UNIVERSITÉ DU QUÉBEC À MONTRÉAL

# A GENERAL FILTER FOR STRETCHED-GRID MODELS

DISSERTATION

PRESENTED

AS PARTIAL REQUIREMENT

OF THE DOCTORATE OF ENVIRONEMENTAL SCIENCES

BY

DORINA SURCEL

OCTOBER 2011

UNIVERSITÉ DU QUÉBEC À MONTRÉAL

# DÉVELOPPEMENT D'UN FILTRE SPÉCIFIQUE POUR UN MODÈLE À RÉSOLUTION VARIABLE

THÈSE

PRÉSENTÉE

COMME EXIGENCE PARTIELLE

DU DOCTORAT EN SCIENCES DE L'ENVIRONNEMENT

PAR

DORINA SURCEL

OCTOBRE 2011

# REMERCIEMENTS

Tout d'abord, je tiens à exprimer mes remerciements et toute ma gratitude au Prof. René Laprise, qui m'a donné l'opportunité de réaliser ce projet. Ses bons conseils, sa rigueur scientifique, ses encouragements ont grandement contribué à finaliser ce travail. Je tiens également à le remercier du soutien financier qu'il m'a offert pendant mes études de maîtrise et de doctorat. Je le remercie aussi pour sa disponibilité permanente, pour sa patience et sa persévérance à m'avoir dirigée toutes ces années.

Je remercie le Centre ESCER et le Réseau canadien de modélisation et diagnostics du climat régional (MDCR) d'avoir mis à ma disposition tout ce dont j'avais besoin pour travailler. Spécialement à Adelina Alexandru, merci beaucoup pour tout ton aide, soit en ta qualité de coordonnatrice du réseau, soit comme très bonne amie. Je veux remercier aussi Georges Huard et Nadjet et Mourad Labassi pour m'aider à résoudre mes problèmes informatiques.

Pendant mon passage à l'UQAM, j'ai connu et j'ai eu la chance de partager de très bons moments avec beaucoup des personnes. Emilia Diaconescu, Cristina et Alexandru Stefanof, Cristina Lupu, Biljana Music et Corina Rosu sont ceux qui ont été un peu plus proches de moi que les autres. Merci beaucoup à tous pour vos mots d'encouragement.

À ma famille, d'ici et de loin, merci d'avoir été patiente avec moi.

# TABLE DES MATIÈRES

# LISTE DES FIGURES

# LISTE DES TABLEAUX

# RÉSUMÉ

Un modèle climatique mondial qui utilise une grille à résolution variable constitue une méthode moderne et efficace pour la modélisation régionale, principalement parce qu'elle évite le problème de pilotage aux frontières latérales caractéristique aux modèles sur aire limitée.

L'approche de grille étirée s'inscrit parmi les méthodes de réduction d'échelle dynamique (*dynamical downscaling*) qui permettent naturellement des interactions réciproques entre les échelles régionales et globales du mouvement. Une augmentation de la résolution seulement dans une région spécifique augmente la précision du modèle, gardant en même temps les coûts de calcul inférieurs aux modèles mondiaux qui utilisent une haute résolution uniforme sur toute la grille. Cependant, l'étirement de la grille conduit à des problèmes liés à l'anisotropie de la grille dans les zones adjacentes à la zone de haute résolution uniforme.

Dans le cadre de cette thèse, un filtre numérique construit à l'aide d'un produit de convolution a été développé pour répondre aux questions associées à l'étirement et à l'anisotropie de la grille de calcul. La caractéristique principale de ce filtre est d'enlever toutes les échelles inférieures à une échelle prescrite par l'utilisateur. L'efficacité et la précision du filtrage représentent un compromis acceptable entre la réponse de filtrage et les coûts de calcul impliqués. Cette approche a été testée sur des grilles étirées unidimensionnelles et bidimensionnelles cartésiennes. Les résultats ont montré que le filtre est efficace même pour une distance de troncature limitée et que la réponse de filtrage est presque isotrope.

Le filtre initialement appliqué sur une grille cartésienne a été adapté dans un deuxième temps pour la grille polaire. Cette étape constitue une démarche nécessaire pour passer ensuite à une grille sphérique latitude-longitude. Les deux grilles, polaire et sphérique, rencontrent le même « problème du pôle » causé par la convergence des méridiens vers les pôles. Des détails sur l'adaptation du filtre pour la grille polaire, ainsi que son application sur une grille polaire uniforme et sur une grille polaire étirée sont présentés. Dans cette partie de la thèse, la performance du filtre près des pôles et dans les régions d'étirement a été testée. Les résultats ont montré que l'opérateur de filtrage est capable d'enlever l'excès de résolution dans les régions polaires, avec des coûts de calculs qui sont inférieurs aux filtres polaires usuels. Le filtre a bien fonctionné en dehors de la région d'intérêt où les échelles qui ne sont pas supportées par la grille ont été enlevées sans déformation ou atténuation des grandes échelles.

L'opérateur de filtrage développé a été appliqué sur une grille polaire étirée pour des variables scalaires et pour des vecteurs. Cette étude a montré des résultats prometteurs, la réponse de filtrage pouvant être optimisée pour différentes fonctions-test ainsi que pour différents types de bruit qui devraient être enlevés.

Mots-clés : filtrage numérique, produit de convolution, fonction de pondération, grille étirée, anisotropie.

# ABSTRACT

Variable-resolution grids are used in global atmospheric models to improve the representation of regional scales over an area of interest, with reduced computational cost compared to uniform high resolution, and avoiding the nesting issues of limited-area models.

The stretched-grid approach provides a dynamical downscaling approach that naturally allows two-way interactions between the regional and global scales of motion. Concentrating the resolution over a subset of the earth's surface increases computational efficiency and reduces the computational costs compared to global uniform high-resolution models; however,it does not come free of some problems related to the variation of resolution.

To adresse these issues associated with the stretching and the anisotropy of the computational grid, a convolution filter with a flexible response function is developped. The main feature of this filter is to locally remove scales shorter than a user-prescribed spatially varying length scale. The filtering effectiveness and computational efficiency of the filter can be custom tailored by an appropriate compromise between the filtering response and the width of the convolution stencil. This approach has been tested in one- and two- dimensional Cartesian geometry. It is shown that an effective filter can be obtained using a limited spatial stencil for the convolution to reduce computational cost, and that an adjustable spatially variable and nearly isotropic response can be obtained for application on variable grids.

The convolution filter that was initially applied in Cartesian geometry is later adapted to cylindrical polar coordinates as an intermediate step towards spherical polar latitude-longitude grids. Both polar grids face the so-called "pole problem" due to the convergence of meridians at the poles. Details related to the adaptation of the filter to cylindrical polar coordinates, for both uniform as well as stretched grids are presented. The results show that the developed operator is skilful in removing the extraneous fine scales around the pole, with a computational cost smaller than that of common polar filters.

The convolution filter was developed for the filtering of scalar and vector variables. The results on a stretched grid are satisfactory and the filter's response can be optimized for different types of test function and noise one wishes to remove.

Keywords: numerical filter, convolution, weighting function, stretched-grid, anisotropy.

# INTRODUCTION

La modélisation atmosphérique est devenue dans les dernières décennies un outil qui répond aux besoins spécifiques concernant la prévision du temps ou la projection de l'évolution du climat. Pour couvrir la vaste gamme d'échelles spatiales et temporelles des phénomènes atmosphériques ou pour mieux représenter les forçages externes, les modèles numériques nécessitent une haute résolution. Bien que la capacité de calcul a augmenté beaucoup depuis qu'on utilise les modèles atmosphériques, il n'est pas rentable et aussi il n'est pas toujours d'intérêt d'utiliser une grille à haute résolution qui couvre la surface entière du globe terrestre, surtout pour des simulations climatiques, donc des simulations sur une longue période de temps. Deux techniques de modélisation régionale sont généralement utilisées par la communauté scientifique pour obtenir une haute résolution au-dessus d'une région d'intérêt (Staniforth 1997, Côté *et al.* 1998).

La première stratégie, celle de l'approche non interactive, consiste en l'utilisation d'un modèle sur aire limitée (*Limited Area Model*, LAM), piloté par un modèle mondial de faible résolution. La difficulté dans cette approche est de spécifier correctement les conditions aux frontières latérales. Ces conditions aux frontières latérales doivent être périodiquement mises à jour, ce qui produit des simulations intermittentes et des résultats qui sont directement liés à la qualité des données utilisées. De plus ces mises à jour périodiques donnent une interaction unidirectionnelle entre les domaines de haute et de basse résolution. Ces modèles sont fiables du point de vue des coûts de calcul parce qu'ils utilisent un domaine restreint, mais il est difficile de représenter les mouvements de grande échelle sur un petit domaine (Fox-Rabinovitz *et al.* 2008).

La deuxième stratégie est celle de l'approche interactive. On utilise un modèle mondial où la résolution varie de la plus fine résolution au-dessus de la zone d'intérêt à une résolution grossière en dehors de cette zone. Cette approche permet non seulement d'obtenir des champs à une haute résolution, mais aussi d'utiliser une orographie et des forçages physiques au-dessus de la zone d'intérêt avec une très fine résolution. Un modèle mondial qui utilise une grille à résolution variable ne nécessite pas des conditions aux frontières latérales, et les caractéristiques de mouvement à l'intérieur et à l'extérieur de la zone d'intérêt interagissent dans un seul système dynamique (Staniforth 1997, Gibelin et Déqué 2003, Fox-Rabinovitz *et al.* 2006, Laprise 2008).

Il y a différentes méthodes pour concevoir la résolution variable. Courtier et Geleyn (1988) et Hardiker (1997) utilisent la transformée conforme de Schmidt (1977) entre deux sphères de manière à préserver l'efficacité de la méthode spectrale. Cette transformation assure localement l'isotropie, mais il y a des limitations quant à l'augmentation de la résolution dans la région d'intérêt comparativement à la région où la résolution demeure faible (Caian et Geleyn 1995). La résolution variable est obtenue en utilisant des éléments finis par Paegle (1989), Paegle *et al.* (1997) et Côté *et al.* (1993).

L'idée de varier graduellement la résolution à partir d'une haute résolution uniforme dans la zone intérêt, vers une résolution faible de côté opposé, constitue le concept de « grille étirée » (*stretched-grid*, SG). Cette approche a été initialement utilisée dans les modèles opérationnels de prévision (Yessad et Bénard 1996, Coté *et al.* 1997 et 1998). Son utilisation pour des simulations climatiques a été initiée au début des années 90 à Météo France dans le cadre du modèle spectral ARPEGE (Déqué et Piedelièvre 1995) et par conséquent par autres groupes de recherche pour des modèles en points de grille (Fox-Rabinovitz *et al.* 1997, McGregor *et al.* 2002).

La nouvelle génération du modèle régional climatique canadien (MRCC) est développée à partir du modèle global environnemental multi-échelle (GEM), qui est présentement utilisé pour les prévisions météorologiques au Service météorologique canadien (Zadra *et al.* 2008). GEM permet plusieurs configurations, incluant une grille globale uniforme, une grille globale étirée avec une zone de haute résolution uniforme au-dessus de la région d'intérêt, ainsi qu'une grille sur aire limitée. Les deux dernières configurations sont envisagées pour l'utilisation dans le cadre du MRCC.

Contrairement à l'approche LAM, l'approche SG ne demande pas de conditions aux frontières latérales et elle permet des simulations indépendantes utilisant un seul modèle mondial (SG-GCM), au lieu de deux modèles, un modèle global à faible résolution uniforme qui va piloter un autre modèle régional à haute résolution uniforme.

Ce type d'approche a aussi été testé lors du projet SGMIP (*Stretched-Grid Model Intercomparison Project*, SGMIP, Fox-Rabinovitz *et al.* 2006 et 2008). Il a réunit quatre groupes de recherche de l'Europe, l'Australie et l'Amérique du Nord qui utilisent l'approche SG dans des modèles climatiques spectraux ou en points de grille. Bien que le projet ait démontré que les résultats de ces modèles sont faisables pour des simulations régionales et globales, les participants ont mentionné la nécessité de respecter certaines conditions de base pour contrôler les problèmes numériques causés par les irrégularités de la grille. Parmi ces conditions, ils mentionnent la nécessité d'avoir un facteur local d'étirement constant pour un étirement graduel qui ne devrait pas dépasser 5 à 10%. Pour préserver la représentation de champs à l'échelle globale, il faut garder une résolution uniforme dans la zone de basse résolution ainsi qu'assurer une résolution minimale de quelques degrés. Une autre condition importante pour l'efficacité de cette approche est d'avoir une haute résolution uniforme dans la région d'intérêt. Même quand les conditions précédentes

sont respectées, la variation de la résolution et l'anisotropie de la grille en dehors de la région de haute résolution uniforme peuvent causer l'apparition d'instabilités numériques qui risquent de contaminer la solution.

Notre attention se concentre sur l'approche de grille étirée sur une grille de type latitude-longitude avec les pôles du système de coordonnées correspondant aux pôles géographiques (Fox-Rabinovitz *et al.* 1997) ou tournés par rapport à celles-ci (Zadra *et al.* 2008). La figure 1.1 montre une représentation simplifiée d'une grille étirée latitude-longitude typique. La région de haute résolution uniforme du domaine (*HR*) est représentée en vert. Cette région est entourée d'une zone dans laquelle la distance entre les points de grille augmente graduellement dans les deux directions (en rose dans la figure 1.1). Au-delà d'une certaine distance, la distance entre les points de grille devient constante, mais le maillage est très anisotrope : ces régions, colorées en orange à la figure 1.1, seront référées comme les « *bras de la croix* ». Ensuite, le domaine est complété par une région de basse résolution uniforme (*LR*) présentée en blanc dans la figure 1.1.

Tous les modèles numériques sont sujets à des instabilités causées par les méthodes de discrétisation, les paramétrages ou les conditions initiales utilisées. Ces instabilités exprimées par l'apparition des ondes de haute fréquence ou de courte longueur d'onde représentent généralement un bruit numérique. Il est possible d'enlever ce bruit ou de limiter son action par l'introduction d'un filtrage dans les modèles. Ce filtrage est défini comme l'élimination des composantes oscillatoires indésirables, généralement de haute fréquence ou courte échelle, d'un ensemble de données ou des solutions d'un ensemble d'équations.

Traditionnellement, deux techniques de filtrage ont été adaptées pour les modèles mondiaux qui utilisent une grille latitude-longitude à résolution variable.

La première méthode est généralement appliquée pour contrôler les instabilités numériques causées par la convergence des méridiens aux voisinages des pôles. Cette convergence des méridiens, connue comme « le problème du pôle », impose des limitations très strictes sur le pas temporel des différents schémas numériques.

Différentes stratégies sont utilisées dans les modèles qui utilisent une grille sphérique pour éliminer le « problème du pôle ». Une première stratégie constitue l'utilisation d'une grille « réduite » dans laquelle la distance physique entre deux points de grille le long des cercles de latitude près du pôle est gardée constante plutôt que la distance azimuthale (Hortal et Simmons 1991). Une autre stratégie fait référence au filtrage des ondes qui deviennent instables pour un certain pas temporel. La plus commune stratégie pour résoudre le « problème du pôle » est l'utilisation d'un filtre polaire de type Fourier. Ce filtre est appliqué au-delà d'une latitude critique $\varphi_c$ (généralement 45° ou 60° dépendant des applications). La puissance de ce filtre augmente graduellement vers le pôle, en augmentant le nombre des ondes zonales affectées et en diminuant leurs amplitudes. L'application d'un filtre de Fourier nécessite des calculs reliés au passage aller-retour de l'espace physique à l'espace spectral, ainsi que la troncature des transformées de Fourier à un certain nombre d'onde. Une troncature abrupte de la transformée de Fourier dans les hautes latitudes affecte l'exactitude des méthodes de discrétisation (Purser 1988). Les filtres de Fourier offrent un contrôle direct de la troncature, mais ont besoin d'un nombre élevé d'opérations de l'ordre de $O\left(N^2 \log^2 N\right)$, avec $N$ le nombre de points de grille sur chaque cercle de latitude.

Une dernière stratégie que nous allons mentionner pour le « problème du pôle » est l'utilisation d'un filtre numérique en une dimension, appliqué dans les hautes latitudes le long des cercles de latitudes avec une puissance qui augmente en s'approchant des pôles. Ces opérateurs (généralement exprimés par un laplacien

unidimensionnel) ont besoin seulement de communications locales, mais la troncature n'est pas toujours bien contrôlée.

Un filtre polaire de type Fourier est appliqué dans le modèle à résolution variable GEOS SG-GCM (Fox-Rabinovitz *et al.* 2001). Ce filtre décrit par Takacs *et al.* (1999) est appliqué aux tendances des variables, plutôt qu'aux variables elles-mêmes. Par conséquent, pour respecter le critère de stabilité numérique près du pôle, les grands nombres d'onde en direction zonale sont plutôt ralentis et non pas amortis.

Une deuxième méthode de filtrage appliquée dans les modèles qui utilisent une grille latitude-longitude étirée est consacrée à l'élimination des instabilités numériques créées par les méthodes de discrétisation ou par la forme de la grille.

Le modèle mondial à grille étirée GEM (Côté *et al.* 1998) utilise au début de l'intégration un filtre digital pour éliminer les oscillations rapides engendrées par les ondes de gravité qui peuvent être présentes dans les champs d'analyse non parfaitement équilibrés. Par la suite, la diffusion horizontale est appliquée sur les variables de quantités de mouvement. Le but de la diffusion horizontale est d'atténuer les plus petites longueurs d'onde pour éviter l'accumulation d'énergie à cause du repliement numérique sur ces longueurs d'ondes. Le schéma semi-lagrangien utilisé dans le modèle GEM étant déjà quelque peu diffusif, le coefficient de diffusion ne nécessite pas d'avoir une valeur très élevée. Surcel (2005) a appliqué la diffusion sur une grille unidimensionnelle variable. Les résultats de l'étude ont montré que la diffusion horizontale appliquée sur une grille qui change la résolution peut produire un lissage uniforme juste pour les ondes moyennes et longues, et non pas pour les ondes courtes.

Le modèle GEOS SG-GCM (Fox-Rabinovitz *et al.* 1997 et 2001) utilise un deuxième filtre (à part le filtre polaire) pour supprimer le bruit causé par le changement de la grille. Ce filtre numérique de Shapiro (1970) d'ordre élevé est

appliqué soit directement sur la grille variable, soit en utilisant une transformation à l'aide des vecteurs propres pour rendre la grille uniforme avant d'appliquer le filtrage. Dans l'étude réalisée par Takacs *et al.* (1999), il y a très peu de différences entre les deux méthodes d'application du filtre de Shapiro, d'où ils concluent que la deuxième méthode plus coûteuse n'est pas rentable.

L'application d'un filtre Shapiro sur une grille à résolution variable est assez contestable. La réponse du filtrage étant dépendant de la résolution de la grille, des champs avec la même longueur d'onde physique seront différemment amortis, en rapport de la localisation sur la grille variable (Surcel 2005). C'est cette constatation qui nous a encouragés à développer une méthode pour construire un filtre universel qui peut effectivement enlever les longueurs d'onde prédéfinies **indépendamment de la grille de calcul**. Le principal objectif de ce filtre sera d'enlever l'anisotropie dans les zones où la résolution varie. Sur une grille qui change la résolution, les seules ondes correctement représentées sont celles qui ont une longueur d'onde plus grande ou égale au double de la distance maximale entre deux points de grille. Ce filtre spécifique permettra de contrôler le repliement numérique des ondes qui sortent de la zone de haute résolution uniforme. L'application de cet opérateur qui agit en fonction de la distance physique sur la grille sera élargie pour le « problème du pôle » et aussi pour éliminer les instabilités numériques caractéristiques à tout modèle.

Le travail effectué dans cette thèse est présenté en deux chapitres correspondant à deux articles écrits en anglais.

Tout d'abord, cette introduction présente une revue des concepts utilisés dans la thèse. L'utilisation de la grille globale étirée est présentée dans la perspective de la modélisation climatique régionale. Deux modèles qui utilisent une grille de type latitude-longitude avec résolution variable sont analysés du point de vue des méthodes de filtrage appliquées. L'objectif général du projet est établi et la méthodologie du projet sera brièvement expliquée.

Le premier chapitre est constitué d'un article intitulé « *A General Filter for Stretched-Grid Models: Application in Cartesian Geometry* » qui a été accepté pour publication dans la revue *Monthly Weather Review*.

Cet article montre la nécessité d'introduire une méthode de filtrage spécifique dans un modèle qui utilise une résolution variable. Cet opérateur de filtrage est construit à l'aide d'un produit de convolution en suivant la méthodologie présentée dans Surcel (2005). Le théorème de convolution (Bracewell 2000) permet d'écrire le produit de convolution entre deux fonctions comme le produit des transformées de Fourier des deux fonctions. À partir de ce théorème la fonction de pondération nécessaire dans le produit de convolution est la transformée inverse de Fourrier de la fonction de réponse qu'on veut obtenir après l'application du filtre. On note que, contrairement aux filtres définis en points de grille, la définition et les propriétés du produit de convolution existent pour l'espace continu et ils ne dépendent pas de l'existence d'une grille spécifique pour son application. Cette propriété sera d'une importance prépondérante pour assurer le développement du filtre spécifique construit à l'aide d'un produit de convolution applicable sur une grille à résolution variable.

Le choix de la fonction de pondération utilisée dans la formulation du filtre est analysé en fonction de la réponse spectrale désirée. Deux méthodes pour approximer la réponse de filtrage sont présentées avec des tests qui montrent les avantages et désavantages de chacune. Le choix entre une distance de troncature plus grande ou l'application répétée du filtre, avec une distance de troncature petite, s'avère un compromis entre la précision du filtre et les coûts de calculs impliqués.

L'opérateur de filtrage développé dans un domaine cartésien à une dimension (1D) est ensuite testé sur une grille variable unidimensionnelle. Le filtre est appliqué sur des fonctions tests composés d'une onde longue correspondant à un signal correctement représenté sur le domaine entier (la solution théorique) et une onde de

courte échelle correspondant à un bruit qui doit être enlevé par le filtre. Les résultats du filtrage sont quantifiés à l'aide de deux métriques, soit une erreur quadratique normalisée et un coefficient de conservation, analysés en fonction de la distance de troncature utilisée.

L'approche théorique développée sur le domaine 1D est généralisée sur le domaine bidimensionnel cartésien. Le produit de convolution bidimensionnel utilise une fonction de pondération qui est le produit des deux fonctions unidimensionnelles, similaires aux celles qui sont utilisées sur le domaine 1D. En pratique, la fonction 2D filtrée sera obtenue par des applications successives du filtre 1D dans chaque direction. La fonction de pondération est symétrique par rapport aux axes *Ox* et *Oy*, et aussi par rapport à toute droite qui passe par le point d'application du filtre.

Le deuxième chapitre continue le développement du filtre pour l'application sur de variables scalaires et vectorielles sur une grille polaire variable. Il est constitué d'un article intitulé « *A General Filter for Stretched-Grid Models: Application in Polar Geometry* » qui a été soumis pour publication dans la revue *Monthly Weather Review*.

Dans la première partie, le filtre construit à l'aide d'un produit de convolution est généralisé pour l'application sur une grille polaire bidimensionnelle. La grille polaire est utilisée comme une simplification d'une grille sphérique latitude-longitude. Les deux types de grilles contiennent des points (les pôles) où les lignes correspondant aux azimuts constants ou aux longitudes constantes convergent. Cette convergence des méridiens connue comme « le problème du pôle » est une caractéristique typique des deux types de grilles et, pour la résoudre, on a besoin d'un traitement particulier.

L'application du filtre sur une grille polaire est obtenue par des applications successives du produit de convolution unidimensionnel en direction azimutale suivi

de l'application en direction radiale. La fonction de pondération utilisée dans le produit de convolution unidimensionnel est identique à la fonction utilisée dans le premier chapitre, mais il faut souligner que cette fonction dépend toujours de la distance physique sur la grille, distance calculée en direction azimutale et en direction radiale.

Dans la deuxième partie on présente l'application du filtre pour des scalaires sur une grille polaire uniforme et sur une grille polaire variable. Le filtre construit à l'aide d'un produit de convolution est appliqué sur des fonctions tests scalaires pour enlever l'anisotropie dans les zones d'étirement ou pour résoudre le « problème du pôle ». Les tests effectués en utilisant des harmoniques cylindriques ou des fonctions similaires à celles qui sont utilisées sur la grille cartésienne ont permis d'évaluer l'erreur quadratique moyenne sur le domaine entier ou dans différentes régions du domaine. Cela a montré l'influence du filtrage sur les ondes représentées dans les zones d'étirement ainsi que l'influence du filtrage sur les ondes longues dans la zone de basse résolution uniforme.

La troisième partie du deuxième chapitre est consacrée à l'application du filtre pour des vecteurs. En sciences atmosphériques, on utilise la représentation des variables par rapport à un système de coordonnées liées au point d'observation, donc liées à un point spécifique sur la grille. C'est pour cette raison que l'application du filtre pour les variables vectorielles, comme le vent horizontal, a dû être adaptée en représentant tous les vecteurs qui seront considérés dans le calcul du produit de convolution relativement au même système de coordonnées centré sur le point d'application du filtre. Les fonctions tests utilisées pour le filtrage des vecteurs sont développées analytiquement à partir des fonctions scalaires similaires à celles qui sont utilisées pour le filtrage des variables scalaires. Le filtre est appliqué sur une grille polaire uniforme pour vérifier son efficacité près du pôle. Par la suite, le filtre est appliqué sur une grille polaire étirée où son efficacité est estimée comme une

erreur quadratique moyenne pour la conservation d'énergie. Cette erreur de filtrage est évaluée sur le domaine entier ou seulement dans les zones d'étirement et dans la zone de basse résolution uniforme.

Les conclusions de cette thèse présentent les résultats obtenus, les contributions, les limites et les perspectives de la recherche. Trois articles soumis au *WGNE Blue Book "Research activities in Atmospheric and Oceanic Modelling, WMO/TD"* (http://collaboration.cmc.ec.gc.ca/science/wgne/index.html) (sans comité de lecture) sont insérés en annexe.

# CHAPITRE I

# UN FILTRE SPÉCIFIQUE POUR UN MODÈLE À RÉSOLUTION VARIABLE : APPLICATION EN COORDONNÉES CARTÉSIENNES

Ce chapitre, rédigé en anglais, est présenté sous la forme d'un article qui a été accepté pour publication dans la revue *Monthly Weather Review*. Il décrit le développement d'un filtre numérique construit à l'aide d'un produit de convolution entre la fonction à filtrer et une fonction de poids. Cette fonction de poids est analysée et testée dans un domaine cartésien unidimensionnel. La conversion du filtre pour un domaine bidimensionnel cartésien à résolution variable, et des tests pour prouver l'efficacité du filtrage, sont ensuite présentés.

L'étude montre que le filtre construit à l'aide d'un produit de convolution est efficace en utilisant une distance de troncature ajustable pour réduire les coûts de calcul. La réponse de filtrage est presque isotropique quand le filtre est appliqué sur une grille à résolution variable.

# A General Filter for Stretched-Grid Models: Application in Cartesian Geometry

Dorina Surcel
and
René Laprise

ESCER Centre
Université du Québec à Montréal, Montréal (Québec), Canada

Published in Monthly Weather Review (2011)
http://journals.ametsoc.org/doi/abs/10.1175/2010MWR3531.1

---

*Corresponding author address:*
Dorina Surcel, Centre ESCER, Université du Québec à Montréal, Case postale 8888, Succursale Centre-ville, Montréal, Québec, CANADA, H3C 3P8.
E-mail: colan@sca.uqam.ca

# Résumé

Un modèle climatique mondial qui utilise une grille à résolution variable constitue une méthode moderne et efficace pour representer les petites échelles sur une région d'intêret, principalement parce qu'elle évite le problème de pilotage aux frontières latérales caractéristique aux modèles sur aire limitée.

L'approche de grille étirée s'inscrit parmi les méthodes de réduction d'échelle dynamique (*"dynamical downscaling"* en anglais) qui permettent naturellement des interactions réciproques entre les échelles régionales et globales. Une augmentation de la résolution seulement dans une région spécifique augmente la précision du modèle, gardant en même temps les coûts de calcul inférieurs aux modèles mondiaux qui utilisent une haute résolution uniforme sur toute la grille. Cependant, l'étirement de la grille conduit à des problèmes liés à l'anisotropie de la grille dans les zones adjacentes à la zone de haute résolution uniforme.

Cette étude présente un filtre numérique construit à l'aide d'un produit de convolution qui a été développé pour répondre aux questions associées à l'étirement et à l'anisotropie de la grille de calcul. La caractéristique principale de ce filtre est d'enlever toutes les longueurs d'onde supérieures à une longueur d'onde prescrite par l'utilisateur. L'efficacité et la précision du filtrage représentent un compromis acceptable entre la réponse de filtrage et les coûts de calcul impliqués. Cette approche a été testée sur des grilles étirées unidimensionnelles et bidimensionnelles cartésiennes. Les résultats ont montré que le filtre est efficace même pour une distance de troncature limitée et que la réponse de filtrage est presque isotrope.

# Abstract

Global climate models with variable resolution are effective means to represent regional scales over an area of interest while avoiding the nesting issues of limited-area models. The stretched-grid approach provides a dynamical downscaling approach that naturally allows two-way interactions between the regional and global scales of motion. Concentrating the resolution over a subset of the earth's surface increases computational efficiency and reduces the computational costs compared to global uniform high-resolution models; however it does not come free of some problems related to the variation of resolution.

To address the issues associated with the stretching and anisotropy of the computational grid, a general convolution filter with a flexible response function is developed. The main feature of this filter is to locally remove scales shorter than a user-prescribed spatially varying length scale. The filtering effectiveness and computational efficiency of the filter can be custom-tailored by an appropriate compromise between the filtering response and the width of the convolution stencil. This approach has been tested in one- and two-dimensional Cartesian geometry. It is shown that an effective filter can be obtained using a limited spatial stencil for the convolution to reduce computational cost, and that an adjustable spatially variable and nearly isotropic response can be obtained for application on variable grids.

## 1.1 Introduction

Regional climate modelling using a variable-resolution global approach is an alternative to the widely used nested limited-area models (LAM). A variable-resolution General Circulation Model (GCM) does not require lateral boundary conditions and it provides self-consistent interactions between global and regional scales of motion (Gibelin and Déqué 2003, Fox-Rabinovitz et al. 2006, Laprise 2008). Concentrating the resolution over a subset of the earth's surface increases computational efficiency, but this does not come free of some issues owing to the variation of resolution. The non-uniformity and anisotropy of the grid can result in computational artefacts and contamination of the physical solution, as does the convergence of meridians near the poles in the case of uniform latitude-longitude grids.

The technique of grid stretching is one of the most extensively used methods for implementing variable resolution in climate models. The stretched-grid (SG) approach was originally used for operational short-term numerical weather prediction (Yessad and Bénard 1996, Coté et al. 1997 and 1998). The implementation of the SG approach for climate simulations was initiated in the early 1990s at Météo-France for the *Action de Recherche Petite Échelle Grande Échelle* (ARPEGE) spectral model (Déqué and Piedelièvre 1995) and later by other groups for grid-point models (Fox-Rabinovitz et al. 1997, McGregor et al. 2002).

In Canada the new generation of the Canadian Regional Climate Model (CRCM5) is being developed within the framework of the existing Global Environmental Multiscale (GEM) model presently used for global and regional numerical weather prediction at the Meteorological Service of Canada (Zadra et al. 2008). GEM supports multiple configurations, including uniform global, stretched-

grid global, and nested limited area; the latter two configurations are contemplated for use in CRCM5.

Unlike the nested approach, the SG by design doesn't require lateral boundary conditions and it allows autonomous multi-year simulations with a single SG-GCM instead of a uniform-resolution GCM driving a nested limited-area model. The SGMIP project (Fox-Rabinovitz et al. 2006, 2008) in its first phase has demonstrated the ability of SG-GCM to provide good-quality regional and global climate simulation results. The authors mentioned the necessity of respecting some basic conditions for controlling computational problems due to grid irregularity. The following conditions must be imposed on the SG design:

- The local stretching factor, which is the ratio between adjacent grid intervals in the stretching zone, must be constant for a gradual stretching;

- The local stretching factor must not exceed 5 - 10% depending on specific application;

- The maximum grid-point distance in the low-resolution part of the domain must not exceed few degrees in order to maintain global accuracy;

- The grid spacing over the high-resolution area must be uniform.

Even when respecting the above constraints for the mesh design, the variation of resolution and anisotropy of the grid outside the uniform high-resolution area can result in numerical artefacts that risk contaminating the simulations. Some of these constrains such as the local isotropy are naturally satisfied by the conformal Schmidt transformation (Schmidt 1977) used in ARPEGE (Courtier and Geleyn 1988); other constrains, however, need to be imposed because of intrinsic limitations of resolution created by this transformation (Caian and Geleyn 1997).

Different grid structures are used in SG models based on spectral numerics (e.g. ARPEGE; Gibelin and Déqué 2003) and grid-point discretisations (e.g. GEOS SG-GCM; Fox-Rabinovitz et al. 1997). In the following we will concentrate on the latter which uses latitude-longitude stretched grids with their computational poles aligned (e.g. Fox-Rabinovitz et al. 1997) or rotated (e.g. Zadra et al. 2008) with respect to the geographical poles. Figure 1.1 shows a simplified sketch of a typical latitude-longitude stretched grid. The uniform high-resolution region (*HR*) of the domain is shown in green. The core *HR* region is surrounded by a region where the grid is stretched in one or both directions; the stretching zones (*SG*) are shown in pink in Fig. 1.1. Beyond some distance the grid spacing becomes constant but the mesh is then very anisotropic: these regions will be referred to as the "arms of the cross" and are shown in orange in Fig. 1.1. The domain is completed by a uniform low-resolution (*LR*) region shown in white in Fig. 1.1. (The line A-A' will be referred to subsequently in 1D tests.)

Traditionally two basic filtering techniques have been adapted in global variable-resolution models. A first filter is generally applied in all models formulated in longitude-latitude grids to control numerical instabilities arising from the convergence of the meridians near the poles; a polar Fourier filter (e.g. Takacs et al. 1999) is often applied in high latitudes. In stretched-grid models it is directly applied on the stretched grid taking into account the stretching. In the GEOS SG-GCM (Fox-Rabinovitz et al. 2005) the polar filter is applied to the tendencies of the prognostic variables rather than to the prognostic variable themselves; as a result high zonal wavenumbers are slowed down rather than being damped, which nevertheless allows respecting the numerical stability criterion near the poles. A second filter is generally applied to remove grid-point noise over the entire domain; this objective is reached with the application of a high-order Shapiro filter (Shapiro 1970). Takacs et al. (1999) found also that the application of Shapiro filter with the eigenvector method produces very small differences compared to its standard application.

The application of a Shapiro filter on a variable-resolution grid is somewhat questionable; the filtering response being dependent on the computational grid distance, fields with a given length scale will be damped differently depending on the local mesh interval of the grid (Surcel 2005). This is what prompted us to design a method for building a general filter that can effectively remove user-defined length scales **independently of the computational mesh**. We will show that the resulting filter can be used among other applications to ensure nearly isotropic resolution even in the stretching region, and to enforce, under the control of the user, smoothly varying effective resolution over the entire domain, independently of the computational mesh, including around the pole where meridians converge and the stretching zone in SG models.

This paper is organized as follows. The next section describes the formulation of the proposed general convolution filter. Section 1.3 presents the application of the filter on one-dimensional uniform and stretched-grid domains, and also provides details and examples of the performance of the filter into a 2D Cartesian stretched grid. In section 1.4 we give some concluding remarks on the application of the filter into a Cartesian domain and general directions for the conversion of the filter to polar geometry.

## 1.2 Description of a general convolution filter

To describe the proposed convolution filter, we recall that the convolution between a signal $\psi$ and a weighting function $w$ can be expressed as follows, in one dimension for simplicity:

$$\overline{\psi}(x) = (\psi * w)(x) = \int_{-\infty}^{\infty} \psi(t)\, w(x-t)\, dt, \tag{1.1}$$

where $\overline{\psi}$ represents the filtered signal. The spectral response of the convolution is obtained by taking the Fourier transform of the filtered $\overline{\psi}$ and original $\psi$ fields, evaluating the ratio of their spectral amplitudes as a function of wavenumbers. The convolution theorem (e.g., Bracewell 2000) shows that, to obtain a desired response from a convolution filter, the required weighting function is the inverse Fourier transform of that response function (e.g., Surcel 2005):

$$w(d) = \frac{1}{2\pi} \int_{-\infty}^{\infty} R(k) \exp(ikd)\, \mathrm{d}k, \tag{1.2}$$

where $R(k)$ is the spectral filtering response. We note that, unlike the usual grid-point filters, the definition and properties of the convolution exist for continuous space and do not rely on the existence of a specific grid for its application; this feature will be of paramount importance for the ensuing development of the proposed general convolution filter applicable to variable-resolution grids.

The standard convolution uses a single weighting function $w(d)$ and it produces a spectral response function $R(k)$ that is constant in space. In some applications it might be desirable to use a filter with a response function that varies

with location, which we note loosely as $R(x,k)$. Modellers sometimes achieve this by using spatially varying diffusion coefficients. A simple, albeit *ad hoc*, modification to the standard convolution can be made to obtain a spatially varying response, consisting in using a weighting function that varies with location: $w(d,x)$. Although it is no more possible then to formally establish the exact response function (noted $R(x,k)$), a WKBJ type of approximation (e.g., Bender and Orszag 1978) leads us to believe that it is reasonable to think in terms of local spectral response, as long as the weighting function varies slowly with location. Empirical evidence from the experimental results presented later will show that this approach renders sensible results even with rather rapid variations of the weighting function.

Whether on a uniform latitude-longitude grid or on a stretched grid, physical grid spacing changes with the location on the grid. On the so-called uniform latitude-longitude grid, the convergence of the meridians towards the poles induces changes in grid spacing in the zonal direction, with maximum grid spacing $\Delta x_{\max}$ near the equator. On a variable-resolution stretched grid, quasi-uniform fine mesh prevails over the area of interest, while outside this area the grid intervals increase in one or both horizontal directions. A geometric progression is often used with a constant local stretching rate defined as:

$$s = \Delta x_i / \Delta x_{i-1}, \tag{1.3}$$

where $\Delta x_i$ and $\Delta x_{i-1}$ are adjacent grid-mesh intervals. The total global stretching factor represents the ratio between the maximum and minimum grid intervals on the mesh:

$$S = \Delta x_{\max} / \Delta x_{\min}\,. \tag{1.4}$$

A generalized convolution filter will be designed to satisfy specific user-defined response function; this filter could be applied to control any undesirable

computational noise, including that arising from the convergence of the meridians near the pole or other non-uniformity and/or anisotropy of a computational grid. Over non-uniform grids, the only waves that can be represented over the entire domain are those with length scales larger than or equal to twice the maximum grid spacing $\Delta x_{\max}$. Therefore, on a uniform latitude-longitude grid, suitable filtering could be used to remove the smaller scales in the zonal direction that are permitted by the convergence of the meridians towards the poles; this would be an effective means of ensuring computational stability as well as isotropy and homogeneity of effective resolution. Similarly in a stretched-grid model, it would be possible to remove some anisotropic features associated with fine-scale structure of the mesh in only one dimension, such as in the arms-of-the-cross region surrounding the high-resolution area of interest; this may be an effective mean of controlling aliasing of fine-scale features while they exit the high-resolution region and enter in the low-resolution part of the domain. In this case the numerical filtering operator could suitably remove the unwanted small scales outside the uniform high-resolution area if the user so desired.

A response function that verifies these conditions can be defined as follows

$$R(k) = \begin{cases} 1 & 0 \le k \le a = \pi/\Delta x_{\max} \\ \cos^2 \dfrac{\pi}{2}\left(\dfrac{k-a}{b-a}\right) & a < k < b \\ 0 & b \le k \le \pi/\Delta x_{\min} \end{cases}, \qquad (1.5)$$

which corresponds to keeping unaltered the large scales with wavenumber smaller than $a$ (corresponding to wavelengths larger than $2\Delta x_{\max}$ that are resolved everywhere on the grid), and removing entirely small scales with wavenumber larger than a chosen value of $b$, with a gradual transition in between to reduce Gibbs' phenomenon. The convolution theorem then gives us the corresponding weighting function as:

$$w(d) = \frac{\pi}{2} \frac{\sin ad + \sin bd}{d\left(\pi^2 - d^2(b-a)^2\right)} \quad , \tag{1.6}$$

with $d = x - t$. We note in passing that a real value of response function corresponds to symmetric weighting functions.

The choice of the $b$ parameter greatly affects the sharpness of the spectral response and the width of the weighting function, as illustrated in Fig. 1.2 for three values of $b$. A relatively small value of $b-a$, corresponding to a narrow response transition such as *R1*, gives rise to a broad weighting function ($w_1$) with oscillating values over a large segment of the domain. On the other hand, a more localized weighting function such as $w_3$, corresponds to very gradual response function (*R3*).

Although the formal definition of the convolution (1.1) exists for continuous space, its practical application requires a version to be defined using a discrete set of points $(x_i)_{i=1,n}$ on a grid. The following general trapezoidal quadrature can be used as follows:

$$\overline{\psi}(x_i) = \frac{\sum_{j=-\infty}^{\infty} \psi(x_j)\, w(d_{i,j})\, \sigma(x_j)}{\sum_{j=-\infty}^{\infty} w(d_{i,j})\, \sigma(x_j)}, \tag{1.7}$$

where $\sigma(x_j)$ is a variable weight assigned to the contribution of each computational point $\sigma(x_j) = (x_{j+1} - x_{j-1})/2$ to account for the stretching. We want to stress that the convolution weights are function of the **physical** distance $d_{i,j} = |x_i - x_j|$ between the application point $x_i$ and all other contributing points $x_j$. The use of physical distance is the distinguishing feature of the proposed approach. In conventional grid-point filtering such as the Shapiro filter, the weights are function of the indices ($|i-j|$)

rather than physical distance. While both approaches render the same results on uniform grid, the use of physical distance in the convolution offers definite advantages over variable grids, as we shall demonstrate.

Returning to the weighting function $w(d)$ (e.g. Fig. 1.2), clearly the presence of non-vanishing values over the entire domain is problematic in practice because of the excessive computational cost. By inspection of the weighting function curve, however, one notices that values become rather small and alternate in sign after some distance from the origin. Hence in the following, we will test various pragmatic approximations to $R$ consisting of truncating $w$ to zero after some distance $d_{\max}$ from the origin, aiming at important reduction in computational cost. Therefore, the filtering formula will be approximated as

$$\overline{\psi}(x_i) = \frac{\sum_{d_{i,j} \le d_{\max}} \psi(x_j)\, w(d_{i,j})\, \sigma(x_j)}{\sum_{d_{i,j} \le d_{\max}} w(d_{i,j})\, \sigma(x_j)}. \qquad (1.8)$$

The three weighting functions represented in Fig. 1.2 will successively be tested considering different values of the cut-off distance $d_{\max}$. We will study the impact on the corresponding response function of using four cut-off distances ($d_1$, $d_2$, $d_3$ and $d_4$) as indicated in Fig. 1.3. The first case corresponds to a wide-footprint weighting function $w_1$ (Fig. 1.3, upper panels). We note that the theoretical response (represented by the curve $d_\infty$) is adequately approximated only with large cut-off distances; otherwise, the response of the filter shows large oscillations corresponding to false amplification or attenuation of the field.

Narrower weighting function such as $w_2$ (Fig. 1.3, middle panels) are much less demanding; a relatively adequate response function is obtained with much smaller cut-off distance, and there is little difference in the response for cut-off distance

$d_{max} > d_2$. An even better approximation is obtained for $w_3$ with a much smaller cut-off distance (Fig. 1.3, bottom panels). This weighting function corresponds to the most gradual variation of the spectral response in our test case.

In summary, the choice of the weighting function is very important for two main reasons. First, a weighting function corresponding to an abrupt change in the spectral response contains large oscillations and needs a large cut-off distance, which would translate to increased computational costs. Second, a gradually varying response function gives rise to a narrow weighting function and thus to a much smaller acceptable cut-off distance in order to approximate adequately the theoretical response. In this case we must be aware that only a small part of the spectrum is completely removed, the rest being only attenuated. This is not necessarily a problem, as we will see later, because repeated applications of such a filter (as it would be the case if the filter is applied at every time step during the integration of the model) would be as effective at removing undesired scales as a wider weighting function, but at a lesser computational cost.

In the next section we will test different weighting functions and will discuss the advantages and disadvantages for the use of different filter configurations.

## 1.3 Applications

This section presents some examples of applications of the proposed convolution filter into 1D and 2D Cartesian domains, initially with uniform resolution and later with a stretched grid. We express the 1D test-function as $\psi(x) = \psi_l(x) + \psi_n(x)$, where $\psi_l$ is a large-scale wave representing the physical signal that is properly represented on the entire domain, and $\psi_n$ is a small-scale wave representing noise. The filter will be aimed at maintaining the large-scale signal but attenuate or remove the small-scale noise.

The skill of the filter will be quantitatively evaluated by comparing the filtered solution $\overline{\psi}$ with the expected analytical solution $\psi_l$, using two scores: the normalized root-mean square error (*NRMS*) and the normalized conservation ratio (*NCR)*. The root-mean square error will be computed between the filtered solution and the expected analytical solution (after subtracting the mean error), normalized by the variance of the analytical solution:

$$NRMS = \frac{\sqrt{\sum_k \left(\overline{\psi}(x_k) - \psi_l(x_k) - \overline{\Psi}\right)^2 \sigma(x_k)}}{\sqrt{\sum_k \left(\psi_l(x_k)\right)^2 \sigma(x_k)}}, \tag{1.9}$$

where $\overline{\Psi} = \dfrac{\sum_k \left(\overline{\psi}(x_k) - \psi_l(x_k)\right) \sigma(x_k)}{\sum_k \sigma(x_k)}$ is the domain-averaged error between the filtered solution and the analytical solution. The *NCR* checks mass conservation as the mean error between the filtered and unfiltered solution, normalized by the variance of the analytical solution:

$$NCR = \frac{\sum_k \left(\overline{\psi}(x_k) - \psi(x_k)\right) \sigma(x_k) \Big/ \sum_k \sigma(x_k)}{\sqrt{\sum_k \left(\psi_l^2(x_k)\, \sigma(x_k)\right) \Big/ \sum_k \sigma(x_k)}}. \tag{1.10}$$

For all the tests we used a function in the form of a sum of single harmonics for both the large-scale signal and small-scale noise

$$\psi(x_i) = A_l \cos(k_l x_i) + A_n \cos(k_n x_i), \tag{1.11}$$

where $A_l$ and $A_n$ are arbitrarily constants, and $k_l$ and $k_n$ are wavenumbers of the signal to be retained and the noise to be removed, respectively. In the following we will use the convention that $x$ covers the interval from 0 to $2\pi$.

### 1.3.1 Application of the convolution filter in a 1D uniform domain

A necessary condition for any filtering method proposed for a variable mesh is to perform adequately for a uniform grid. In this section, we test the performance of various configurations of the convolution filter in idealized conditions on a uniform-resolution 1D domain.

Three test functions will be used, noted $\psi_1$, $\psi_2$ and $\psi_3$, defined on 256 grid points so that $256\Delta x = 2\pi$. All test functions will use the same signal with wavenumber $k_l = 2\dfrac{2\pi}{256\Delta x} = \dfrac{2\pi}{128\Delta x}$ corresponding to 2 oscillations around the periodic domain and a wavelength of $\lambda_l = 128\Delta x$. Three test functions will be used with different noise scales characterized by the following wavenumbers and wavelengths: $k_{n_1} = 32\dfrac{2\pi}{256\Delta x} = \dfrac{2\pi}{8\Delta x}$ and $\lambda_{n_1} = 8\Delta x$ for the first,

$k_{n_2} = 64\dfrac{2\pi}{256\Delta x} = \dfrac{2\pi}{4\Delta x}$ and $\lambda_{n_2} = 4\Delta x$ for the second, and $k_{n_3} = 128\dfrac{2\pi}{256\Delta x} = \dfrac{2\pi}{2\Delta x}$ and $\lambda_{n_3} = 2\Delta x$ for the third test function.

There are three main parameters that control the response of the filter as defined: $a$ and $b$ characterize the formal filtering response (large scales with wavenumbers smaller than $a$ are kept intact while small scales with wavenumbers larger than $b$ are removed entirely, with a gradual transition in between), and the finite width of the stencil $d_{\max}$ affects the accuracy of the actual filter. We will use a single value for the parameter $a = \dfrac{2\pi}{16\Delta x} = 16\dfrac{2\pi}{256\Delta x}$ corresponding to an ideal response in which all length scales larger than or equal to $16\Delta x$ are kept. We will vary the $b$ parameter as $b_1 = 2a = \dfrac{2\pi}{8\Delta x} = 32\dfrac{2\pi}{256\Delta x}$, $b_2 = 4a = \dfrac{2\pi}{4\Delta x} = 64\dfrac{2\pi}{256\Delta x}$ and $b_3 = 8a = \dfrac{2\pi}{2\Delta x} = 128\dfrac{2\pi}{256\Delta x}$, which corresponds to removing all length scales shorter than or equal to $8\Delta x$, $4\Delta x$ and $2\Delta x$, respectively. These choices parameters correspond to three weighting functions in the convolution formulation, $w_1$, $w_2$ and $w_3$ as shown in the left panels of Fig. 1.3. We will assess the performance of the filters on the test functions, using various stencil widths.

Figure 1.4 shows visually the results of the three filters applied on $\psi_1$ (Figs. 1.4a, c, e) and $\psi_2$ (Figs. 1.4b, d, f) using a stencil that is wide enough to approximate well the theoretical response as seen in Fig. 1.3. The first filter (using $b_1$) was designed in such a way that it should remove entirely the noise for both $\psi_1$ and $\psi_2$ test functions because $b_1 \le \left(k_{n_1}, k_{n_2}\right)$; Figs. 1.4a,b confirm the expectation. In this case the truncation distance $d_{\max} = d_4 = 21\Delta x$ was used in $w_1$ (see the upper-left panel in Fig. 1.3). The second filter (using $b_2$) was designed such as to remove entirely the

noise of $\psi_2$ because $k_{n_2} \geq b_2$, but only attenuate weakly the noise of $\psi_1$ because $k_{n_1} < b_2$; Figs. 1.4c,d again confirm the expectation. Because this second filter has a broader spectral response, a shorter truncation distance $d_{\max} = d_3 = 10\Delta x$ was sufficient to approximate $w_2$, as seen in the middle left panel of Fig. 1.3. The third filter (using $b_3$) was designed to only attenuate the noise of $\psi_1$ and $\psi_2$ because $\left(k_{n_1}, k_{n_2}\right) < b_3$; Figs. 1.4e,f confirm the expectation, and in fact this filter has very little effect on $\psi_1$. Because this third filter has an even broader spectral response, a very short truncation distance $d_{\max} = d_2 = 4\Delta x$ was sufficient to approximate $w_3$, as seen in the lower-left panel of Fig. 1.3. We note that all three filters were very effective in removing entirely the noise in the third test function $\psi_3$ characterised by $2\Delta x$ short-scale noise, and for this reason the figures are not shown.

We now proceed to the quantitative evaluation of the filtering response for the three test functions $\psi_1$, $\psi_2$ and $\psi_3$. In Fig. 1.5 the *NRMS* is shown as a function of the truncation distance used for the stencil in the convolution. In the case of the first filter with a sharp spectral response function and, therefore, a broad weighting function $w_1$, the noise is completely removed only if the truncation distance is large enough to approximate the theoretical response (Fig. 1.5a). The other two filters have more gradual response functions and thus narrower weighting functions $w_2$ and $w_3$; in this case the *NRMS* converges more rapidly to the value that represents the amplitude of the noise remaining after filtering according to the theoretical response in the definition of the weighting function (Fig. 1.5 b,c).

In all cases the conservation ratio was verified and the *NCR* scores were within the round-off error of the computer used for these tests.

We note a sharp spectral response to the filter implies a broad-structure weighting function in the convolution, and that the increase of the stencil width improves the accuracy of the filter, which is then able to produce the theoretical

response. But this increase of stencil width has drawbacks: first it is computationally expensive (especially in many dimensions), and second it involves large volumes of data motion for implementation on distributed-memory parallel computers. Narrower stencils are computationally more efficient in the convolution, but with very narrow stencils, the filter only approximates the theoretical response, which may result in reducing the amplitude of the noise one wishes to eliminate, but without removing it entirely as in the theoretical response. In practice, however, filters can be applied at time intervals - possibly at every time steps - in atmospheric models. The repeated application of a less-expensive filter using a narrow stencil, which only damps without suppressing entirely undesired noise, can be as efficient and effective as a more accurate but expensive filter using a wide stencil.

We proceed to illustrate the effect of repeated application of a filter. We recall that the third filter (using $b_3$) was designed such as to remove entirely the noise in the third test function $\psi_3$ characterised by very short-scale noise with wavenumber $k_{n_3}$, but to only attenuate the larger scale noise of $\psi_1$ and $\psi_2$; in fact this filter had very weak damping effect on the noise of $\psi_1$. Figure 1.6a shows the response of the repeated application of the filter. The small-scale noise of the test function $\psi_2$ with wavenumber $k_{n_2}$ is essentially eliminated after 10 applications. For the test function $\psi_1$, the noise with wavenumber $k_{n_1}$ still remains even after 40 applications, and we also note a small attenuation of the large-scale signal (at wavenumber $a$) caused by the repeated applications of the filter. The variation of the *NRMS* for the noise component as a function of the number of applications of the filter to $\psi_1$ and $\psi_2$ is shown in Fig. 1.6b. Figure 1.7 shows the results on test function $\psi_2$ after 4 and 10 applications (Fig. 1.7a,b), and on test function $\psi_1$ after 4 and 40 applications. As expected this particular choice of compact filter is more effective at damping short-scale noise than larger scale one; but repeated application of the filter succeeds at reducing substantially even larger scale noise.

### 1.3.2 Application of the convolution filter into a 1D stretched-grid

The application of the convolution filter for a variable resolution domain is tested considering a periodic 1D stretched grid. The domain $[0,2\pi]$ is divided into four main zones: a uniform fine-resolution zone with grid mesh $\Delta x_{\min}$ located in the centre of the domain, bordered by two stretching zones where the resolution is gradually degraded, and completed by a uniform low-resolution zone with grid mesh $\Delta x_{\max}$, as represented in Fig. 1.8. Such configuration is typical of the varying resolution around a latitude circle in the region outside the uniform high-resolution area of the domain, as indicated for example by the line segment A-A' in Fig. 1.1, which slices through "the arms of the cross" region in the latitude-longitude grid.

One purpose of the 1D stretched-grid tests will be to verify the ability of the general convolution filter to actually render uniform-resolution fields despite the varying grid mesh. If effective, such filter could be used in 2D to remove the anisotropy of the grid in the "arms of the cross" region of the grid. The test functions used for the following 1D stretched-grid tests are in the form analogous to (1.11) that was used for the uniform resolution, but here the noise amplitude is chosen to be zero in the *LR* part of the domain, gradually increased in the *SG* areas, and is maximum in the *HR* area that is here taken to represent the anisotropic-grid "arms of the cross" region of a 2D domain. Two grid designs will be used in the following experiments (see Table 1.1). We mention in passing that for both grids, the number of grid points located in the uniform high-resolution area represents 60 - 64 % from the total number of grid points, even if the area represents only 1/3 from the entire domain.

In the following tests we will interpret the high-resolution part of the 1D grid as corresponding to the anisotropic arm-of-the-cross region of a 2D grid; the convolution will be applied with the aim of filtering some small-scale noise that a user may want to remove outside the uniform high-resolution zone. Therefore, in our

1D variable-domain, the filter will be designed to render quasi-uniform resolution fields by removing scales with wavelengths shorter than twice the maximum grid mesh in the domain; consequently the parameter $a$ in the weighting function, which controls the largest wavenumber retained on the entire grid, is chosen as $a = \frac{2\pi}{2\Delta x_{\max}}$. Various values of the parameters $b$ and $d_{\max}$ will be tested and results will be presented through examples of filtered functions and *NRMS* and *NCR* statistics for the two stretched grids mentioned above.

A first example is shown for grid SG2 in Figure 1.9. In this case, the test function contained a noise with wavenumber $k_n = \frac{2\pi}{4\Delta x_{\min}}$. A convolution filter $w_1$ was chosen to completely remove the smallest resolved scale in the high-resolution region, using parameter $b = 1.5a$, hence $k_n < b$. Figure 1.9 shows the result obtained with a truncation distance $d_{\max} = 5\Delta x_{\max}$ for the weighting function. We see that the goal is reached: the short-scale noise is completely removed and the large-scale signal perfectly maintained.

We study the effects of different stretching rates by running tests on two variable-resolution grids, SG1 and SG2, that have the same total stretching factor ($S \cong 4$), but the stretching rate of SG1 is 3 times larger than that of SG2. We will use the same test function as in the previous case, and use two convolution filters aiming at removing entirely small-scale noise, with weighting functions $w_1$ ($a = \frac{2\pi}{2\Delta x_{\max}}$; $b = 1.5a$) and $w_2$ ($a = \frac{2\pi}{2\Delta x_{\max}}$; $b = 2a$). The *NRMS* scores are shown in Fig. 1.10a. It is seen that the noise is completely removed if an adequate truncation distance is used; this distance is shorter for the filter with the more gradual response ($w_2$). There appears to be little impact of the stretching rate on the *NRMS* score. For the *NCR* score (Fig. 1.10b), we note that better conservation is obtained with the filter

with the more gradual response ($w_2$) and on the grid with smaller stretching rate (SG2).

As mentioned before, a large truncation distance permits one to completely remove scales smaller than $b$ and maintain conservation, but wide stencils come with increased computational costs. For this reason it may be preferable to use convolution filters using weighting function with a narrow stencils, even if such filters remove only a fraction of the noise at every application.

For the next experiment we use the same test function and stretched grids, and apply two convolution filters with theoretical response corresponding to removing only a fraction of the noise at every application, with weighting functions $w_3$ ($a = \frac{2\pi}{2\Delta x_{\max}}; b = 3a$) and $w_4$ ($a = \frac{2\pi}{2\Delta x_{\max}}; b = 3.5a$) corresponding to stronger and weaker filtering of the shorter scales, respectively. The truncation distance used for these applications was $6\Delta x_{\min}$ for $w_3$ and $4\Delta x_{\min}$ for $w_4$. Figure 1.11a shows that the *NRMS* score initially decreases as a function of the truncation distance but, after a certain truncation distance, it becomes constant but not zero, meaning that a part of the noise is still present; increasing the truncation distance will not improve the score because the response of the filter then reproduces exactly the theoretical response corresponding to removing only a fraction of the noise. To remove completely the noise using such weighting functions, the filter must be repeatedly applied. Figure 1.11b shows the *NRMS* score with repeating the application of the filter; for these tests, we chose the truncation distance for which the *NRMS* was nearly constant, indicated by the dot in Fig. 1.11a. We can see that just after few applications the *NRMS* is almost zero. We note, however, a slight but systematic attenuation of the largest scales with several applications of the filter; this shows in Fig. 1.11b as a non-zero value of *NRMS* and in Fig. 1.11c as a linear increase of *NCR* for repeated

applications. The mass non-conservation is particularly pronounced for the grid with the larger stretching rate (SG1) and for the less scale-selective filter ($w_4$).

We next illustrate the results of the convolution filter on SG2 using the same test function that was used in Fig. 1.9, with a noise characterised by wavenumber $k_n = \frac{2\pi}{2\Delta x_{\min}}$. In Fig. 1.12 the blue and red lines represent the initial and the filtered functions, respectively. The left column shows results for the weighting function $w_3$ ($a = \frac{2\pi}{2\Delta x_{\max}}; b = 3a$) with a truncation distance $d_{\max} = 8\Delta x_{\min}$, and the right column for $w_4$ ($a = \frac{2\pi}{2\Delta x_{\max}}; b = 3.5a$) with a truncation distance $d_{\max} = 6\Delta x_{\min}$; the first row shows results after one application of the filter, and the second row after four applications. After one application of the $w_3$ filter, the amplitude of the noise is reduced by 52%, and after four applications only 5% of the noise remains. For comparison, after one application of the $w_4$ filter, 36% of the noise is removed, and after four applications 17% of the noise is still present.

A general filtering technique applied on a variable-resolution domain must be able to remove at the same time any noise that may result from the anisotropy in the stretching zones, but also the computational noise characteristic of any numerical model. We next consider a test function composed from three harmonics. The first one represents a large-scale signal to be preserved under filtering. The second harmonic represents a computational noise, present anywhere on the grid. The third one represents another noise that may be resulting from the stretching of the grid; we will introduce it only in the stretching region and the high-resolution area that we will interpret here as corresponding to the anisotropic arm-of-the-cross region of a 2D grid. We used the following test function:

$$\psi(x_i) = A_l \cos(k_l x_i) + A_{n_l} \cos(k_{n_l} x_i) + A_{n_h} \cos(k_{n_h} x_i),$$

where $A_l$, $A_{n_l}$ and $A_{n_h}$ are arbitrary amplitudes, and $k_l$, $k_{n_l}$ and $k_{n_h}$ are the wavenumbers of the large-scale signal and of the two types of noises.

For the test shown in Fig. 1.13, we used the values $k_l = 2\dfrac{2\pi}{256\Delta x_{\max}} = \dfrac{2\pi}{128\Delta x_{\max}}$, $k_{n_1} = \dfrac{2\pi}{4\Delta x_{\max}}$ and $k_{n_2} = \dfrac{2\pi}{4\Delta x_{\min}}$, and a convolution filter with a weighting function $w_5$ with parameters ($a = \dfrac{2\pi}{8\Delta x_{\max}}$; $b = 1.5a$) and a truncation distance of $8\Delta x_{\max}$. Using appropriate weighting function and truncation distance, the filter is able to eliminate both noises, as we see in Fig. 1.13.

The ability of the convolution filter to remove noises everywhere on a stretched-grid emphasizes the definition of the weighting function independently of the computational mesh. To highlight this property we use the same test function as in Fig.1.13 but with $A_{n_h} = 0$ and $k_{n_1} = \dfrac{2\pi}{2\Delta x_{\max}}$. To remove this noise the convolution filter uses a weighting function $w_6$ with parameters ($a = \dfrac{2\pi}{8\Delta x_{\max}}$; $b = 2.5a$) and a truncation distance of $6\Delta x_{\max}$. Figure 1.14a shows the initial and the filtered functions; it can be seen that the noise is completely removed everywhere, including in the low-resolution, in the high-resolution, and in the stretched zones of the domain. Next, we apply the Shapiro filter to the same test function; as can be seen in Fig. 1.14b the noise is completely removed only in the low-resolution zone, and it is only attenuated in the high-resolution and the stretched zones. The amount by which the noise is attenuated or removed corresponds to $R(L) = 1 - \sin^2(\pi\Delta x/L)$ where $L = 2\Delta x_{\max} \cong 8\Delta x_{\min}$; because the response depends on the computational grid-point distance, we conclude that the Shapiro operator is not really appropriate for a variable mesh.

For all tests performed on 1D stretched grids, the convolution filter worked appropriately. With suitable parameter choices, the noise is removed in regions chosen by the user (such as in the stretching zones and/or over the entire domain), the total mass is relatively well conserved, and there is little attenuation of the initial signal. In practice the choice of the weighting function and truncation distance must be made as a compromise between the cost of the application and the precision of the filter.

### 1.3.3 Application of the convolution filter into a 2D Cartesian stretched-grid

The formal approach developed in 1D is generalized for two-dimensional domains. The two-dimensional convolution uses a weighting function that is the product of two one-dimensional functions, similar with those used in one-dimensional case. The approximation of a 2D convolution using a sequence of 1D convolutions requires reduced computations while producing equally valid analyses when compared with those of the 2D filter scheme, as shown by Thatcher and McGregor (2009) who used this approach in the context of a scale-selective filter for dynamical downscaling.

Considering a signal $\psi(x,y)$, the filtered value $\overline{\psi}(x,y)$ is:

$$
\begin{aligned}
\overline{\psi}(x,y) &= (\psi * w)(x,y) \\
&= \int_{-\infty}^{\infty}\int_{-\infty}^{\infty} \psi(s,t)\, w(x-s, y-t)\, ds\, dt \\
&= \int_{-\infty}^{\infty}\left(\int_{-\infty}^{\infty} \psi(s,t)\, w_{1D}(x-s)\, ds\right) w_{1D}(y-t)\, dt, \\
&= \int_{-\infty}^{\infty} \left(\psi * w_{1D}\right)(x,t)\, w_{1D}(y-t)\, dt \\
&= \left(\left(\psi * w_{1D}\right) * w_{1D}\right)(x,y)
\end{aligned}
\tag{1.12}
$$

where $w(x,y) = w_{1D}(x)\, w_{1D}(y)$ with $w_{1D}$ representing the same 1D function as in Eq. (1.6). In practice, the 2D filtered function will be obtained conveniently by successive applications of 1D filter in each direction. The weighting function is symmetrical with respect to $x$ and $y$ directions, and also with respect to any line that passes through an application point.

The convolution is expressed as a quadrature for a grid point in the stretched domain as follows:

$$
\overline{\psi}(x_i, y_j) = \frac{\sum_{\substack{k \\ d_{i,k} \le d_{\max}}} \sum_{\substack{l \\ d_{j,l} \le d_{\max}}} \psi(x_k, y_l)\, w(d_{j,l})\, w(d_{i,k})\, \sigma(x_k)\, \sigma(y_l)}{\sum_{\substack{k \\ d_{i,k} \le d_{\max}}} \sum_{\substack{l \\ d_{j,l} \le d_{\max}}} w(d_{j,l})\, w(d_{i,k})\, \sigma(x_k)\, \sigma(y_l)}, \tag{1.13}
$$

where $d_{i,k}$, $d_{j,l}$, $\sigma(x_k)$ and $\sigma(y_l)$ have the same meaning as in Eq. (1.7). It is important to reiterate that in our proposed convolution filter approach, the weights are calculated using physical distances rather than grid-point indices. In practice the width of the weighting function stencil is truncated to a finite distance from the application point when the distance in $x$ or $y$ direction exceeds the maximum prescribed distance $d_{\max}$; this results in an approximately isotropic 2D weighting function.

A 2D stretched-grid was built following a similar approach as for the 1D grid. In the centre of the mesh is the uniform high-resolution area and, outside of this zone, the grid spacing increases in both directions as a geometric progression with a constant stretching factor of 7.2% until a maximum grid spacing is attained. We chose a total stretching factor $S \approx 4$ in $x$ and $y$ directions, similar to the SG1 previously used in the one-dimension tests.

The purpose of our simplified 2D tests with the convolution filter will be to remove the small scales outside the uniform high-resolution core region of the domain, thus correcting for the anisotropy of a test-function field in the arms-of-the-cross and stretching areas where the resolution varies with direction or the resolution is not uniform.

Similarly to our tests in 1D, we define a test function using 2D sinusoidal waveforms. One will represent a large-scale signal $\psi_l(x,y)$ that will be represented on the entire grid and that we wish to retain with the filter. The second waveform will be a small-scale component $\psi_n(x,y)$ that will be present in the uniform high-resolution region where it will represent a fine-scale signal we wish to be retained with the application of the filter; the small-scale component will also be progressively added in the stretching regions, where it will be considered as noise that the filter should remove. The test-function will be represented as

$$\psi(x,y) = \psi_l(x,y) + \psi_n(x,y) \ ,$$

or for grid-point representation:

$$\psi(x_i,y_j) = A_l \cos(k_l x_i) \cos(l_l y_j) + A_n \cos(k_n x_i) \cos(l_n y_j),$$

where $A_l$ and $A_n$ are arbitrarily amplitudes, and ($k_l$, $l_l$) and ($k_n$, $l_n$) are the large-scale and small-scale wavenumbers in $x$ and $y$ directions, respectively. The tests were

performed on a grid with a total stretching factor $S \approx 4$ in $x$ and $y$ directions, similar to SG1 previously used in one dimension. The initial field is presented in the upper panel of Fig. 1.15.

The middle row presents the results using a filter with the weighting function $w_1$ with parameters $(a = \frac{2\pi}{2\Delta x_{\max}}; b = 1.5a)$ and a truncation distance of $d_{\max} = 10\Delta x_{\min}$ (left panel) and $d_{\max} = 21\Delta x_{\min}$ (right panel). We note that the filter successfully removes completely the "noise" when using a large enough truncation distance, and there are no visible deformations of the signal at the borders of the uniform high-resolution area.

The lower row presents the results using a less scale-selective filter with a weighting function $w_3$ with parameters $(a = \frac{2\pi}{2\Delta x_{\max}}; b = 3a)$ with a truncation distance of $d_{\max} = 10\Delta x_{\min}$. The left panel shows the result after one application of the filter, and the right panel after six applications of the filter. The broad spectral response of this filter allows the use of a narrower stencil for the weighting function, but the filter only damps the noise without suppressing it entirely; however, repeated applications of the filter can effectively remove the noise.

## 1.4 Conclusion

We described a filtering approach based on the convolution operator that can be applied effectively on stretched grids. The filter can be effective to remove unwanted small scales outside the uniform high-resolution area of the global variable-resolution domain. This approach can be used to render quasi-isotropic fields on variable-resolution grids. The weighting function in the convolution can simply be calculated as the inverse Fourier transform of the spectral response desired for the filter. A key element of the approach is that the weights are based on the physical distance between grid points rather than grid-point indices; it is this feature that makes this approach attractive for use on variable-resolution grids. The method has here been tested in 1D periodic domain and 2D Cartesian mesh, on uniform as well as variable-resolution stretched grids.

In the first part of the paper, we presented the mathematical formulation for the convolution filter and an analysis of the weighting function for a uniform periodic one-dimensional domain. We noted that the design of a convolution filter with a sharp cut-off spectral response requires a large number of grid points in the weighting function in order to reproduce the desired response, but such filter incurs a high computational cost. Truncating the weighting function after some distance can save on computational cost, but the resulting filter only reproduces approximately the desired spectral response, and in general only results in an attenuation of the small scales one wishes to filter. Multiple applications of such approximate filter can be a pragmatic compromise. We showed that in the simplified context of periodic domain, sinusoidal fields, large truncation distance for the weighting function, the convolution filter conserves perfectly the mass, the noise is removed and the large-scale signal is completely preserved.

The second part of the paper was dedicated to the adaptation of the convolution filter for 1D variable-resolution grids. Because the weighting function in the proposed convolution filter depends on the physical distance rather than grid-point indices, we showed that the response of the filter is almost independent of the stretching of the underlying computational mesh. The only repercussion of the changing resolution is computational: if the application point is located in a high-resolution area, the number of grid points participating in the quadrature is large.

The experiments performed on test-functions represented by single harmonics on the one- and two-dimensional periodic stretched-grid have shown that the proposed convolution filter can effectively remove completely the small-scale noise while conserving the large-scale signal.

In summary, the proposed approach appears to be a valuable alternative to conventional grid-point based smoothing operator for stretched-grid models. In forthcoming papers, we will expand the present Cartesian-geometry scalar formulation to polar geometry and vectors. The convolution filter approach developed for 1D variable grid and generalized to two-dimensional Cartesian geometry will be adapted for polar geometry as an intermediated step towards spherical latitude-longitude grid. On the polar grid, the convolution filter will be used not only in the stretching area but also near the poles. As in the present study, we chose for simplicity and efficiency a filter formulation obtained by the separate application of the convolution in radial and azimuthal directions, but preserving the paramount concept of physical distance. Because the number of grid points for a given physical distance in the azimuthal direction varies with radial distances, it will be important to apply first the convolution in azimuthal direction, followed by the application of the convolution in radial direction.

*Acknowledgments.*

This research was done as part of the Doctoral project of the first author and as a project within the Canadian Regional Climate Modelling and Diagnostics (CRCMD) Network, funded by the Canadian Foundation for Climate and Atmospheric Sciences (CFCAS), the Ouranos Consortium for Regional Climatology and Adaptation to Climate Change, and National Centre of Excellence (NCE) Mathematics of Information Technology and Complex Systems (MITACS). Ouranos also provided office space during a large part of this work.

# References

Bender, C.M., and S.A. Orszag, 1978: *Advanced mathematical methods for scientists and engineers.* McGraw-Hill International Series in Pure and Applied Mathematics, 593 pp.

Bracewell, R. N., 2000: *The Fourier transform and its applications.* McGraw-Hill International Editions, third edition, 640 pp.

Caian, M., and J.-F. Geleyn, 1997: Some limits to the variable mesh solution and comparison with the nested-LAM solution. *Quart. J.Roy. Meteor. Soc.,* **123,** 743–766.

Côté, J., S. Gravel, A. Méthot, A. Patoine, M. Roch, and A. Staniforth, 1997: Preliminary results from a dry global variable-resolution primitive equations model. *Numerical methods in Atmospheric and Oceanic Modelling: The André J. Robert Memorial Volume*, edited by C. Lin, R. Laprise and H. Richie, 245-259, CMOS, Ottawa, Canada.

Côté, J., S. Gravel, A. Méthot, A. Patoine, M. Roch, and A. Staniforth, 1998: The operational CMC-MRB Global Environmental Multiscale (GEM) Model. Part I : Design considerations and formulation. *Mon. Wea. Rev.*, **126**, 1373-1395.

Courtier, P., and J.-F. Geleyn, 1988: A global numerical weather prediction model with variable resolution: Application to the shallow-water equations. *Quart. J. Roy. Meteor. Soc.,* **114,** 1321– 1346.

Déqué, M., and J. P. Piedelièvre, 1995: High resolution climate simulation over Europe. *Climate Dyn.*, **11**, 321-339.

Fox-Rabinovitz, M., L. Stenchikov, M. Suarez, and L. Takacs, 1997: A finite-difference GCM dynamical core with a variable-resolution stretched grid. *Mon. Wea. Rev.*, **125**, 2943-2968.

Fox-Rabinovitz, M.S., E. H. Berbery, L. Takacs, and R. C. Govindaraju, 2005: A multiyear ensemble simulation of the U.S climate with a stretched-grid general circulation model. *Mon. Wea. Rev.*, **133**, 2505-2525.

Fox-Rabinovitz, M., J. Côté, B. Dugas, M. Déqué, and J.L. McGregor, 2006: Variable resolution general circulation models: Stretched-grid model

intercomparison project (SGMIP). *J. Geophys. Res.*, **111**, D16104, doi:10.1029/2005JD006520.

Fox-Rabinovitz, M., J. Coté, B. Dugas, M. Déqué, J.L. McGregor, and A. Belochitski, 2008: Stretched-grid Model Intercomparison Project: decadal regional climate simulations with enhanced variable and uniform-resolution GCMs. *Meteor. Atmos. Phys.*, **100**, 159-177.

Gibelin A. L., and M. Déqué, 2003: Anthropogenic climate change over the Mediterranean region simulated by a global variable resolution model. *Clim. Dyn.* **20,**327-339.

Laprise R., 2008: Regional climate modelling. *J. Comput. Phys.*, **227**, 3641-3666.

McGregor J.L., K.C. Nguyen, and J.J. Katzfey, 2002: Regional climate simulations using a stretched-grid global model. Research Activities in Atmospheric and Oceanic Modelling, Report 32 WMO/TD- No. 1105, 3.15-16.

Schmidt, F., 1977: Variable fine mesh in the spectral global models. *Beitr. Phys. Atmos.*, **50,** 211–217.

Shapiro, R., 1970: Smoothing, filtering and boundary effects. *Rev. Geophys. Space Phys.*, **8**, 359-387.

Surcel, D., 2005: Filtres universels pour les modèles numériques à résolution variable. Mémoire de maîtrise en Sciences de l'atmosphère, Université du Québec à Montréal. 104 pp.

Takacs, L., W. Sawyer, M. J. Suarez, and M. S. Fox-Rabinovitz, 1999: Filtering techniques on a stretched grid General Circulation Model. *NASA Tech. Memo. 104606*, Vol. 16, 45 pp. [Available from Data Assimilation Office, NASA GSFC, Greenbelt, MD 20771].

Thatcher M., and J. L. McGregor, 2009: Using a scale-selective filter for dynamical downscaling with the Conformal Cubic Atmospheric Model. *Mon. Wea. Rev.*, **137**, 1742-1752.

Yessad K., and P. Bénard, 1996: Introduction of a local mapping factor in the spectral part of the Meteo-France global variable mesh numerical weather forecast model. *Quart. J. Roy. Meteorol. Soc.*, **122**, 1701-1719.

Zadra, A., D. Caya, J. Côté, B. Dugas, C. Jones, R. Laprise, K. Winger, and L.-P. Caron, 2008: The next Canadian Regional Climate Model. *Physics in Canada,* **64**, 75-83.

Table 1.1 Parameters of 1D stretched-grids used to verify the performance of the convolution filter.

| | *High-resolution zone* | *Stretched-grid zones* | *Local stretching factor «s»* | *Total stretching factor «S»* |
|---|---|---|---|---|
| SG 1 | $\left[\frac{2\pi}{3},\frac{4\pi}{3}\right]$ | $\left[\frac{7\pi}{12},\frac{2\pi}{3}\right]\cup\left[\frac{4\pi}{3},\frac{17\pi}{12}\right]$ | 7.2% | 4 |
| SG 2 | $\left[\frac{2\pi}{3},\frac{4\pi}{3}\right]$ | $\left[\frac{5\pi}{12},\frac{2\pi}{3}\right]\cup\left[\frac{4\pi}{3},\frac{19\pi}{12}\right]$ | 2.4% | 4 |

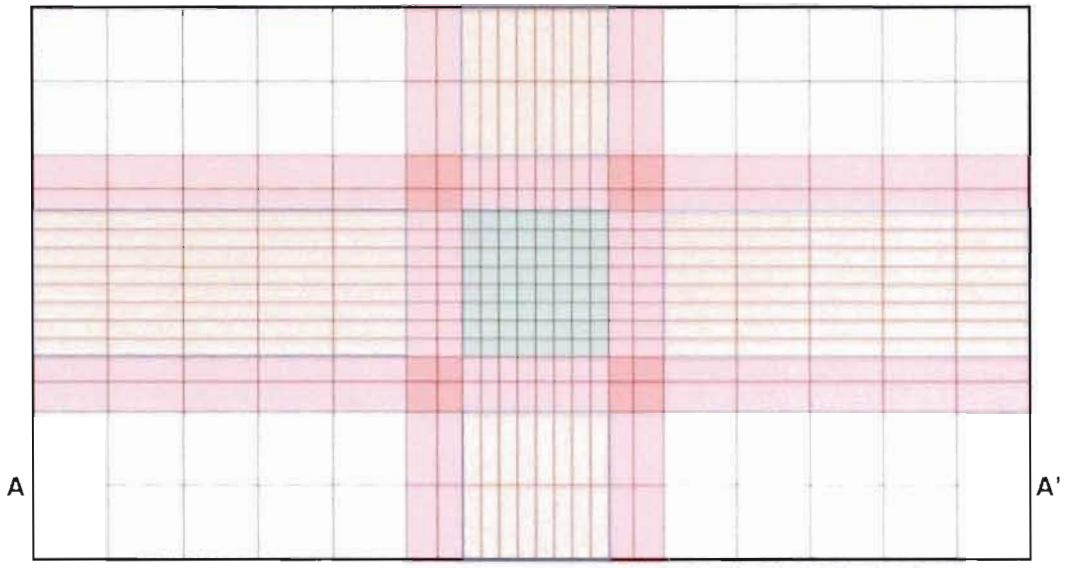


Figure 1.1 Simplified sketch showing a typical latitude-longitude stretched grid. The uniform *HR* core region of the domain is shown in green; the *SG* is shown in pink; the anisotropic "arms of the cross" regions are shown in orange, and the uniform *LR* region is shown in white. The line A-A' will be referred to subsequently in 1D variable-grid tests.

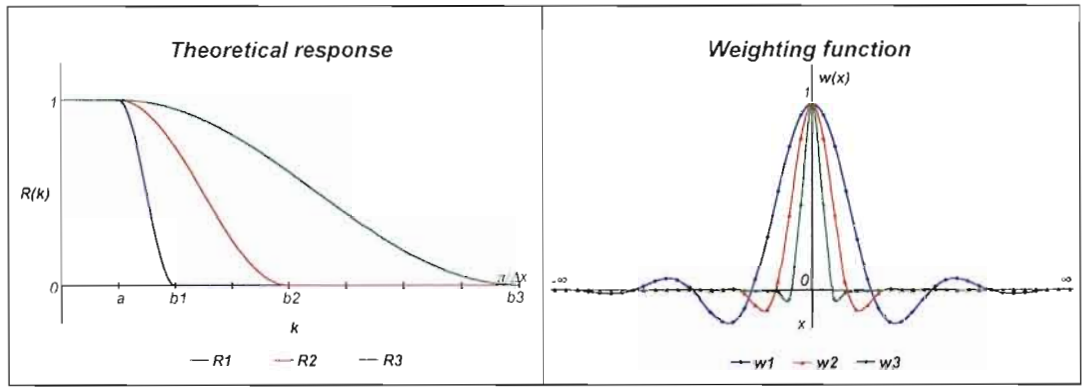


Figure 1.2 (left) Examples of three different spectral responses as a function of wavenumber and (right) corresponding weighting functions as a function of distance; the weighting functions are normalized by their maximum value.

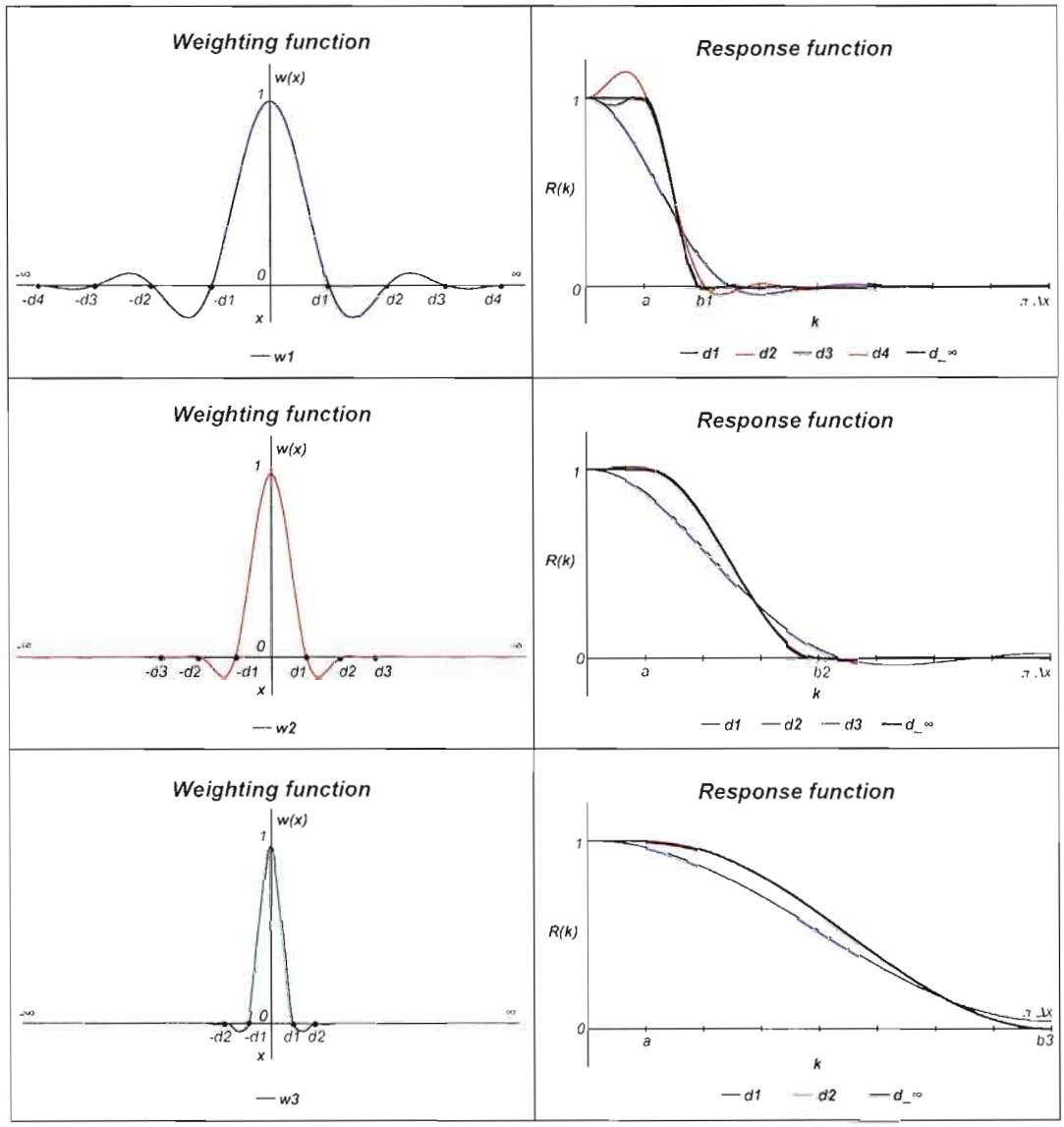


Figure 1.3 (left) The three weighting functions represented in Fig. 1.2 with the location of various arbitrary truncation distances noted $d_1$ to $d_4$. (right) The corresponding spectral responses obtained after the application of the convolution filter with the truncated weighting functions; the exact responses are the curves in black labelled $d_\infty$.

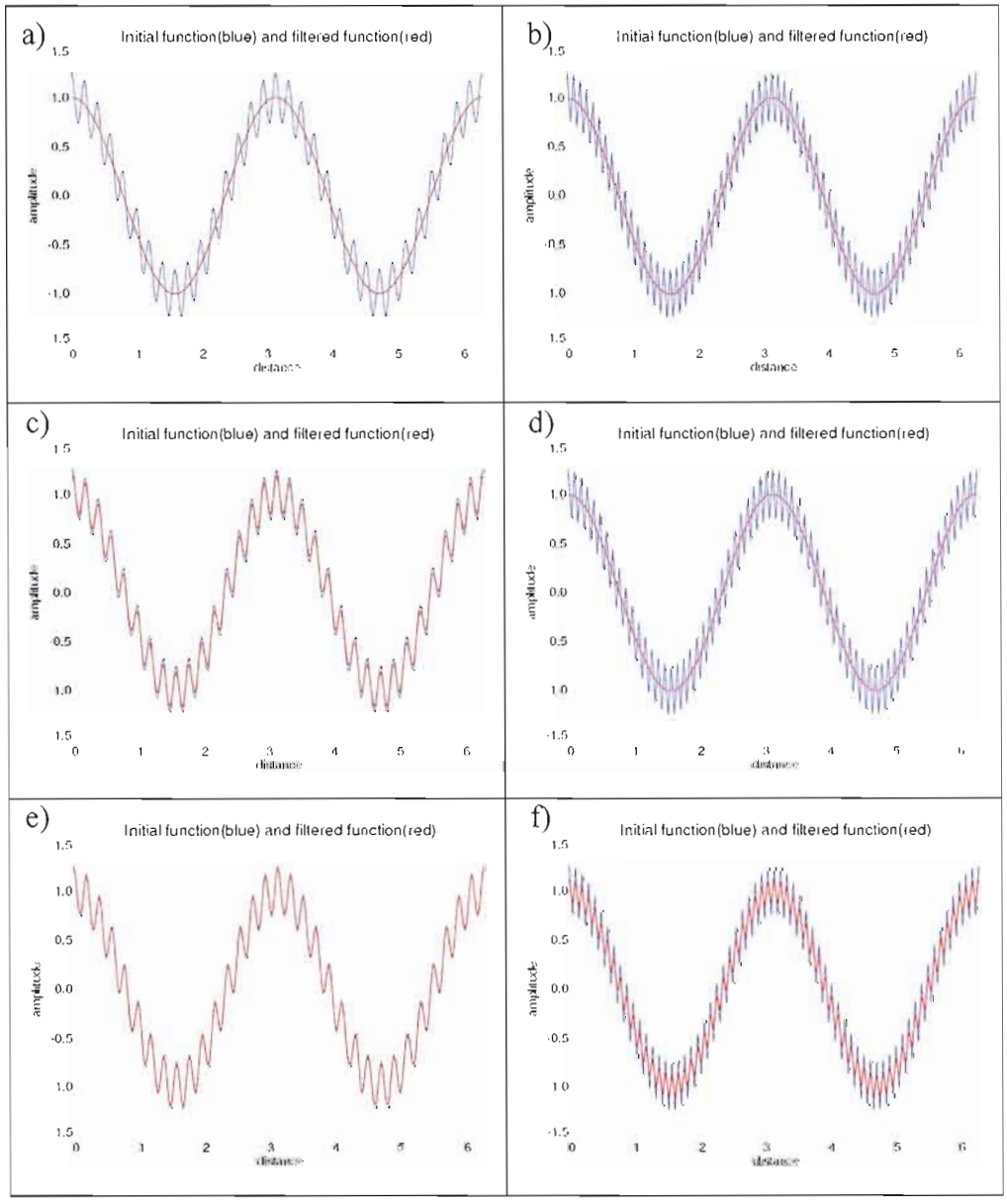


Figure 1.4 The test functions (left) $\psi_1$ and (right) $\psi_2$ in blue and the filtered fields in red. (a),(b) The filter used the weighting function $w_1$ and a truncation distance of $21\Delta x$; (c),(d) the filter used the weighting function $w_2$ and a truncation distance of $10\Delta x$; and (e),(f) the filter used the weighting function $w_3$ and a truncation distance of $4\Delta x$.

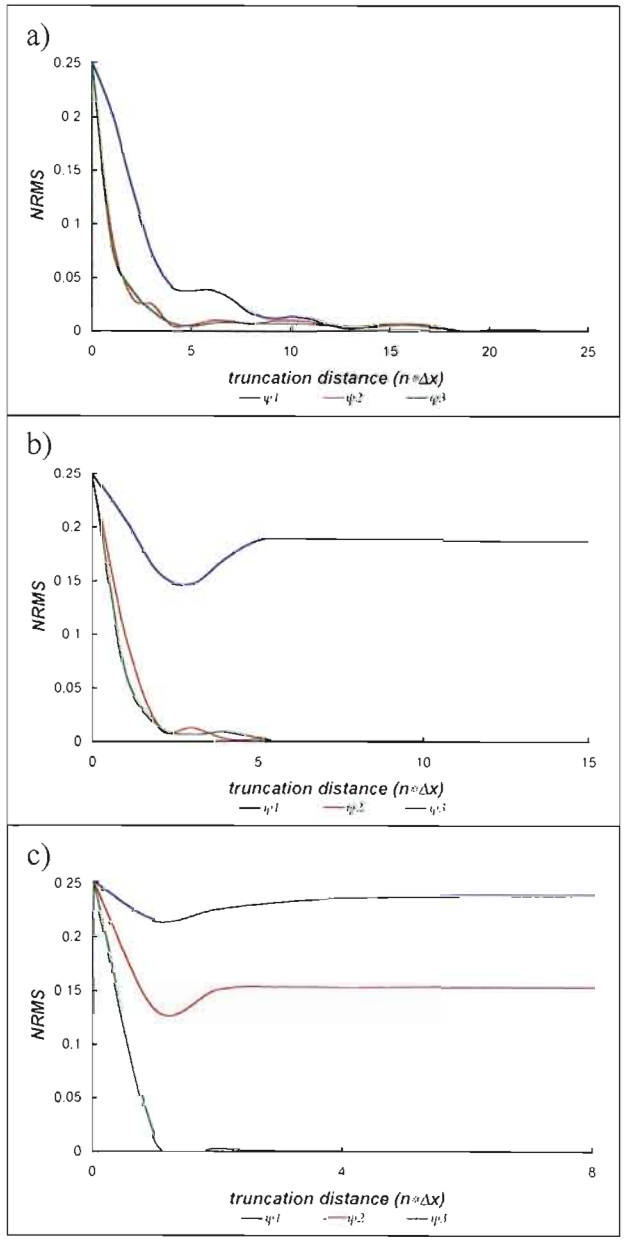


Figure 1.5 Variation of the *NRMS* scores as a function of the truncation distance, for the test functions $\psi_1$, $\psi_2$ and $\psi_3$, using the weighting functions (a) $w_1$, (b) $w_2$, and (c) $w_3$.

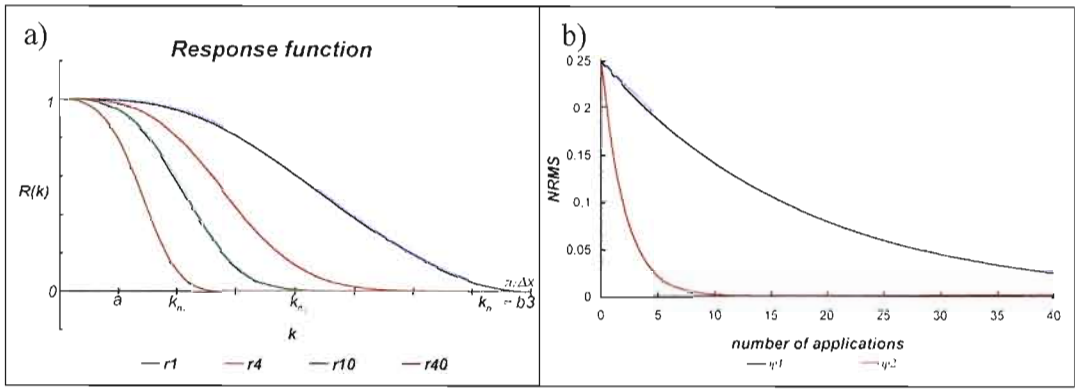


Figure 1.6 (a) Spectral response after 1, 4, 10 or 40 applications of the convolution filter using weighting function $w_3$. The wavenumbers corresponding to the test functions $\psi_1$, $\psi_2$ and $\psi_3$ are indicated on the horizontal axis. (b) The *NRMS* score as a function of the number of applications of the convolution filter using weighting function $w_3$ on the test functions $\psi_1$ and $\psi_2$.

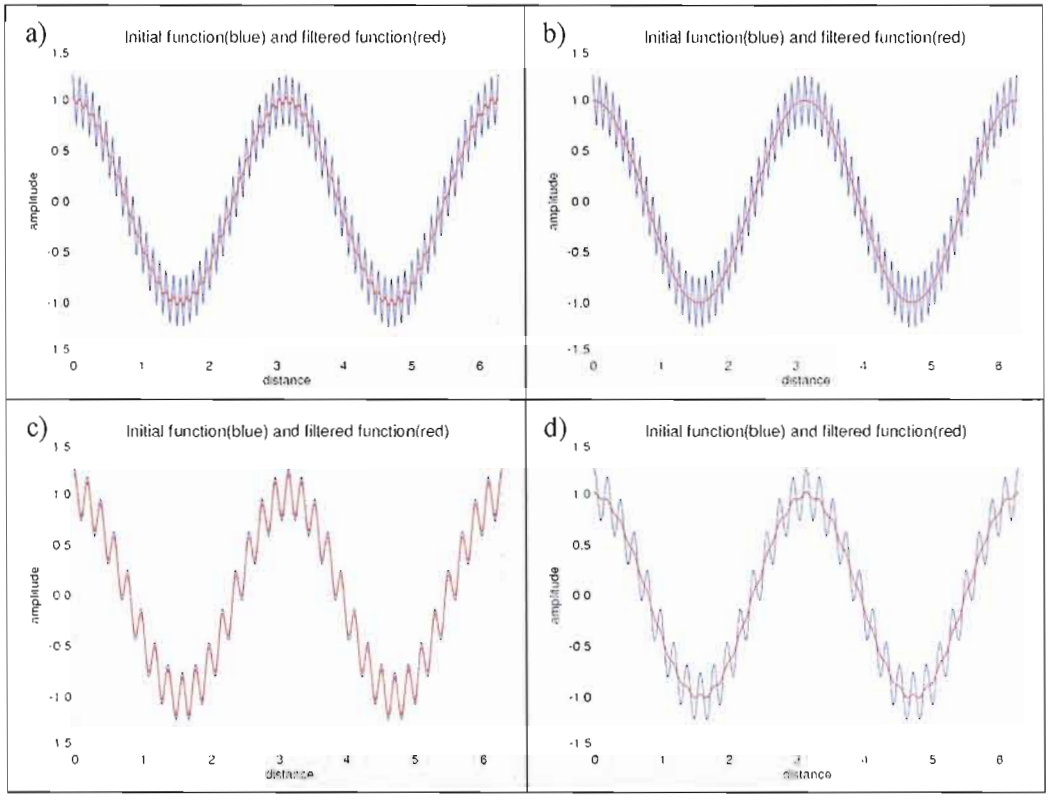


Figure 1.7 (top) The initial test function $\psi_2$ (blue) and the filtered field (red) after (a) 4 and (b) 10 applications of the convolution filter with weighting function $w_3$ and truncation distance is $d_{\max} = 4\Delta x_{\min}$. (bottom) The corresponding results for test function $\psi_1$ after (c) 4 and (d) 10 applications of the same convolution filter.

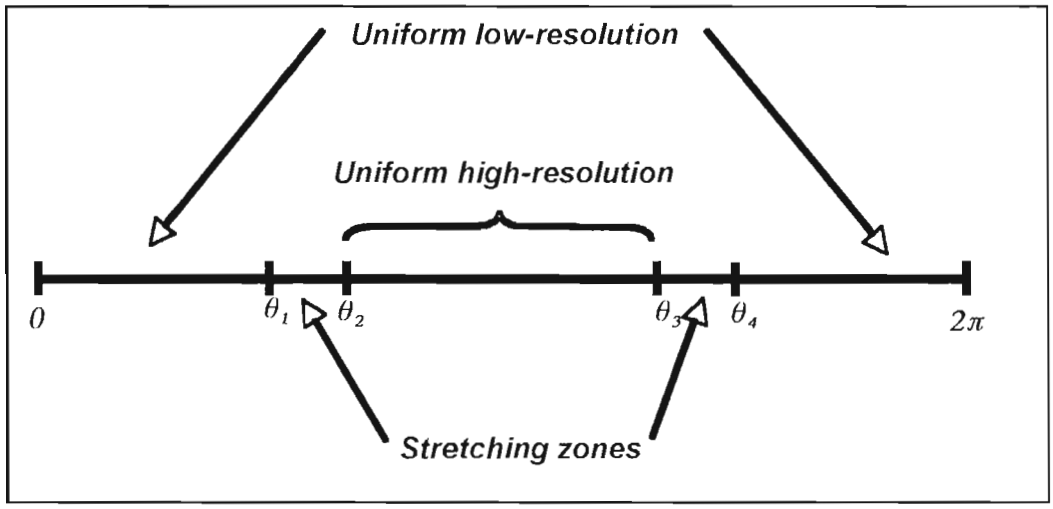


Figure 1.8 General configuration of 1D stretched grid.

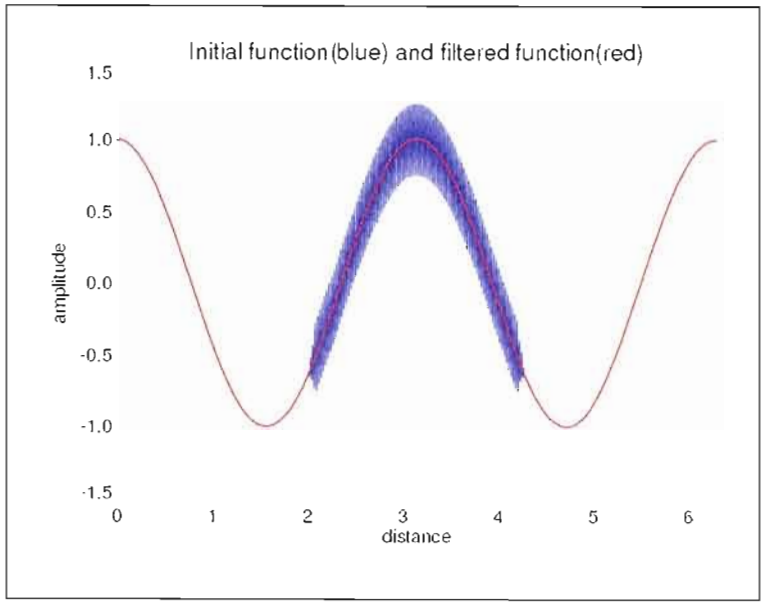


Figure 1.9 The initial test function (blue) and the filtered field (red) on the SG2 grid with $S \cong 4$. For the convolution, the weighting function used parameters $a = \frac{2\pi}{2\Delta x_{\max}}$ and $b = 1.5a$, and a truncation distance $d_{\max} = 5\Delta x_{\max}$; the noise in the test function had a wavenumber of $k_n = \frac{2\pi}{4\Delta x_{\min}}$.

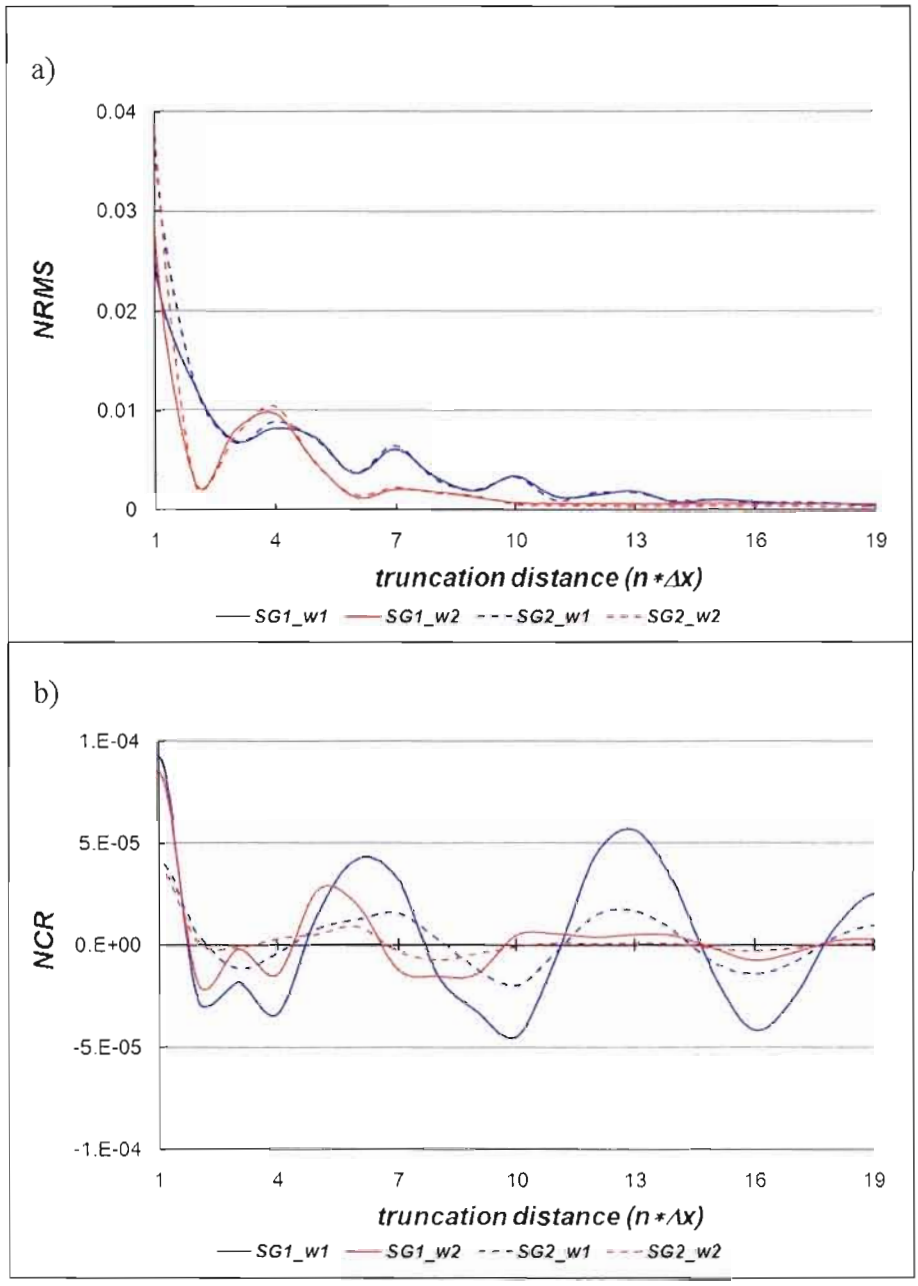


Figure 1.10 The (a) *NRMS* and the (b) *NCR* scores as a function of the truncation distance, for two convolution filters with weighting functions $w_1(a=\frac{2\pi}{2\Delta x_{\max}}; b=1.5a)$ and $w_2(a=\frac{2\pi}{2\Delta x_{\max}}; b=2a)$, applied on SG1 and SG2 stretched grids.

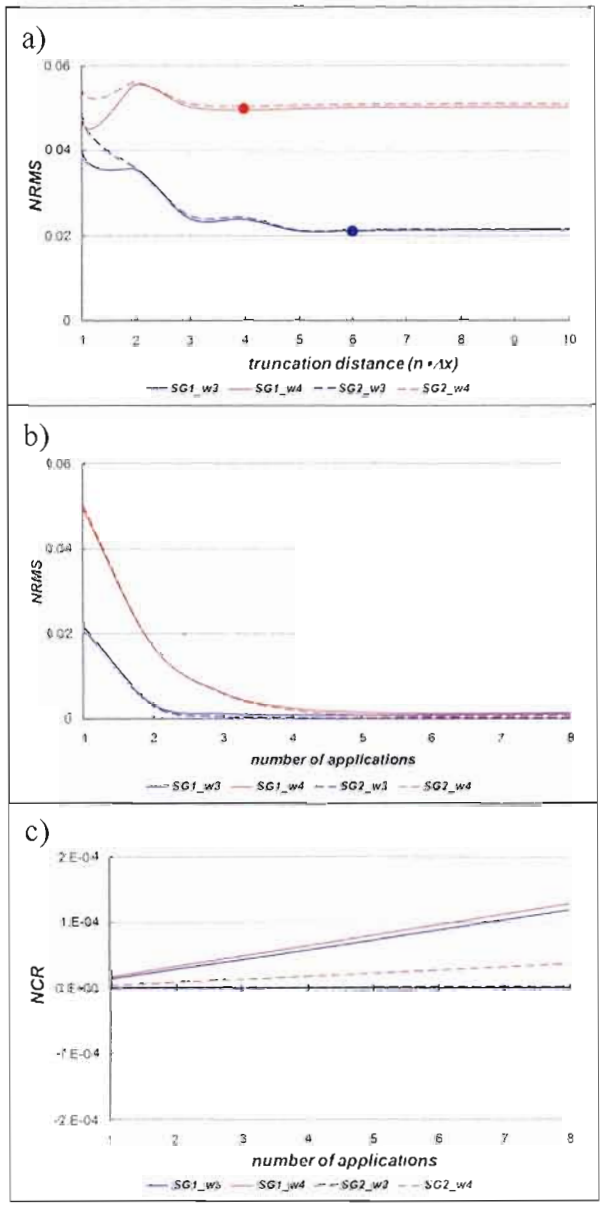


Figure 1.11 (a) The *NRMS* score as a function of the truncation distance, for two convolution filters with weighting functions $w_3(a=\frac{2\pi}{2\Delta x_{\max}}; b=3a)$ and $w_4(a=\frac{2\pi}{2\Delta x_{\max}}; b=3.5a)$, applied on SG1 and SG2 stretched grids. (b) The *NRMS* score as a function of the number of application of convolution filters with weighting functions $w_3$ with a truncation distance of $6\Delta x_{\min}$ and $w_4$ with a truncation distance of $4\Delta x_{\min}$. (c) As in (b), for the *NCR* score.

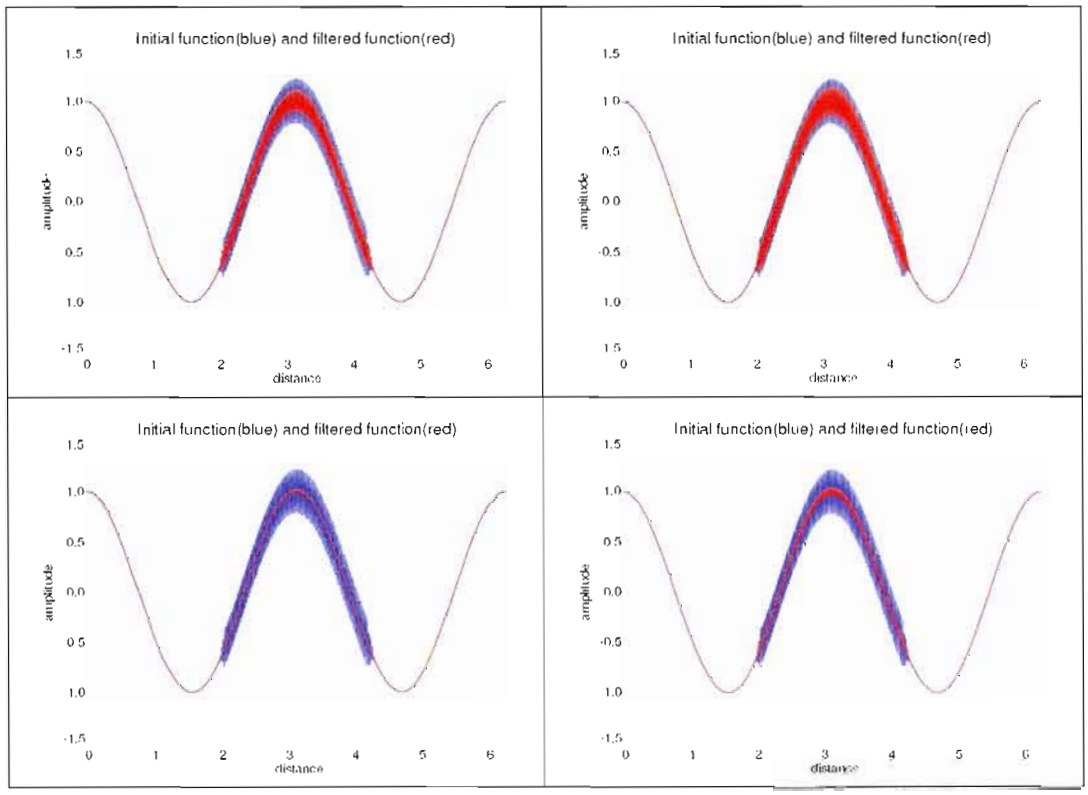


Figure 1.12 The initial test function (blue) with noise of wavenumber $k_n = \frac{2\pi}{4\Delta x_{\min}}$ on the SG2 grid, and the filtered field (red) after 1 (first row) and 4 applications (second row) of the convolution filter. (left) Results obtained using a weighting function $w_3$ with parameters ($a = \frac{2\pi}{2\Delta x_{\max}}; b = 3a$) and a truncation distance of $8\Delta x_{\min}$, and (right) a weighting function $w_4$ ($a = \frac{2\pi}{2\Delta x_{\max}}; b = 3.5a$) with a truncation distance $d_{\max} = 6\Delta x_{\min}$.

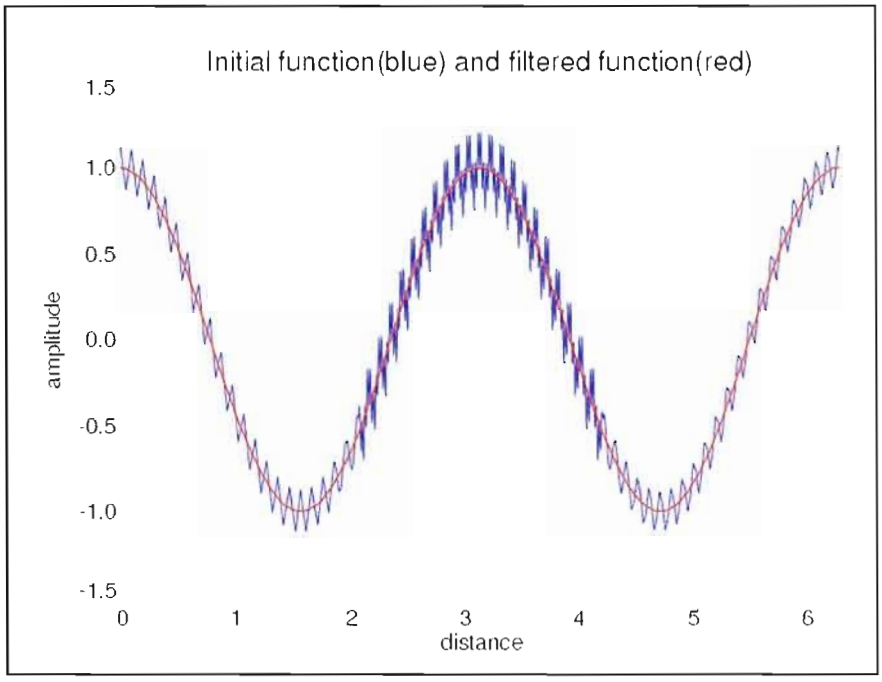


Figure1.13 The initial test function (blue) on the SG1 grid and the filtered field (red). The noise on the entire grid has wavenumber $k_{n_1} = \frac{2\pi}{4\Delta x_{\max}}$, and the noise on the stretching region and high-resolution area has wavenumber $k_{n_2} = \frac{2\pi}{4\Delta x_{\min}}$. The convolution filter used a weighting function $w_5$ with parameters $a = \frac{2\pi}{8\Delta x_{\max}}$ and $b = 1.5a$, and a truncation distance of $8\Delta x_{\max}$.

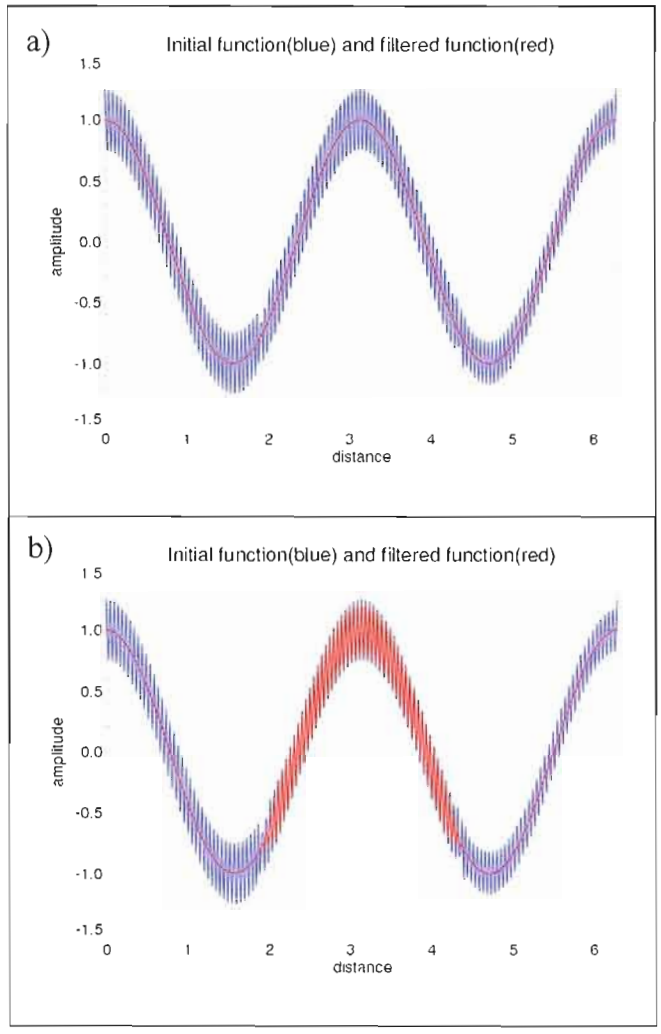


Figure 1.14 The initial test function (blue) on the SG1 contains a noise represented on the entire grid with wavenumber $k_{n_1} = \frac{2\pi}{2\Delta x_{\max}}$. (a) The filtered field (red) is obtained using a convolution filter with a weighting function $w_6$ with parameters $a = \frac{2\pi}{8\Delta x_{\max}}$ and $b = 2.5a$, and a truncation distance of $6\Delta x_{\max}$. (b) The filtered field (red) is obtained using the Shapiro filter.

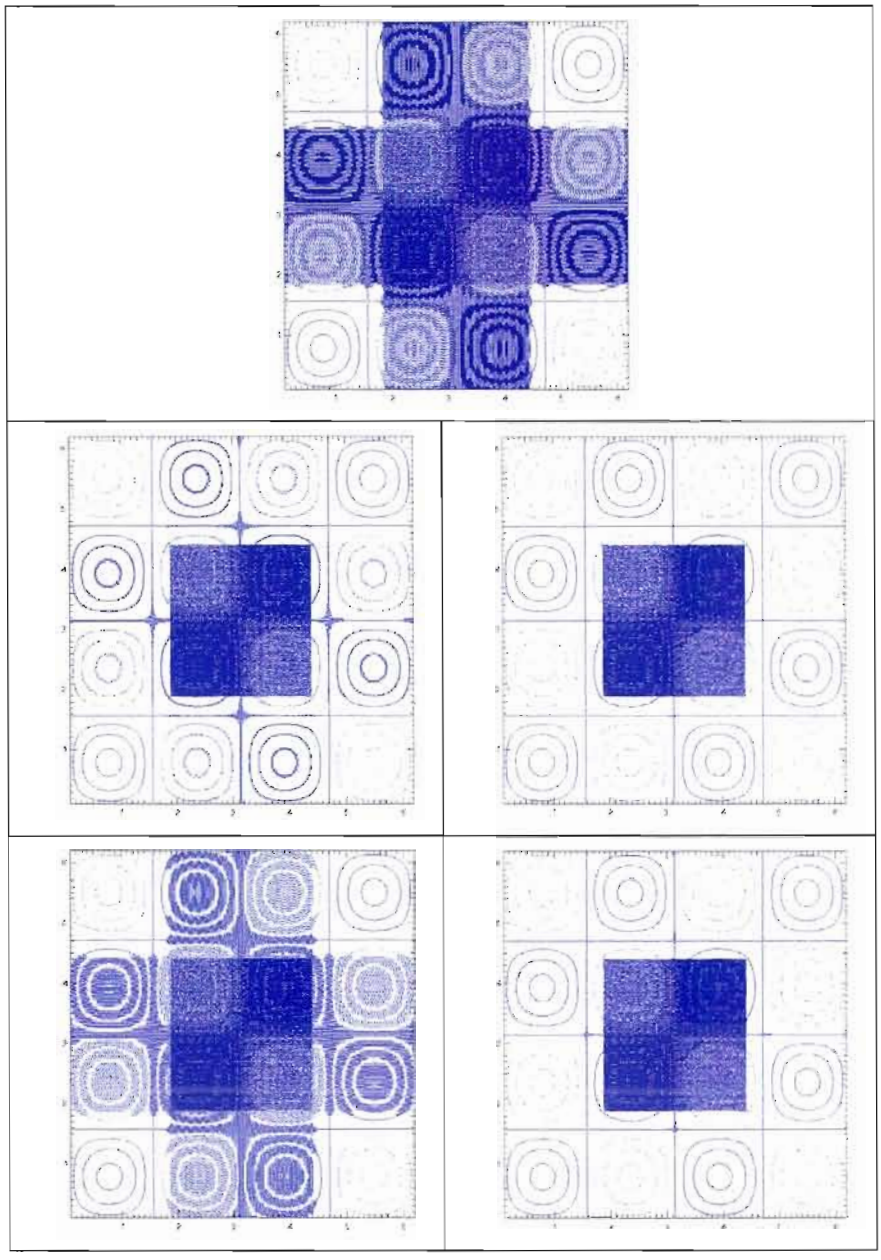

Figure 1.15 (top) The initial test field on the 2D stretched-grid with $S \cong 4$. (middle) The filtered fields after application of a convolution filter with 1D weighting function $w_1$ and a truncation distance of (middle left) $10\Delta x_{\min}$ and (middle right) $21\Delta x_{\min}$. (bottom) The filtered fields after application of a convolution filter with 1D weighting function $w_4$ and a truncation distance is $10\Delta x_{\min}$; the result after (bottom left) one and (bottom right) six applications of the filter.

# CHAPITRE II

# UN FILTRE SPÉCIFIQUE POUR UN MODÈLE À RÉSOLUTION VARIABLE : APPLICATION SUR LA GRILLE POLAIRE

Ce chapitre, rédigé en anglais, est présenté sous la forme d'un article qui a été soumis pour publication dans la revue *Monthly Weather Review*. Il décrit la conversion du filtre construit à l'aide d'un produit de convolution pour la grille polaire. Le produit de convolution utilise une fonction de pondération qui dépend de la distance physique sur la grille de calcul. Le filtre est appliqué sur une grille polaire pour des variables scalaires ainsi que pour des vecteurs. L'efficacité du filtrage est quantifiée en utilisant une erreur quadratique normalisée représentée en fonction de la distance de troncature.

L'étude montre que le filtre construit à l'aide d'un produit de convolution est efficace dans les régions prés du pôle et aussi dans les zones d'étirement. La fonction filtrée ne présente ni atténuation ni déformation en dehors de la zone de haute résolution uniforme. L'application du filtre pour des scalaires et des vecteurs en utilisant la même procédure fait de cette approche une option intéressante, facile à utiliser et qui mérite d'être exploitée sur une grille sphérique.

# A General Filter for Stretched-Grid Models: Application in Two-Dimension Polar Geometry

Dorina Surcel
and
René Laprise

ESCER Centre
Department of Earth and Atmospheric Sciences,
Université du Québec à Montréal, Montréal (Québec), Canada

Accepted for publication in *Monthly Weather Review*
August 2011

http://journals.ametsoc.org/doi/abs/10.1175/MWR-D-11-00058.1

---

*Corresponding author address:*
Dorina Surcel, Centre ESCER, Université du Québec à Montréal, Case postale 8888, Succursale Centre-ville, Montréal, Québec, CANADA, H3C 3P8.
E-mail: colan@sca.uqam.ca

# Résumé

Les modèles atmosphériques mondiaux utilisent des grilles à résolution variable pour mieux représenter les échelles régionales au-dessus d'une région d'intêret avec des coûts de calcul inférieurs aux modèles modiaux qui utilisent des grilles uniformes avec une haute résolution. Mais l'utilisation d'une résolution variable conduit aux problèmes liés à l'anisotropie de la grille dans les zones adjacentes à la zone de haute résolution uniforme. Pour éviter ces problèmes, un filtre spécifique a été dévéloppé.

Ce filtre initialement appliqué sur une grille cartésienne est maintenant adapté pour la grille polaire. Cette étape constitue une démarche nécessaire pour passer ensuite à une grille sphérique latitude-longitude. Les deux grilles, polaire et sphérique, rencontrent le même « problème du pôle » causé par la convergence des méridiens vers les pôles. Des détails sur l'adaptation du filtre pour la grille polaire, ainsi que son application sur une grille polaire uniforme et sur une grille polaire étirée sont présentés. La performance du filtre près des pôles et dans les régions d'étirement a été testée. Les résultats ont montré que l'opérateur de filtrage est capable l'enlever l'excès de résolution dans les régions polaires, avec des coûts de calculs qui sont inférieurs aux filtres polaires usuels. Le filtre a bien fonctionné en dehors de la région d'intérêt où les échelles qui ne sont pas supportées par la grille ont été enlevées sans déformation ou atténuation des grandes échelles.

L'opérateur de filtrage développé a été appliqué sur une grille polaire étirée pour des variables scalaires et pour des vecteurs. Cette étude a montré des résultats prometteurs, la réponse de filtrage pouvant être optimisée pour différentes fonctions-test ainsi que pour différents types de bruit qui devraient être enlevés.

# Abstract

Variable-resolution grids are used in global atmospheric models to improve the representation of regional scales over an area of interest, with reduced computational cost compared to uniform high resolution, and avoiding the nesting issues of limited-area models. In order to address some concerns associated with the stretching and anisotropy of the variable-resolution computational grid, a general convolution filter operator was developed.

The convolution filter that was initially applied in Cartesian geometry in a companion paper is here adapted to cylindrical polar coordinates as an intermediate step towards spherical polar latitude-longitude grids. Both polar grids face the so-called "pole problem" due to the convergence of meridians at the poles.

In this work we will present some details related to the adaptation of the filter to cylindrical polar coordinates, for both uniform as well as stretched grid. The first objective is to establish the performance of the filter near the poles. The results show that the developed operator is skilful in removing the extraneous fine scales around the pole. The computational cost related to the application of the filter is smaller than the cost associated with usual polar filters. The second objective is to apply the filter on a stretched grid for vector as well as scalar test functions. The results are satisfactory and the filter's response can be optimized for different types of test function and noise one wishes to remove.

## 2.1 Introduction

Numerical models have been used for climate modelling for half of a century, and they are powerful tools for reproducing the interactions between different components of the Earth's system. Such virtual laboratories would however require computational resources that are not commonly affordable when using high-resolution grids to cover the entire globe for long-term simulations. Two dynamical downscaling techniques are commonly used by the climate modelling community to reduce the computational costs and achieve high resolution over an area of interest, thus providing potential added value compared with uniform low-resolution global circulation models (IPCC 2007).

The first and the most common approach is the one-way nesting of a regional, limited-area model (LAM), which is a non-interactive approach (e.g., Giorgi and Bates 1989, Pielke et al. 1992, Christensen et al. 1998, Caya and Laprise 1999, Wang 2001, Jacob 2001, Döscher et al. 2002, Skamarock and Klemp 2008). LAMs need the specification of time-dependent boundary values that control the regional simulation. Nested models are computationally efficient due to the use of a limited-area domain, but this approach makes achieving an adequate representation of large scales challenging (Fox-Rabinovitz et al. 2008).

A second way to achieve high resolution over an area of interest is the interactive approach of a global variable-resolution model. A variable-resolution General Circulation Model consists of using high resolution over a specific region of interest and lower resolution over the rest of the globe. It allows naturally two-way interaction between global and regional domains (Fox-Rabinovitz et al. 2008, Laprise 2008). The concentration of the resolution over a subset of the Earth's surface increases computational efficiency, but this does not come free of some problems

owing to the variation of resolution. Variable resolution can be achieved in different ways, but the technique of grid stretching is one of the most extensively used methods and it allows varying the resolution simultaneously in both coordinate directions in a flexible manner. Over the last few years the approach of grid stretching in regional climate modelling gained in popularity. In the international "Stretched-Grid Model Intercomparison Project" (SGMIP) (Fox-Rabinovitz et al. 2006, 2008) four major groups from Australia (Mc. Gregor and Dix 1997, 2001), France (Déqué and Piédelièvre 1995), Canada (Côté et al. 1997, 1998) and United States (Fox-Rabinovitz et al, 1997) evaluated the performance of several Stretched-Grid General Circulation Models (SGGCMs) against observations and reanalyses, and also compared variable- and uniform-resolution Global Circulation Models (GCMs) for North American regional climate.

Despite the fact that the variable-resolution approach allows continuous multi-year simulations to be autonomously performed and that it provides consistent interactions between global and regional scales of motion, the anisotropy of the grid outside the uniform high-resolution area gives rise to a local degradation in accuracy, which may result in local flow distortions. Surcel and Laprise (2011; hereinafter SL11 argued for the benefits of introducing a special filter to remove the modes improperly represented in the stretching areas, thus providing a nearly isotropic and smoothly varying representation on the entire mesh. Their filter operator is designed to be used both in the stretching areas of a variable latitude-longitude grid (the anisotropic "arms of the cross" regions) as well as to alleviate the "pole problem" specific to latitude-longitude grids. The filter can also be applied to control potential numerical instabilities common to all numerical models. The filtering operator is built as the convolution between a field and a specific weighting function. A key aspect of the proposed convolution that makes it particularly suitable to stretched grids, is that the weighting function is defined in terms of the physical distance from the application point, rather than grid point count. In SL11 the filter was applied in

uniform and stretched 1D and 2D Cartesian grids. In this paper we pursue the development of the convolution filter by extending it to cylindrical polar coordinates as an intermediate step towards spherical polar longitude-latitude grid.

The origin of a polar coordinate system, and the north and south poles on a sphere, constitute point of convergence for the lines of constant polar angle or constant longitude. This convergence of meridians results in the so-called "pole problem" with latitude-longitude grids, which imposes severe time-stepping limitations with most numerical schemes. This issue has been circumvented in different ways.

One possibility is to use a "reduced" grid in which the longitudinal grid interval is kept reasonably constant in term of physical distance rather than angular distance; this can even be beneficial in spectral models (Hortal and Simmons 1991). Another possibility is to use a stabilizing procedure related to the filtering of the waves that would become unstable for a chosen time step (e.g. Williamson and Laprise 2000).

Another stabilizing procedure is a polar Fourier filter, applied poleward of a specified critical latitude $\varphi_c$ (typically 45° or 60° depending on specific applications). The strength of the filter is gradually increased toward the pole, by increasing the number of affected zonal wavenumbers and the damping strength. The application of Fourier filtering requires direct and inverse Fourier transforms on latitude circles, with a specified wavenumber truncation. Abrupt Fourier truncation at high latitudes is damaging to the accuracy of zonal differencing regardless of the nominal order of accuracy of the used differencing method (Purser 1988). Even when a smooth scalar field has only intrinsic scales greater than some particular limit, the zonal wavenumbers present on even the smallest circle of latitude are not correspondingly band-limited. Any Fourier truncation applied on such a circle of data inevitably affects the representation of scales larger than those intended. The Fourier filter offers

a relatively direct control of truncation and it needs data communication of all longitudes for the latitudes where it is applied.

Another procedure is to filter in the high-latitude regions using a 1D digital operator applied on latitude circles, with increased filtering strength as the poles are approached, typically 1D Laplacian on latitude circles, with repeated applications as the poles are approached. This filter only needs local data communication, but the truncation is poorly controlled.

Ideally smoothing techniques applied in the polar regions of a latitude-longitude stretched-grid should offer the possibility of maintaining nearly uniform resolution in the fields, as should be in any region of a variable-resolution stretched grid. When filters are scaled with the grid length rather with the physical distance, then filtering on anisotropic grids leads to anisotropic damping. The purpose of filtering on a variable grid should be to render the solution effectively isotropic and grid-independent. The specific convolution filter will be adapted here to the polar geometry. One important point in the development of this operator is that the weighting function in the convolution will depend on the physical distance rather than on the computational mesh distance. The second point to note is that this specific operator could be used for vectors as well as for scalar fields.

This paper is organized as follows. The next section reviews the formulation of the convolution filter in one dimension and presents the adaptation of the filter for a polar stretched grid. The third section presents examples of filter application for different scalar tests functions: the filter first is applied on a uniform polar grid to test the control of the pole problem, and then on a variable-resolution polar grid to verify that the filter can remove the noise in the anisotropic region outside the high-resolution area. The fourth section deals with the filtering of vectors. It is shown that the vectors at the points contributing to the convolution need to be expressed in the same reference system. The performance of the convolution operator on vector fields

is tested first on a uniform polar grid and then on a variable polar grid. Conclusions are presented in the last section.

## 2.2 Description of the convolution filter in polar geometry

Variable-resolution stretched grids usually have a uniform high resolution over the area of interest. Outside this area the grid intervals are increased or stretched in one or both horizontal directions, often as a geometric progression with a constant local stretching factor $s$ defined as follows:

$$s = \Delta x_i / \Delta x_{i-1} \tag{2.1}$$

where $\Delta x_i$ and $\Delta x_{i-1}$ are adjacent grid intervals. The total (or global) stretching factor is defined as

$$S = \Delta x_{\max} / \Delta x_{\min}, \tag{2.2}$$

where $\Delta x_{\max}$ and $\Delta x_{\min}$ are the maximum and minimum grid intervals over the domain.

To control potential computational problems due to the non-uniformity and anisotropy of the grid, a numerical filtering operator is here designed, which aims in part to removing the unwanted small scales outside the uniform high-resolution area. The convolution operator was chosen to design the filtering scheme. For a field $\psi$, the filtered value $\overline{\psi}$ is given by

$$\overline{\psi}(x) = (\psi * w)(x) = \int_{-\infty}^{\infty} \psi(s)\, w(x-s)\, ds \tag{2.3}$$

The spectral response of the convolution is obtained as the ratio of the spectral amplitudes, as a function of wavenumbers, of the Fourier transform of the filtered $\overline{\psi}$ and original $\psi$ fields. SL11 reviewed the well-known mathematical property that the

weighting function $w$ in the convolution should be the inverse Fourier transform of the desired response function after the application of the filter so:

$$w(d) = \frac{1}{2\pi} \int_{-\infty}^{\infty} R(k) \exp(ikd)\, \mathrm{d}k.$$

These studies also showed that this formal result could be extended to spatially varying response function, as long as the variation is made gradually. It is thus necessary to first choose a response function and its spatial variation. The degradation of resolution outside the high-resolution area gives rise to an anisotropic grid and hence to an anisotropic solution. To prevent the propagation of small-scale signals from the high-resolution region into the regions where the resolution is degraded, we choose to impose that the filter operator will remove the fine scales that are not correctly represented outside the uniform high-resolution region. The response function is defined as $R(k) = 1$ in the uniform high-resolution region; outside this region we choose

$$R(k) = \begin{cases} 1 & 0 \le k \le a = \pi/\Delta x_{\max} \\ \cos^2 \dfrac{\pi}{2}\left(\dfrac{k-a}{b-a}\right) & a < k < b \\ 0 & b \le k \le \pi/\Delta x_{\min} \end{cases} \qquad (2.4)$$

This function is dependent on the wavenumbers $a$ and $b$. The parameter $a$ is well determined: $a = \pi/\Delta x_{\max}$. In practice the parameter $b$ is adjusted such as to minimise the Gibbs' phenomenon associated with the change of resolution. The parameters that characterize the convolution can be expressed in term of wavelengths that must either be retained or removed; therefore $a = 2\pi/L_a$ where $L_a$ is the shortest wavelength that will be entirely preserved after the application of the filter, and $b = 2\pi/L_b$ where $L_b$ is the longest wavelength that will be completely removed by the filter. All scales with wavelengths between $L_a$ and $L_b$ will be partly removed.

Since the response function is even, the inverse Fourier transform that represents the weighting function will be symmetrical with respect to the application point. Hence Eq. (2.4) then implies that

$$w(x) = \frac{\pi}{2} \cdot \frac{\sin ax + \sin bx}{x} \cdot \frac{1}{\pi^2 - x^2(b-a)^2} \tag{2.5}$$

As shown by SL11, the computational cost can be greatly reduced by truncating the convolution to a user-prescribed finite distance $d_{\max}$ between the application point and the points contributing to the convolution. The resulting filter's response then only approximates the chosen response, but this may often be adequate for practical applications. SL11 presented two-dimensional filtering in Cartesian geometry. For simplicity and computational cost reduction reasons, these filters were obtained by successive applications of one-dimensional filtering in each direction, with the convolution weighting function depending on the physical distance. The study showed that the resulting filter was nearly isotropic.

The formal approach is here generalized to two-dimensional polar geometry. On the polar grid the convolution filter will be used not only in the stretching area but also near the poles. In polar coordinates, a point is specified by the radius $r$, which is the distance from a point to the origin of the coordinate system, and the azimuthal angle $\lambda$. The Cartesian coordinates $x$ and $y$ are connected to the polar coordinates through the relations

$$\begin{cases} x = r \cdot \cos\lambda \\ y = r \cdot \sin\lambda \end{cases} \tag{2.6}$$

where $\begin{cases} r = \left(x^2 + y^2\right)^{1/2} \\ \lambda = \tan^{-1}\left(\dfrac{y}{x}\right) \end{cases}$, and $0 \le r < \infty$ and $0 \le \lambda \le 2\pi$.

We chose a filter formulation obtained by the separate application of the convolution in the radial and the azimuthal directions, for simplicity and efficiency considerations, while preserving the paramount concept of physical distance. The filtered function can formally be written in integral form as

$$\overline{\psi}(r,\lambda)=\left(\overline{\left(\overline{\psi}\right)^{\lambda}}\right)^{r}(r,\lambda)=\int_{r'=0}^{\infty}\int_{\lambda'=0}^{2\pi}\psi(r',\lambda')\,w\left(r'(\lambda-\lambda')\right)w(r-r')\,r'\,dr'\,d\lambda' \qquad (2.7)$$

On a discrete polar grid $(r_i,\lambda_j)$, the field to be filtered is represented by $\psi_{i,j}=\psi(r_i,\lambda_j)$, with $i=1,\ldots,n;j=1,\ldots,m$ and $r_i\in[0,R_e]\lambda_j\in[0,2\pi]$ where $R_e$ is the distance from the centre of the grid to the boundary (henceforth referred to as the equator). Then the convolution formula is discretized as follows:

$$\begin{aligned}\overline{\psi}^{r,\lambda}(r_i,\lambda_j)&=\frac{\sum_k\overline{\psi}^{\lambda}(r_k,\lambda_j)\cdot w(d^r_{i-k})\cdot s(r_k)}{\sum_k w(d^r_{i-k})\cdot s(r_k)}\\&=\frac{\sum_k\sum_l\psi(r_k,\lambda_l)\cdot w(d^{\lambda}_{j-l})\cdot w(d^r_{i-k})\cdot s(r_k)\cdot s(\lambda_l)}{\sum_k\sum_l w(d^{\lambda}_{j-l})\cdot w(d^r_{i-k})\cdot s(r_k)\cdot s(\lambda_l)}\end{aligned} \qquad (2.8)$$

where $d^r_{i-k}$ and $d^{\lambda}_{j-l}$ are the radial and azimuthal distances between two grid points $(r_i,\lambda_j)$ and $(r_k,\lambda_l)$, and $s(r_k)\cdot s(\lambda_l)=s(r_k,\lambda_l)$ is the surface area around the $(r_k,\lambda_l)$ grid point. It must be noted that the weighting function varies with the physical distances, and is not based on grid-point count, which is in fact the critical ingredient in the design of the proposed convolution filter.

As for the Cartesian coordinate case discussed in SL11, the discrete convolution will be truncated by calculating the summation up to a user-prescribed distance $d_{\max}$ between the application point and the points contributing to the convolution; this will greatly reduce the computational cost, when an approximate

filter's response suffices. For simplicity and further computational efficiency, the convolution is calculated by successive applications of one-dimensional filtering in each direction. Because the number of grid points for a given physical distance in the azimuthal direction varies with radial distances (in integral (2.7) the azimuthally weighting function depends on the radial distance), it will be important to apply first the convolution in the azimuthal direction, followed by the application of the convolution in the radial direction. The convolution in the azimuthal direction gives

$$\overline{\psi}^{\lambda}\left(r_k,\lambda_j\right)=\frac{\sum\limits_{l}\psi\left(r_k,\lambda_l\right)\cdot w\left(d^{\lambda}_{j-l}\right)\cdot s\left(\lambda_l\right)}{\sum\limits_{\substack{l\\ d^{\lambda}_{j-l}\le d_{\max}}} w\left(d^{\lambda}_{j-l}\right)\cdot s\left(\lambda_l\right)}\qquad(2.9)$$

where $d^{\lambda}_{j-l}=r_k\cdot\left(\lambda_j-\lambda_l\right)$ is the distance between two points $\left(r_k,\lambda_j\right)$ and $\left(r_k,\lambda_l\right)$ situated on the same circle $r_k=\text{const.}$, and $s\left(\lambda_l\right)=r_k\cdot\left(\lambda_{l+1}-\lambda_{l-1}\right)/2$ is the scale factor in azimuthal direction corresponding to the grid point $\left(r_k,\lambda_l\right)$. The convolution in the radial direction is calculated as follows

$$\overline{\psi}\left(r_i,\lambda_j\right)=\left(\overline{\overline{\psi}^{\lambda}}\right)^{r}\left(r_i,\lambda_j\right)=\frac{\sum\limits_{k}\overline{\psi}^{\lambda}\left(r_k,\lambda_j\right)\cdot w\left(d^{r}_{i-k}\right)\cdot s\left(r_k\right)}{\sum\limits_{\substack{k\\ d^{r}_{i-k}\le d_{\max}}} w\left(d^{r}_{i-k}\right)\cdot s\left(r_k\right)}\qquad(2.10)$$

where $d^{r}_{i-k}=r_i-r_k$ is the distance between two points $\left(r_i,\lambda_j\right)$ and $\left(r_k,\lambda_j\right)$ situated on the same azimuth $\lambda_j=\text{const.}$, and $s\left(r_k\right)=\left(r_{k+1}-r_{k-1}\right)/2$ is the scale factor corresponding to the radial direction. Figure 2.1 shows the grid points participating to the convolutions in the azimuthal and the radial directions.

The computer implementation is greatly simplified by introducing an extended grid for $\lambda < 0$ and $\lambda > 2\pi$. Periodicity considerations give $\psi(r,\lambda) = \psi(r,\lambda \pm 2n\pi)$ with $n$ an integer. Similarly, in order to avoid having to resort to special treatment at the pole and equator, we will also use an extended domain that represents an extension of the physical domain to $r < 0$ and $r > R_e$. For $r < 0$ the extended grid is built considering the symmetry of scalars around the pole:

$$\psi(r,\lambda) = \psi(-r, \lambda \pm \pi).$$

The field $\psi(r,\lambda)$ was extended for $r > R_e$ by simply using the analytical functions prescribed for our tests. The extension of the domain for $r > R_e$ is only needed due to the polar grid used in this study; on the spherical latitude-longitude grid, this problem does not exist, the computational grid will need only to be extended beyond the poles.

## 2.3 Application to scalar fields

By the application of the filter on the polar grid we want to achieve two objectives: to remove both the "pole problem" and the anisotropy outside the uniform high-resolution area of the stretched polar grid. We will investigate first the effects of the filtering operator on scalar test-functions. Considerations regarding the application of the filter on vector fields will be dealt with in the next section.

For evaluating the skill of the proposed filtering approach, we choose a test-function composed of a large-scale field $\psi_l$, referred to as the signal or physical component, and a small-scale field $\psi_n$, referred to as the noise, defined in every grid point as follows:

$$\psi(r_i,\lambda_j) = \psi_l(r_i,\lambda_j) + \psi_n(r_i,\lambda_j) \tag{2.11}$$

As for the one-dimensional stretched-grid version of the convolution filter (SL11), the quality of the filter will be quantitatively assessed using two main metrics: the normalized root-mean square error (*NRMS*) and the normalized conservation ratio (*NCR*). The root-mean square error will be computed between the filtered solution $\overline{\psi}$ and the expected analytical solution $\psi_l$ (after subtracting the mean error $\overline{\Delta\Psi}$), normalized by the variance of the analytical solution:

$$NRMS = \frac{\sqrt{\sum_i \sum_j \left(\overline{\psi}(r_i,\lambda_j) - \psi_l(r_i,\lambda_j) - \overline{\Delta\Psi}\right)^2 \cdot s(r_i,\lambda_j)}}{\sqrt{\sum_i \sum_j \left(\psi_l(r_i,\lambda_j)\right)^2 \cdot s(r_i,\lambda_j)}} \tag{2.12}$$

where $\overline{\Delta\Psi} = \dfrac{\sum_i \sum_j \left(\overline{\psi}(r_i,\lambda_j) - \psi_l(r_i,\lambda_j)\right) \cdot s(r_i,\lambda_j)}{\sum_i \sum_j s(r_i,\lambda_j)}$ is the domain-averaged error between the filtered solution and the analytical solution. The normalized conservation ratio (*NCR)* checks mass conservation as the mean error between the filtered and unfiltered solution, normalized by the variance of the analytical solution:

$$NCR = \frac{\sum_i \sum_j \left(\overline{\psi}(r_i,\lambda_j) - \psi(r_i,\lambda_j)\right) \cdot s(r_i,\lambda_j) \Big/ \sum_i \sum_j s(r_i,\lambda_j)}{\sqrt{\sum_i \sum_j \psi_l^2(r_i,\lambda_j) \cdot s(r_i,\lambda_j) \Big/ \sum_i \sum_j s(r_i,\lambda_j)}} \tag{2.13}$$

where $s(r_i,\lambda_j) = r_i \cdot \dfrac{r_{i+1} - r_{i-1}}{2} \cdot \dfrac{\lambda_{j+1} - \lambda_{j-1}}{2}$ is the area around the $(r_i,\lambda_j)$ point.

Two types of test functions will be considered to represent the large-scale signal:

a) A double cosine in physical space:

$$\psi_l(r_i,\lambda_j) = A_l \cos(k_l r_i \cos\lambda_j) \cos(l_l r_i \sin\lambda_j),$$

where $k_l = l_l = 2\pi/L_l$, $L_l$ (expressed in km) represents the wavelength, and $A_l$ is the amplitude of the large-scale signal.

b) A cylindrical harmonic, eigenfunction of the Laplacian on the polar grid:

$$\psi_l(r_i,\lambda_j) = A_l J_{l_l}(k_l r_i) \cos(l_l \lambda_j),$$

where $J_{l_l}(k_l r_i)$ is the Bessel function of the first kind and order $l_l$ (Bowman, 1958), $k_l$ is the radial wavenumber, $l_l$ the azimuthal wavenumber and $A_l$ the amplitude of the large-scale signal.

The small-scale noise will also represented by two different test functions:

a) A double cosine in physical space:

$$\psi_n(r_i,\lambda_j) = A_n \cos\left(k_n r_i \cos\lambda_j\right) \cos\left(l_n r_i \sin\lambda_j\right),$$

where $k_n = l_n = 2\pi/L_n$, $L_n$ (expressed in km) represents the wavelength, and $A_n$ is the amplitude of the small-scale noise.

b) A checkerboard-like noise on the polar grid:

$$\psi_n(r_i,\lambda_j) = A_n \left(\pm 1\right)^{i+j}$$

Such noise corresponds to wavenumbers that vary with radial distance, with a minimum value at the equator corresponding to a wavelength of $2\Delta\lambda$.

In order to avoid difficulties with the extension beyond the artificial boundary of the domain ($r = R_e$) for computer implementation of the convolution, the noise field is gradually diminished to zero over the last four grid points in the radial direction.

The weighting function used in the convolution filter formulation represents the inverse Fourier transform of the desired response. It is important to choose a response or transfer function with a gradual cutoff, first to minimize the Gibbs' phenomena (Sardeshmukh and Hoskins 1984) and second because a smooth cut-off will give rise to a narrow weighting function and the truncation errors related to the application to a finite set of points will be decreased. As we saw in Eq. (2.5), the parameters that define the weighting function, $a = 2\pi/L_a$ and $b = 2\pi/L_b$, depend on the physical length scale that a user chooses to preserve or remove. The convolution will be calculated considering all grid-points located up to a user-chosen maximum distance $d_{\max}$ in radial or azimuthal directions from the application point.

### 2.3.1 Application of the filter for scalars on a uniform polar grid

To test the skill of the filter at alleviating the pole problem, we employ a "uniform" polar grid, i.e. a uniform radial resolution $\Delta r$ and isotropic resolution near the equator $R_e \Delta\lambda = \Delta r$. With $n$ radial grid points, this implies $n = R_e/\Delta r + 1$, i.e. $\Delta r = R_e/(n-1)$ (with grid points both at the pole and the equator). With $m$ equally spaced azimuths $\Delta\lambda = 2\pi/m$, this implies $m = 2\pi(n-1)$, i.e. $n = m/2\pi + 1$. In the following tests we have used arbitrarily $R_e = 10{,}000\,\text{km}$, the approximate distance between the pole and the equator on Earth. To summarise, the discrete uniform polar grid used for our experiments was represented by $(r_i, \lambda_j)$ with $r_i \in [0, R_e]$, $i = 1,\ldots,n$ and $\lambda_j \in [0, 2\pi]$, $j = 1,\ldots,m$ and $R_e \Delta\lambda = \Delta r$.

The tests performed on the uniform polar grid, using scalar test-functions, were designed to verify the skill of the filter at removing the small-scale noise around the pole while preserving the large-scale signal, and to evaluate the influence of using different choices of weighting functions.

For the first objective of handling the pole problem, Fig. 2.2 presents four examples of filtering with different test functions. The uniform polar grid has a resolution of 1° in azimuthal direction, resulting in an isotropic resolution near the equator of $\Delta r \cong 175\,\text{km}$. In the first example presented in Fig. 2.2a, the test-function is composed of a large-scale signal in the form of a double cosine with $k_l = l_l = 2\pi/L_l$ and $L_l = 20{,}000\,\text{km}$, and a small-scale noise represented also by a double cosine with $k_n = l_n = 2\pi/L_n$ and $L_n = 500\,\text{km}$. The amplitude of the large-scale signal is $A_l = 1$ and the amplitude of the noise is $A_n = 1/4$ except for the last four grid points in radial direction where this amplitude is gradually reduced to zero. The parameters of the convolution weighting function were chosen to be $L_a = 2{,}400\,\text{km}$ and $L_b = 800\,\text{km}$, so the filter should preserve the large-scale signal and remove entirely the small-scale

noise. With these parameters, the response function is relatively smooth and the weighting function needs a truncation distance of $d_{\max} = 1{,}600\,\text{km}$ for an adequate accuracy of the convolution. The test-function represented in Fig. 2.2b is composed of a large-scale signal in form of a cylindrical harmonics with $k_l = l_l = 2$, and a small-scale noise in form of a double cosine with $k_n = l_n = 2\pi/L_n$ and $L_n = 600\,\text{km}$. The amplitude of the large-scale signal was set to $A_l = 1$ and, to keep almost the same proportion between the amplitude of the signal and the noise as in the first example, we chose $A_n = 1/8$ excepting the last four grid points where the amplitude is diminish gradually to zero. To remove the noise we used a weighting function where $L_a = 2{,}400\,\text{km}$ and $L_b = 1{,}000\,\text{km}$. Because this weighting function has a wider footprint then an increased truncation distance is necessary for a proper response of the filter, so we chose $d_{\max} = 2{,}300\,\text{km}$. The last two examples presented in Fig. 2.2c and Fig. 2.2d used test-functions composed of large-scale signals identical with those used in the first two examples, but with checkerboard-like noises with amplitudes equals to 1/8 for c) and 1/16 for d). To remove these noise patterns the convolution filter employed the same weighting function and truncation distances as in the first two examples. In all four tests shown in Fig. 2.2, the convolution filter appears to adequately remove the noise and preserve the signal; we will next verify this assessment with a quantitative score.

We now assess quantitatively the influence of the truncation distance and filtering cut-off scale $L_b$. Three different weighting functions will be tested in the convolution filter applied to the test function used in Fig. 2.2a. All three weighting functions are designed to remove the noise, as $L_n \le L_b$, while keeping the large-scale signal; the parameters that characterise these weighting functions are:

$$w1: \begin{cases} L_a = 2{,}400\,\text{km} \\ L_b = 1{,}000\,\text{km} \end{cases} \quad w2: \begin{cases} L_a = 2{,}400\,\text{km} \\ L_b = 800\,\text{km} \end{cases} \quad w3: \begin{cases} L_a = 2{,}400\,\text{km} \\ L_b = 600\,\text{km} \end{cases}.$$

Figure 2.3 shows the curves *NRMS* and *NCR* for truncation distances varying between 200km and 2,400 km. Figure 2.3a shows the *NRMS* for different weighting functions. Overall the error decreases as the truncation distance is increased, although not monotonically; the oscillations are larger for $w1$ than for $w3$ due to the Gibbs' phenomenon associated with narrower response function which necessitates wider stencil for accurate representation. The normalized conservation ratio (*NCR)* is shown in Fig. 2.3b. The *NCR* curves exhibit important oscillations; while the conservation error even increases with overly small truncation distance, all curves eventually asymptote towards zero for large truncation distances, indicating then good conservation of filtered quantities at large truncation distances. We note that broader response functions (such as $w3$) converge faster due to reduced spurious Gibbs' phenomenon. Beyond a truncation distance of 2,400 km the weighting functions have values that become very small and hence their contribution is unimportant in the convolution, and the curves *NRMS* and *NCR* asymptote toward zero.

We now investigate how the sensitivity to the truncation distance varies depending on the scale of the noise one intends to remove. In Fig. 2.4 we chose a test function composed of a large-scale signal with $k_l = 2\pi/L_l$ and $L_l = 20{,}000\,\text{km}$, and five different double cosine noises with wavenumbers $k_{n_j} = 2\pi/L_{n_j}$, $(j = 1,...,5)$, with $L_{n_1} = 500\text{km}$, $L_{n_2} = 600\text{km}$, $L_{n_3} = 700\text{km}$, $L_{n_4} = 800\,\text{km}$ and $L_{n_5} = 900\,\text{km}$. We chose a weighting function characterised by $w: \begin{cases} L_a = 4{,}000\,\text{km} \\ L_b = 1{,}000\,\text{km} \end{cases}$, which should be adequate to remove all the above small-scale noises; this weighting function has non negligible values over a distance of 1,600 km. Figure 2.4 shows that shorter scale noises are most effectively removed and they tolerate shorter truncation distance in the convolution filter; as the length scale of the noise increases, convergence is slower and an increased truncation distance is required. However, it can be noted that the

error asymptotically converge to zero beyond some truncation distance (in our case 800 km) for all tested noises.

### 2.3.2 Application of the filter to scalars on a variable polar grid

We now turn our attention to verify the skill of the filter at removing the anisotropy on a stretched polar grid. We use a "uniform" high-resolution domain ($D_{HR}$) defined by

$$D_{HR}:\left(r,\frac{\lambda}{2\pi}\right)\in\left(r_1,r_2\right)\times\left(t_1,t_2\right)=\left(3{,}500\,\text{km};7{,}500\,\text{km}\right)\times\left(\frac{5}{8},\frac{7}{8}\right)\text{ with }t_i=\frac{\lambda_i}{2\pi},$$

where the radial resolution is chosen to be $\Delta r\cong 15\text{km}$ and the azimuthal resolution $\Delta\lambda\cong\pi/1080$. This implies that resolution will be isotropic in the middle of the high-resolution sector, at $\left(r,\frac{\lambda}{2\pi}\right)=\left(5{,}500\,\text{km};\frac{3}{4}\right)$. A gradual stretching zone, with local stretching rate of $s_r=8\%$ in the radial direction and $s_\lambda=3.8\%$ in the azimuthal direction is used adjacent to the high-resolution area, which defines the stretching domain ($D_{SG}$):

$$D_{HR}\cup D_{SG}:\left(r,\frac{\lambda}{2\pi}\right)\in\left\{\left(r_3,r_4\right)\times\left(0,1\right)\cup\left(0,R_e\right)\times\left(t_3,t_4\right)\right\}$$

$$=\left\{\left(2{,}500\,\text{km};8{,}500\,\text{km}\right)\times\left(0,1\right)\cup\left(0;10{,}000\,\text{km}\right)\times\left(\frac{9}{16},\frac{15}{16}\right)\right\}$$

and $D_{HR}\cap D_{SG}=\varnothing$.

Low resolution is used elsewhere in the domain, with $\Delta r\cong 90\,\text{km}$ and $\Delta\lambda\cong\pi/180$ ($D_{LR}$), resulting in a total stretching factor of $S_r\cong S_\lambda\cong 6$.

The test functions used to verify the performance of the filter when is applied on variable polar stretched grid are similar to those used for the uniform polar grid.

The difference consists in the representation of the small-scale component, which is added in the uniform high-resolution area and in the adjacent stretching regions where the grid is anisotropic. In the uniform high-resolution area ($D_{HR}$), the small-scale component will be interpreted as part of the signal; it constitutes the added value provided by the stretched grid, and hence the convolution filter will be designed to keep the small-scale component in the uniform high-resolution area. Outside the uniform high-resolution area, the small-scale component will be interpreted as noise that the convolution filter should remove.

The first two examples are shown in Fig. 2.5. The test-functions are composed of large-scale double cosines with wavelengths of 20,000 km and 10,000 km, and small-scale component in the form of double cosines with wavelengths of 400 km and 500 km, respectively. The initial fields are represented in the left panels and the filtered fields in the right panels. For the first case (upper panels), the convolution filter uses a weighting function characterized by $L_a = 2{,}400\text{km}$ and $L_b = 1{,}000\text{km}$, with a truncation distance of 2,300 km. In the second case (lower panels), the weighting function used in the convolution is characterized by $L_a = 2{,}400\text{km}$ and $L_b = 600\text{km}$, and a shorter truncation distance of 1,000 km is used, which is sufficient because of the smoother response than in the first case, resulting in a narrower footprint of the weighting function. Figure 2.5 shows that the convolution filter adequately removes the fine-scale noise outside the uniform high-resolution area.

The next two examples shown in Fig. 2.6 present the results with test-functions composed of cylindrical harmonics as large-scale signals and double cosines as small-scale components. The large-scale signals have wavenumbers $k_l = l_l = 3$ and $k_l = l_l = 2$, and the small-scale component have wavelengths of 400 km and 500 km, respectively. The weighting functions used to remove the noise are characterized by $L_a = 2{,}400\text{km}$ and $L_b = 1{,}000\text{km}$ with a truncation distance of 2,300 km for the

example presented in the upper panels, and $L_a = 2{,}400\text{km}$ and $L_b = 600\text{km}$ with a truncation distance of 1,000 km for those presented in the bottom panels. Again we see in Fig. 2.6 that the convolution filter adequately removes the fine-scale noise outside the uniform high-resolution area.

We will next quantify the skill of the convolution filter at removing the small-scale noise outside the uniform high-resolution area, while keeping the signal (large and small scales) in the high-resolution area, using similar quantitative scores as for the uniform polar grid. We first establish the following notation:

$$\text{for the test function } \psi(r,\lambda) = \begin{cases} \psi_{HR} & \text{if} \quad (r,\lambda) \in D_{HR} \\ \psi_{SG} & \text{if} \quad (r,\lambda) \in D_{SG} \\ \psi_{LR} & \text{if} \quad (r,\lambda) \in D_{LR} \end{cases},$$

$$\text{and for the filtered function } \overline{\psi}(r,\lambda) = \begin{cases} \psi_{HR} & \text{if} \quad (r,\lambda) \in D_{HR} \\ \overline{\psi}_{SG} & \text{if} \quad (r,\lambda) \in D_{SG} \\ \overline{\psi}_{LR} & \text{if} \quad (r,\lambda) \in D_{LR} \end{cases}.$$

We remark that the convolution filter is applied only outside the uniform high-resolution area, so the filter does not affect the test function in this domain. We can then estimate the normalised root mean square error on the entire domain, considering the expected analytical solution $\psi_{as}$ as:

$$\psi_{as}(r,\lambda) = \begin{cases} \psi_{HR}(r,\lambda) & \text{if } (r,\lambda) \in D_{HR} \\ \psi_i(r,\lambda) & \text{for all other } (r,\lambda) \end{cases}.$$

*NRMS* will be calculated as:

$$NRMS = \frac{\sqrt{\sum_i \sum_j \left(\overline{\psi}(r_i,\lambda_j) - \psi_{as}(r_i,\lambda_j) - \overline{\Delta\Psi_{SG}}\right)^2 \cdot s(r_i,\lambda_j)}}{\sqrt{\sum_i \sum_j \left(\psi_l(r_i,\lambda_j)\right)^2 \cdot s(r_i,\lambda_j)}} \tag{2.14}$$

where $\overline{\Delta\Psi}_{SG} = \dfrac{\sum_i \sum_j \left(\overline{\psi}(r_i,\lambda_j) - \psi_{as}(r_i,\lambda_j)\right) \cdot s(r_i,\lambda_j)}{\sum_i \sum_j s(r_i,\lambda_j)}$.

We compute similar scores $NRMS\_SG$ and $NRMS\_LR$ only for parts of the domain; so for the stretching domain $D_{SG}$ and the low-resolution domain $D_{LR}$, we calculate:

$$NRMS\_\alpha = \frac{\sqrt{\sum_i \sum_j \left(\overline{\psi}_\alpha(r_i,\lambda_j) - \psi_{as}(r_i,\lambda_j)\right)^2 \cdot s(r_i,\lambda_j)}}{\sqrt{\sum_i \sum_j \left(\psi_l(r_i,\lambda_j)\right)^2 \cdot s(r_i,\lambda_j)}} \tag{2.15}$$

$$\text{where} \quad \begin{cases} \alpha \equiv SG & \text{for} \quad (r_i,\lambda_j) \in D_{SG} \\ \alpha \equiv LR & \text{for} \quad (r_i,\lambda_j) \in D_{LR} \end{cases} \tag{2.16}$$

To check the conservation of filtered quantities, $NCR$ is calculated as in Eq. (2.13).

Three different weighting functions will be used in the convolution applied to the same test function as used in the first example in Fig. 2.5. By definition, all those functions should remove the noise, as $L_n \le L_b$, keeping unchanged the large-scale signal. The parameters characterising the weighting functions are:

$$w1: \begin{cases} L_a = 2{,}400\text{km} \\ L_b = 1{,}000\text{km} \end{cases} \quad w2: \begin{cases} L_a = 2{,}400\text{km} \\ L_b = 800\text{km} \end{cases} \text{ and } \quad w3: \begin{cases} L_a = 2{,}400\text{km} \\ L_b = 600\text{km} \end{cases}.$$

Figure 2.7a shows that *NRMS* error generally decreases as the truncation distance increases, although not monotonically. The curves exhibit oscillations that are larger for the weighting function corresponding to the most abrupt response due to Gibbs' phenomenon. These oscillations are reduced as the truncation distance increases and the error then asymptotes towards zero, as is the case for the weighting function *w*3, which only requires a shorter truncation distance in order to reproduce the theoretical spectral response from which was conceived. The conservation scores are shown in Fig. 2.7b. With sufficiently wide weighting function the *NCR* curves eventually approach zero when using large truncation distance.

The lower two panels in Fig. 2.7c and Fig. 2.7d show the normalised error over only the stretching domain (*NRMS_SG*) and the low-resolution domain (*NRMS_LR*). The *NRMS_SG* curves have similar shape as the *NRMS* curves, which we interpret to imply that the main errors arise from the application of the filter in the stretching region. For a truncation distance smaller than 600 km, *NRMS* and *NRMS_SG* generally decrease while *NRMS_LR* is small, which implies that the convolution filter is effective at removing the noise in the stretching domain. For an increased truncation distance the *NRMS* error decreases more slowly and the *NRMS_LR* begins to increase till a value of about 1,000km is reached; this means that the truncation distances smaller than this value are inadequate to reproduce the expected spectral response and that Gibbs' oscillations produce false amplifications or attenuations of the large-scale signal. When the truncation distance is further increased beyond 1,000km, then the error in the low-resolution domain is mostly responsible for the total value of *NRMS*. All errors decrease toward zero when the truncation distances became large enough to reach vanishing values of the weighting functions.

In order to substantiate the above interpretation, we will show where in the domain the error occurs, using the case already presented in Fig. 2.5a. The spatial

distribution of the quadratic error is computed as the square of the difference between the filtered function and the analytical solution:

$$\sigma^2(r_i,\lambda_j) = \left(\overline{\psi}(r_i,\lambda_j) - \psi_{as}(r_i,\lambda_j)\right)^2 \tag{2.17}$$

Figure 2.8a shows the quadratic error for a truncation distance of 400 km. We note that the errors are generally located in the stretching zones where some noise remains after the application of the filter. When the truncation distance is increased to 1,000 km (Fig. 2.8b), then the noise remains in the regions where the resolution varies rapidly. When the truncation distance is further increased to 1,400 km, then the error is practically removed, but then the Gibbs' oscillations give attenuation or amplification of the large scales, resulting in the error pattern shown (Fig. 2.8c). The spatial error decreases under the values of $10^{-5}$ (the minimal value shown in Figs. 2.8) when the truncation distance exceeds 1800km.

The experiments realized on the polar grid showed the ability of the convolution filter to adequately remove small-scale noise both in the polar region and also in the anisotropic "arms-of-the-cross" regions of the variable polar stretched grid. The convolution filter can be applied at the same time to address the pole problem and also to remove anisotropic noise in the stretching region of the grid, by choosing appropriate parameters for the convolution weighting function. These parameters depend on the length scales that a user wants to be retained or removed in each region of the domain. We reiterate that because the convolution filter is designed in terms of physical distance on the grid and not on grid-point counts, the resulting response is almost isotropic and independent of grid-point spacing.

## 2.4 Application to vector fields

When the convolution is applied to vectors such as the horizontal wind, care has to be taken to use a representation of the vector components relative to the same reference system, chosen here to correspond to the application point. As the polar grid used in this paper is an intermediate step to the application of the filter on a spherical latitude-longitude stretched grid, the representation of the vector components will be made by analogy with the spherical grid.

Coordinates on a polar grid are defined by $(r,\lambda)$, with $r$ the distance from the centre of the grid (the equivalent on the sphere would be the radius of the Earth multiplied by the co-latitude angle) and $\lambda$ the azimuth angle (equivalent to longitude on the sphere). The horizontal wind is defined related to the local coordinate system, as shown in Fig. 2.9, with

$$\mathbf{V}_h = (u,v) = \left(r\frac{d\lambda}{dt}, -\frac{dr}{dt}\right)$$

where $(u,v)$ correspond to the "zonal" and "meridional" wind components (using the terminology on the sphere), with the sign convention that $u$ is positive eastward and $v$ is positive northward. Hence the position on the polar grid is defined by $(r_i,\lambda_j)$ and the horizontal wind components as

$$\begin{cases} u_{i,j} = u(r_i,\lambda_j) \\ v_{i,j} = v(r_i,\lambda_j) \end{cases} \text{ with } i=1,\ldots,n; \quad j=1,\ldots,m; \; r_i \in [0,R_e]; \quad \lambda_j \in [0,2\pi]. \tag{2.18}$$

Following the meteorological tradition, the wind components are defined relative to a locally orthogonal reference system whose base vectors change with location (only with longitude in fact for the polar grid). Therefore the application of the filter operator will require representing the wind components contributing to the convolution at a point in the same coordinate system as that point.

For each point $P_0(r_i,\lambda_j)$ where the convolution filter is applied for $(u,v)$, we need to transform all wind vectors in the neighbouring points $P(r_k,\lambda_l)$ contributing to the convolution, i.e. those for which their distance is within the chosen truncation distance for the convolution. The wind components at point $P(r_k,\lambda_l)$ are expressed in the coordinate system relative to the application point $P_0$ as follows:

$$\begin{pmatrix} u \\ v \end{pmatrix}_{P_0}(k,l) = \begin{bmatrix} \cos(\lambda_l - \lambda_j) & -\sin(\lambda_l - \lambda_j) \\ \sin(\lambda_l - \lambda_j) & \cos(\lambda_l - \lambda_j) \end{bmatrix} \begin{pmatrix} u \\ v \end{pmatrix}_{P}(k,l) \tag{2.19}$$

We note that the conversion only involves the longitude angle, not the radial distance; so no transformation is required for points aligned on the same meridian.

As for scalars, it is convenient to introduce an extended grid that allows applying the general convolution equation without having to use special treatments near the boundaries of the domain. Hence, if $\lambda < 0$ or $\lambda > 2\pi$, periodicity considerations give $\begin{cases} u(r,\lambda) = u(r,\lambda \pm 2n\pi) \\ v(r,\lambda) = v(r,\lambda \pm 2n\pi) \end{cases}$ with $n$ an integer. Symmetry considerations at the pole suggest the following extrapolation for $r < 0$:

$$\begin{cases} u(r,\lambda) = -u(-r,\lambda \pm \pi) \\ v(r,\lambda) = -v(-r,\lambda \pm \pi) \end{cases}.$$

Again in order to avoid difficulties with the application of the convolution near the artificial boundary of the domain ($r = R_e$), the noise field is gradually diminished to zero over the last four grid points in radial direction.

We define test wind fields by constructing rotational and divergent motions using the Helmholtz theorem for two-dimensional vector field $\mathbf{V}_h$ as:

$$\mathbf{V}_h = \mathbf{V}_R + \mathbf{V}_D = \mathbf{k} \otimes \nabla\psi + \nabla\chi \tag{2.20}$$

where $\psi$ is the streamfunction and $\chi$ the velocity potential. We then employ test functions similar with those presented in the previous subsection, for use as streamfunction or velocity potential, and we develop analytically the corresponding zonal and meridional wind components in polar coordinates. We will use a signal corresponding to either a pure rotational or divergent large-scale motion, and then add to it a small-scale noise that is also either rotational or divergent.

### 2.4.1 Application of the filter for vectors on a uniform polar grid

The filter's ability for application to vectors was tested first on a uniform polar grid. We verified the performance of the convolution filter representing a large-scale wind field, considered as analytical solution, a perturbed wind field created by adding a noise to the analytic wind field, and the filtered wind field that must be identical with the analytical solution if the filter works properly.

For the first test shown in the Fig. 2.10, a streamfunction represented by a double cosine with wavelengths of 20,000 km is used to define a purely rotational large-scale wind field. To this large-scale signal we added a small-scale noise in the form of double cosines with wavelengths of 500 km, either as divergent wind (middle left panel) or as rotational wind (bottom left panel). We chose a convolution filter with a weighting function characterized by $\begin{cases} L_a = 3{,}000\,\text{km} \\ L_b = 800\,\text{km} \end{cases}$ and a truncation distance of 1,100 km. The filtered fields (shown in the right panels of Fig. 2.10) show that the large-scale signal is preserved and the noise removed.

A similar experience was repeated, but now using a velocity potential function represented by double cosines with wavelengths of 20,000 km that define a purely divergent large-scale signal wind (upper panel of Fig. 2.11). Again small-scale noises in the form of double cosines with wavelengths of 500 km were added, as a divergent

wind noise in the middle left panel of Fig. 2.11 and as a rotational noise in the bottom panel of Fig. 2.11. We chose a convolution filter with weighting function characterized by $\begin{cases} L_a = 3{,}000\,\text{km} \\ L_b = 600\,\text{km} \end{cases}$ and a truncation distance of $900\,\text{km}$. As shown in Fig. 2.11 the filtered fields (right panels) are similar with the initial large-scale field represented in the upper panel.

The tests presented in Fig. 2.10 and Fig. 2.11 used test fields developed analytically from large-scale double cosines located specifically such as to have not zero winds at the pole. Numerically the pole is considered as $\left(r_1, \lambda_j\right)$ with $j = 1,\ldots,m$ and the convolution filter is applied there as for all other grid-points. The tests revealed that the convolution filter works properly in the vicinity of the pole, and the large-scale fields are recovered without distortions near the pole.

These two experiments were repeated for a large-scale signal represented by streamfunction or velocity potential in form of cylindrical harmonics with Bessel function of the first kind.

In Fig. 2.12 in the upper panel we show a pure rotational wind field developed from a large-scale cylindrical harmonic as streamfunction with radial wavenumber $k_l = 1$ and azimuthal wavenumber $l_l = 2$. As before this large-scale field is perturbed by either a pure divergent or a pure rotational wind noise developed from a small-scale double cosine as velocity potential or streamfunction fields with wavelengths of $500\,\text{km}$. The convolution filter uses the same weighting function and truncation distance as for the examples presented in Fig.2.10. Again we note in the right panels that, after the application of the filter, the noise is removed and the filtered fields recover the analytical solution shown in the upper panel.

We repeated the same experiment for an initial pure divergent wind field developed from a large-scale cylindrical harmonic as velocity potential field with

radial wavenumber $k_l = 1$ and azimuthal wavenumber $l_l = 2$ (Fig. 2.13 upper panel). This field is perturbed either by a pure divergent or a pure rotational noise created from small-scale fields in form of double cosines with wavelengths of 500 km (Fig. 2.13 middle and bottom left panels). We used a convolution filter that uses the same weighting function and truncation distance as in Fig. 2.11. We remark in the middle and bottom right panels of Fig. 2.13 that the noise is removed and the large-scale signal is recovered.

To quantitatively assess the performance of the filter when is applied for vector fields, we employ the *Wind_RMS* score calculated as:

$$Wind\_RMS = \sqrt{\frac{\left|\overline{\mathbf{V}} - \mathbf{V}_l\right|^2}{\left|\mathbf{V}_l\right|^2}} = \frac{\sqrt{\sum_i \sum_j \left[\left(\overline{u}(r_i,\lambda_j) - u_l(r_i,\lambda_j)\right)^2 + \left(\overline{v}(r_i,\lambda_j) - v_l(r_i,\lambda_j)\right)^2\right] \cdot s(r_i,\lambda_j)}}{\sqrt{\sum_i \sum_j \left[\left(u_l(r_i,\lambda_j)\right)^2 + \left(v_l(r_i,\lambda_j)\right)^2\right] \cdot s(r_i,\lambda_j)}} \tag{2.21}$$

where $\mathbf{V} = \mathbf{V}_l + \mathbf{V}_n$, $\mathbf{V}_l$ represents the large-scale wind vector or the expected analytical solution, $\mathbf{V}_n$ represents the small-scale wind vector or the noise that will be removed, and $\overline{\mathbf{V}}$ is the filtered wind vector solution.

Figure 2.14 shows the *Wind_RMS* score as function of truncation distance for convolution filters using different values of $L_a$ and $L_b$ in the weighting functions. These tests were carried out with a test-wind field composed of a large-scale purely divergent wind with wavelengths of 20,000km and small-scale rotational noise with wavelengths of 500km. Panel a) shows results obtained with various values of $L_b$, using $L_a$ = 3,000km:

$$w1:\begin{cases} L_a = 3{,}000\,\text{km} \\ L_b = 1{,}000\,\text{km} \end{cases},\ w2:\begin{cases} L_a = 3{,}000\,\text{km} \\ L_b = 800\,\text{km} \end{cases} \text{ and } w3:\begin{cases} L_a = 3{,}000\,\text{km} \\ L_b = 600\,\text{km} \end{cases}.$$

We note that beyond a certain truncation distance, the error is smaller than 0.4% of the error obtained when the truncation distance is very small. As was to be expected the convergence is faster for convolutions with narrower weighting functions such as $w2$ and $w3$. The next tests shown in panel b) were obtained using $L_b = 600\,\text{km}$ with various values of $L_a$:

$$w3:\begin{cases} L_a = 3{,}000\,\text{km} \\ L_b = 600\,\text{km} \end{cases},\ w4:\begin{cases} L_a = 2{,}600\,\text{km} \\ L_b = 600\,\text{km} \end{cases} \text{ and } w5:\begin{cases} L_a = 2{,}200\,\text{km} \\ L_b = 600\,\text{km} \end{cases}.$$

The errors show relative insensitivity to changing $L_a$. We hypothesise that this reflects the fact that the error also contains a contribution from disturbing the large-scale signal.

In order to test this hypothesis we compare the performance of filters using the weighting functions $w1$ and $w4$ that have the same attenuation wavelength bandwidth $L_a - L_b = 2{,}000\,\text{km}$. Test-functions similar to those in the previous tests were used, but with two different large-scale signal characterized by $L_{l_1} = 16{,}000\,\text{km}$ and $L_{l_2} = 12{,}000\,\text{km}$, and small-scale noise with $L_n = 500\,\text{km}$. The resulting *Wind_RMS* score is represented in Fig. 2.15. It is evident that $w4$ performs better, and both filters are more effective for larger scale signals $L_{l_1} = 16{,}000\,\text{km}$. We note that the curves obtained with $w1$ weighting function exhibit larger oscillations, but they eventually decreases towards zero for larger truncation distance (around 2,200 km).

### 2.4.2 Application of the filter for vectors on a variable polar grid

We proceed to tests on a stretched grid, using wind field test functions similar to those used on the uniform polar grid, in order to check the skill of the filter to remove the noise outside of the uniform high-resolution domain. The test functions are composed of a large-scale wind field, which is either purely rotational or purely divergent wind developed analytically from a streamfunction or a velocity potential in form of double cosines in physical space or cylindrical harmonics, with a wavelength $L_l$, and a small-scale field that is either rotational or divergent developed similarly to the large-scale field but with wavelength $L_n$. This small-scale field is gradually added in the stretching zones where it will be interpreted as noise, and in the uniform high-resolution area where it will be part of the signal and represents the added value of using variable resolution; therefore in this latter region the filter will not be applied.

Figure 2.16 shows a large-scale purely rotational wind field with $L_l = 20{,}000\text{km}$ (upper panel) perturbed by divergent or rotational small-scale fields (left middle and bottom panels) with $L_n = 400\text{km}$. The filter uses a weighting function defined by $w: \begin{cases} L_a = 3{,}000\text{km} \\ L_b = 1{,}000\text{km} \end{cases}$ and a truncation distance of $2{,}000\,\text{km}$. Because we apply the filter only outside the uniform high-resolution area, and to better display the effect of the filter in the stretching zones, we only present the test-function outside the uniform high-resolution zone. Visually we observe that the convolution filter is able to remove the noise, and after the application of the filter, the large-scale signal is recovered.

A second test presented in Fig. 2.17 used a test function composed of a large-scale purely divergent wind with $L_l = 20{,}000\text{km}$ (upper panel) perturbed by divergent or rotational small-scale fields (left middle and bottom panels) with $L_n = 400\text{km}$. For this test we employed a weighting function with parameters

$w:\begin{cases} L_a = 3{,}000\text{km} \\ L_b = 600\text{km} \end{cases}$ and a truncation distance of 900 km. This distance is sufficient to completely remove the noise because the weighting function corresponds to a smoother theoretical response and $L_n < L_b$. Again no deformations were noted around the high-resolution domain and the filter works properly in the stretching zones as well as around the pole.

Next the experiments will use different large-scale wind fields. In Fig. 2.18 the large-scale field is defined by a purely rotational wind developed from a cylindrical harmonic as streamfunction with radial wavenumber 1 and azimuthally wavenumber 2. The small-scale fields are similar with those used in Fig. 2.16. A weighting function with parameters $w:\begin{cases} L_a = 1{,}800\text{km} \\ L_b = 600\text{km} \end{cases}$ will need, in this case, a truncation distance of 1,200 km in order to remove the noise. After the application of the filter the resulting wind field (right panels) looks similar to the initial large-scale wind field presented in the upper panel.

Finally Fig. 2.19 shows a purely divergent wind field built from a velocity potential function in form of cylindrical harmonic with radial wavenumber 1 and azimuthally wavenumber 2 (upper panel), and perturbed by small-scale fields similar with those used in Fig. 2.17, using a weighting function with parameters $w:\begin{cases} L_a = 1{,}000\text{km} \\ L_b = 600\text{km} \end{cases}$. This weighting function has a broad footprint because it corresponds to a relatively abrupt response function (only 400 km between $L_a$ and $L_b$) and, for this reason, it needs a truncation distance of 1,800 km to remove the noise. The results show suitable performance, with the initial large-scale signal being recovered and no apparent deformations of the wind fields in the stretching regions.

The performance of the filter in removing noise for vector quantities on the stretched polar grid will be quantified using the *Wind_RMS* score calculated over the entire grid or separately in the stretching zones or the low-resolution region of the domain. If we consider a wind field composed from a large-scale signal and a noise, then we set up the following notations:

$$\text{for the test field } \mathbf{V} = \begin{cases} \mathbf{V}_{HR} & \text{if} \quad (r,\lambda) \in D_{HR} \\ \mathbf{V}_{SG} & \text{if} \quad (r,\lambda) \in D_{SG} \\ \mathbf{V}_{LR} & \text{if} \quad (r,\lambda) \in D_{LR} \end{cases},$$

$$\text{and for the filtered field } \overline{\mathbf{V}} = \begin{cases} \mathbf{V}_{HR} & \text{if} \quad (r,\lambda) \in D_{HR} \\ \overline{\mathbf{V}}_{SG} & \text{if} \quad (r,\lambda) \in D_{SG} \\ \overline{\mathbf{V}}_{LR} & \text{if} \quad (r,\lambda) \in D_{LR} \end{cases}.$$

We computed the *Wind_RMS* score considering the analytical solution:

$$\mathbf{V}_{as} = (u_{as}, v_{as}) = \begin{cases} \mathbf{V}_{HR} & \text{if} \quad (r,\lambda) \in D_{HR} \\ \mathbf{V}_{l} & \text{for all other } (r,\lambda) \end{cases}.$$

For the stretched grid three score will be calculated following the next relationships:

$$Wind\_RMS = \sqrt{\frac{\left|\overline{\mathbf{V}} - \mathbf{V}_{as}\right|^2}{\left|\mathbf{V}_l\right|^2}}$$

$$= \frac{\sqrt{\sum_i \sum_j \left[ \left( \overline{u}(r_i,\lambda_j) - u_{as}(r_i,\lambda_j) \right)^2 + \left( \overline{v}(r_i,\lambda_j) - v_{as}(r_i,\lambda_j) \right)^2 \right] \cdot s(r_i,\lambda_j)}}{\sqrt{\sum_i \sum_j \left[ \left( u_l(r_i,\lambda_j) \right)^2 + \left( v_l(r_i,\lambda_j) \right)^2 \right] \cdot s(r_i,\lambda_j)}},$$

$$Wind\_RMS\_SG = \sqrt{\frac{\left|\overline{\mathbf{V}}_{SG} - \mathbf{V}_{as}\right|^2}{\left|\mathbf{V}_I\right|^2}}$$

$$= \frac{\sqrt{\sum_{(r_i,\lambda_j)\in D_{SG}} \sum \left[\left(\overline{u}_{SG}(r_i,\lambda_j) - u_{as}(r_i,\lambda_j)\right)^2 + \left(\overline{v}_{SG}(r_i,\lambda_j) - v_{as}(r_i,\lambda_j)\right)^2\right] \cdot s(r_i,\lambda_j)}}{\sqrt{\sum_i \sum_j \left[\left(u_I(r_i,\lambda_j)\right)^2 + \left(v_I(r_i,\lambda_j)\right)^2\right] \cdot s(r_i,\lambda_j)}} \quad \text{and}$$

$$Wind\_RMS\_LR = \sqrt{\frac{\left|\overline{\mathbf{V}}_{LR} - \mathbf{V}_{as}\right|^2}{\left|\mathbf{V}_I\right|^2}}$$

$$= \frac{\sqrt{\sum_{(r_i,\lambda_j)\in D_{LR}} \sum \left[\left(\overline{u}_{LR}(r_i,\lambda_j) - u_{as}(r_i,\lambda_j)\right)^2 + \left(\overline{v}_{LR}(r_i,\lambda_j) - v_{as}(r_i,\lambda_j)\right)^2\right] \cdot s(r_i,\lambda_j)}}{\sqrt{\sum_i \sum_j \left[\left(u_I(r_i,\lambda_j)\right)^2 + \left(v_I(r_i,\lambda_j)\right)^2\right] \cdot s(r_i,\lambda_j)}} \cdot$$

These tests performed for vectors on the stretched grid used a test-wind field composed of a large-scale purely divergent wind with wavelengths of 20,000 km and small-scale rotational noise with wavelengths of 400 km. The same three weighting function as for the uniform polar grid were employed, characterized by:

$$w1: \begin{cases} L_a = 3{,}000\,\text{km} \\ L_b = 1{,}000\,\text{km} \end{cases}, \quad w2: \begin{cases} L_a = 3{,}000\,\text{km} \\ L_b = 800\,\text{km} \end{cases} \text{ and } \quad w3: \begin{cases} L_a = 3{,}000\,\text{km} \\ L_b = 600\,\text{km} \end{cases}.$$

The scores are represented as function of the truncation distance with values between 200 km and 2,200 km. The *Wind_RMS* score for the entire domain is represented in Fig. 2.20a. We can remark that the error decreases gradually to zero as the truncation distance increases. This error begins to stabilize after 900 km if the weighting function $w3$ is used, after 1,500 km if the weighting function $w2$ is used, and after 2,000 km if the weighting function $w1$ is used. As is to be expected, the required truncation distance is function of the width of the weighting function

footprint, which is the largest for $w1$ and the narrowest for $w3$. After the truncation distance reaches large values, the errors decrease to less than 0.4% of the error when the truncation distance is small.

The convolution filter applied on a variable polar grid must remove the noise outside the uniform high-resolution area. The filtering error represents the effect of the filter operator on the signal in the stretching zones and in the uniform low-resolution domain. For this reason we represent the error separately in the stretching domain (the *Wind_RMS_SG* score) and in the uniform low-resolution domain (the *Wind_RMS_LR* score). The curve *Wind_RMS_SG* represented in Fig. 2.20b has similar shape with the curve *Wind_RMS* and the errors stabilize after the same truncation distance is reached. This means that the most important part of the error results from the application of the filter in the stretching area. After the stabilization of the error this is about 0.3% of the error calculated if the truncation distance is small, so we conclude that about 75% of the total error derives from the stretching area. The last curve represented in Fig. 2.20c shows the effect of the convolution filter on the large-scale signal. Because the small-scale signal is introduced gradually in the stretching domain and in the uniform high-resolution domain, the only signal represented in the low-resolution area is the large scale one. Inspecting the shape of the *Wind_RMS_LR* curve we remark that for the weighting function $w3$ this is almost flat, meaning that in this case the filter does not affect the large-scale signal. This weighting function has the narrowest footprint corresponding to the smoother spectral response (the attenuation bandwidth is 2,400 km). If the attenuation bandwidth is decreased, so the spectral response is less smooth, then the weighting function has a lager footprint and it needs a larger truncation distance in order to provide a good filter response. It is explained by the oscillations that appear on the *Wind_RMS_LR* curve shape for $w2$ and $w1$. As in the previous cases, the errors stabilize after the same truncation distance is reached. The values of *Wind_RMS_LR* score are close to zero for large truncation distances, but there is always a small difference of 0.2%

from the initial error, which can be explained by unavoidable numerical approximations due to the application of the filter on the variable mesh.

## 2.5 Conclusion

The approach of variable resolution has proven to be a viable alternative solution to nested limited-area models for regional climate modelling. Gradually varying resolution of the stretched grid away from the area of interest reduces the computational noise, but it does not resolve the issue of the anisotropy of the grid outside the uniform high-resolution zone.

An adequate filtering technique designed for variable stretched grid can be a powerful tool to control small scales improperly represented outside the high-resolution region of the interest zone. The so-called "arms of the cross" regions are characterized by differences between grid-points spacing in latitudinal and longitudinal directions, which may induce all sorts of numerical artefacts as well as make difficult the parameterisation of subgrid-scale physical processes.

A convolution filter developed by SLI1 was here adapted in this study for polar geometry. The convolution filter uses a weighting function that is the inverse Fourier transform of the desired response function in one dimension. In practice the convolution can be truncated at some finite distance, where the weighting function becomes sufficiently small, which reduces substantially the computational cost, especially in two dimensions. The main ingredient of this convolution filter is its formulation based on physical distance rather than on grid-point distances. Being independent on the underlying grid structure, this filter provides an almost isotropic response, which can conveniently be used by a user to control small-scale noise outside the uniform high-resolution area. The application of this filter for a polar grid can also naturally handle the "pole problem" characteristic of all spherical grids.

In the first part of the paper, the mathematical formulation for the convolution filter adapted for 2D polar geometry was described. We found that for application on a polar grid, the 2D convolution could be conveniently cast into the successive applications of 1D convolution in radial and azimuthal directions.

The second part of the paper presented applications in 2D uniform and variable stretched grids. The convolution filter adapted for polar geometry could be applied for scalar variables to resolve the anisotropy of the computational stretched grid or for the pole problem. Choosing cylindrical harmonics or double cosines signals as test-functions, we showed that weighting functions could be designed to remove specific noises. This is an important point in the design of this filter operator because it can resolve at the same time both problems mentioned earlier, without the necessity of changing the filter formulation to respond of a certain type of noise. In order to save on computations, the convolution can be truncated at some finite distance where the weighting function becomes sufficiently small, resulting then in an approximate response. Tests have revealed that the error decreases for larger truncation distances and that the filter conserves approximately the filtered quantities.

It is a common practice to filter the fields (or sometimes their tendencies) in order to remove high wavenumbers that otherwise will affect the accuracy of a climate model. Generally these damping methods are applied to variables such as temperature, pressure and humidity, and if filtering is needed for momentum, it is generally applied to corresponding scalar quantities such as streamfunction and velocity potential, or vorticity and divergence. In our study we proceed to the filtering the wind vectors themselves. The filter is applied simultaneously for both wind components and the convolution is applied successively in radial and azimuthally directions. With appropriate definition constraints and representing the winds components for all points contributing to the convolution relative to the same

reference system as the application point, we were able to remove small-scale noise superimposed on large-scale signals.

In conclusion, the proposed filtering approach appears to be an attractive alternative to conventional grid-point based smoothing operator for stretched-grid models. Its versatility, applicability for all variables of a model, and filtering for different purposes, such as removing the anisotropy of a variable grid or resolving the pole problem, offers an attractive possibility to adapt this approach for spherical variable-resolution global climate models.

*Acknowledgments*

This research was done as part of the Doctoral project of the first author and as a project within the Canadian Regional Climate Modelling and Diagnostics (CRCMD) Network, funded by the Canadian Foundation for Climate and Atmospheric Sciences (CFCAS), the Ouranos Consortium for Regional Climatology and Adaptation to Climate Change, and National Centre of Excellence (NCE) Mathematics of Information Technology and Complex Systems (MITACS). Ouranos also provided office space and computational resources during a large part of this work.

# References

Bowman, F., 1958: Introduction to Bessel functions, Dover Publications Inc., New York, 135 pp.

Caya, D._and R. Laprise, 1999: A semi-Lagrangian semi-implicit Regional Climate Model: The Canadian RCM. *Mon. Wea. Rev.*, **127**, 341-362.

Christensen, O. B., J. H. Christensen, B. Machenhauer and M. Botzet, 1998: Very-High-Resolution Regional Climate Simulations over Scandinavia. Present Climate. *J. Climate*, **11**, 3204-3229.

Côté, J., 1988: A Lagrange multiplier approach for the metric terms of semi-Lagrangian models on the sphere. *Quart. J. Roy.Meteor. Soc.*, **114**, 1347-1352.

Côté, J., S. Gravel, A. Méthot, A. Patoine, M. Roch and A. Staniforth, 1997: Preliminary results from a dry global variable-resolution primitive equations model. *Numerical methods in Atmospheric and Oceanic Modelling: The André J. Robert Memorial Volume*. C. Lin, R. Laprise and H. Richie (eds.), CMOS, Ottawa, Canada, 245-259.

Côté, J., S. Gravel, A. Méthot, A. Patoine, M. Roch and A. Staniforth, 1998: The operational CMC-MRB Global Environmental Multiscale (GEM) Model. Part I : Design considerations and formulation. *Mon. Wea. Rev.*, **126**, 1373-1395.

Déqué, M. and J. P. Piédelièvre, 1995: High resolution climate simulation over Europe. *Climate Dyn.*, **11**, 321-339.

Döscher, R., U. Willén, C. Jones, A. Rutgersson, H. E. M. Meier, U. Hansson and P. Graham, 2002: The development of the coupled ocean-atmosphere model RCAO. *Boreal Env. Res.*, **7**, 183–192.

Fox-Rabinovitz, M.S., G. L. Stenchikov, M. J. Suarez and L.L. Takacs, 1997: A finite-difference GCM dynamical core with a variable resolution stretched-grid. *Mon. Wea. Rev.*, **125**, 2943-2968.

Fox-Rabinovitz, M., J. Côté, B. Dugas, M. Déqué and J.L. McGregor, 2006: Variable resolution General Circulation Models: Stretched-Grid model intercomparison project (SGMIP). *J. Geophys. Res.*, **111**, D16104, doi:10.1029/2005JD006520.

Fox-Rabinovitz, M., J. Côté, B. Dugas, M. Déqué, J.L. McGregor and A. Belochitski, 2008: Stretched-grid Model Intercomparison Project: Decadal regional climate simulations with enhanced variable and uniform-resolution GCMs. *Meteor. Atmos. Phys.*, **100**, 159-177.

Giorgi, F., and G.T. Bates, 1989: The climatological skill of a regional model over complex terrain. *Mon. Wea. Rev.*, **117**, 2325-2347.

Hortal, M., and A. J. Simmons, 1991: Use of reduced Gaussian grids in spectral models. *Mon. Wea. Rev.*, **119**, 1057-1074.

IPCC, 2007: Climate Change 2007: The Physical Science Basis. Contribution of Working Group I to the Fourth Assessment Report of the Intergovernmental Panel on Climate Change [Solomon, S., D. Qin, M. Manning, Z. Chen, M. Marquis, K.B. Averyt, M. Tignor and H.L. Miller (eds.)]. Cambridge University Press, Cambridge, United Kingdom and New York, NY, USA, 996 pp.

Jacob D., 2001: A note to the simulation of the annual and inter-annual variability of the water budget over the Baltic Sea drainage basin. *Meteorol. Atmos. Phys.*, **77**, 61-73.

Laprise R., 2008: Regional climate modelling. *J. Comput. Phys.*, **227**, 3641-3666.

McGregor, J. L. and M. R. Dix, 1997: Development of a global conformal-cubic primitive equations model. *Research Activities in Atmopheric and Oceanic Modelling*, **25**, A. Staniforth (ed.), WMO/TD-792, 3.27 – 3.28.

McGregor, J. L. and M. R. Dix, 2001: The CSIRO conformal-cubic atmospheric GCM, *IUTAM Symposium on Advances in Mathematical Modelling of Atmosphere and Ocean Dynamics*, P. F. Hodnett (ed.), Kluwer Academic Publishers, 197-202.

Pielke, R.A., W. R. Cotton, R. L. Walko, C. J. Trembaek, W. A. Lyons, L. D. Grasso, M. E. Nieholls, M. D. Moran, D. A. Wesley, T. J. Lee and J. H. Copeland, 1992 : A comprehensive meteorological modeling system—RAMS. *Meteor. Atmos. Phys.*, **49**, 69-91.

Purser R. J., 1988: Degradation of numerical differencing caused by Fourier filtering at high latitudes. *Mon. Wea. Rev.*, **116**, 1057-1066.

Sardeshmukh, P.D., and B. I. Hoskins, 1984: Spatial Smoothing on the Sphere. *Mon. Wea. Rev.*, **112**, 2524-2529.

Skamarock, W. C., and J. B. Klemp, 2008: A time-split nonhydrostatic atmospheric model for research and NWP applications. *J. Comp. Phys.*, **227**, special issue on environmental modeling, 3465–3485.

Surcel, D., 2005: Filtres universels pour les modèles numériques à résolution variable. Mémoire de maîtrise en Sciences de l'atmosphère, Département des Sciences de la Terre et de l'Atmosphère, Université du Québec à Montréal, 105 pp.

Surcel, D., and R. Laprise, 2011: A General Filter for Stretched-Grid Models: Application in Cartesian Geometry. *Mon. Wea. Rev.* **139**, 1637-1653

Zhang, H., and M. Rancic, 2005: A Global Eta Model on Quasi-uniform Grids. *Quart. J. Roy. Meteor. Soc.*, **133**, 517-528.

Wang, Y., 2001: An explicit simulation of tropical cyclones with a triply nested movable mesh primitive equation model: TCM3. Part I: Model description and control experiment. *Mon. Wea. Rev.*, **129**, 1370–1394.

Williamson, D., and R. Laprise, 2000: Numerical approximations for global atmospheric General Circulation Model, *Numerical modeling of global atmosphere in the climate system*, P. Mote and A. O'Neil (eds.) Kluwer Academic Publishers, 127-219.

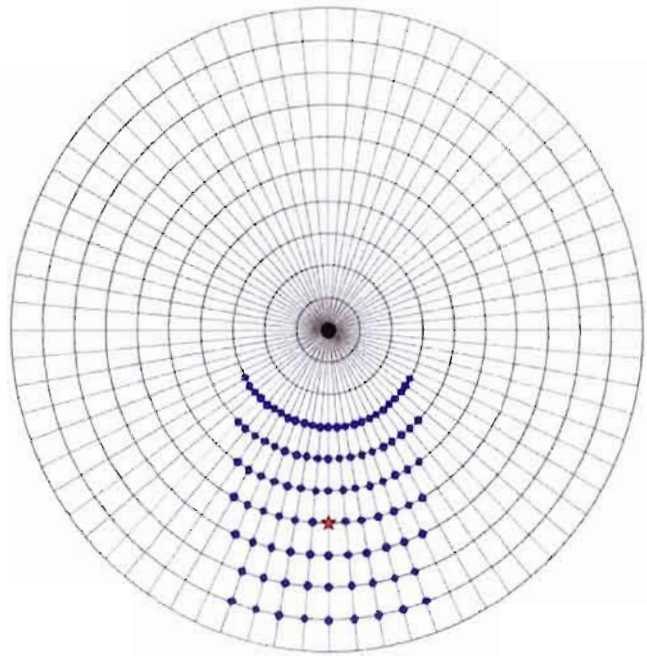

Figure 2.1 Simplified sketch showing a typical uniform polar grid. The red star represents the grid-point where the filter is applied and the blue circles the grid points contributing to the convolution.

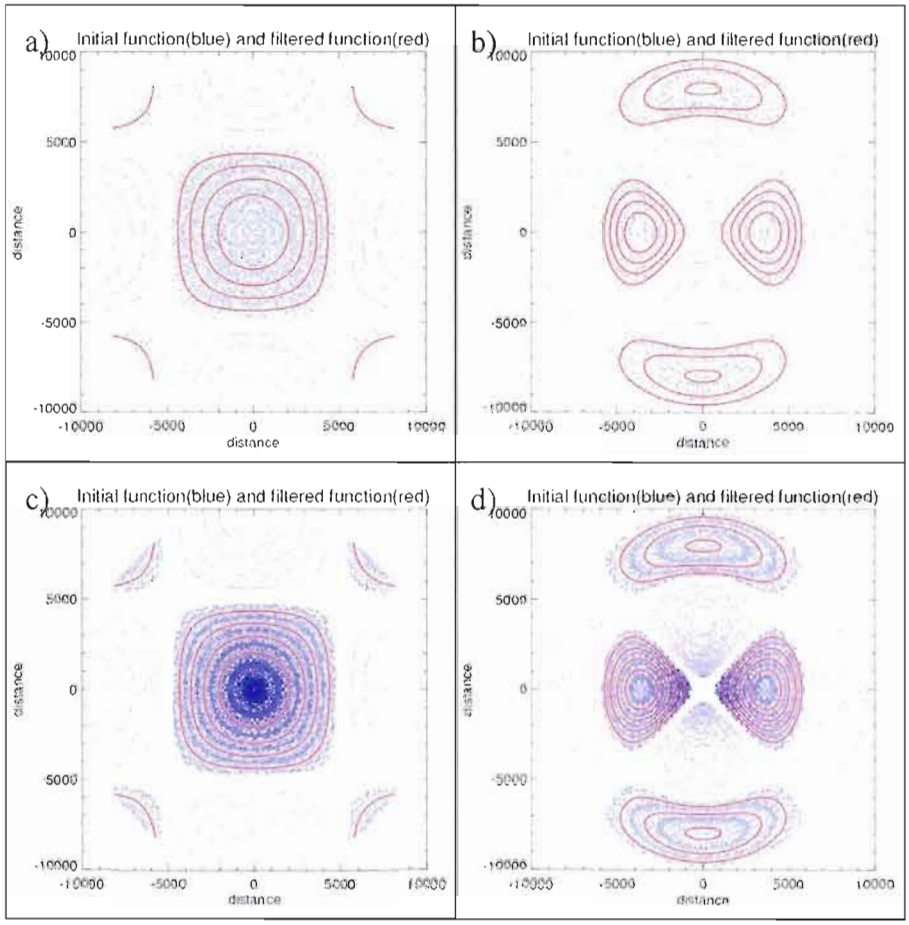


Figure 2.2 a) An initial function shown in blue was composed of a large-scale signal defined as double cosine with $L_l = 20{,}000\text{km}$ and a small-scale noise in form of a double cosine with $L_n = 500\text{km}$; the resulting filtered function is represented in red. The weighting function used in the convolution aimed at keeping all waves larger than 2,400 km and removing all waves smaller than 800 km. The truncation distance was chosen as $d_{\max} = 1{,}600\text{km}$. b) An initial function shown in blue was composed of a large-scale cylindrical harmonics with $k_l = l_l = 2$ and a small-scale noise in form of a double cosine with $L_n = 600\text{km}$; the filtered function is represented in red. The weighting function used in the convolution kept all waves larger than 2,400 km and removed all waves smaller than 1,000 km. The truncation distance was $d_{\max} = 2{,}300\text{km}$. c) The initial function is composed from the large-scale signal identical to that used in a) but with a random noise. The same weighting function and truncation distance as in a) were used. d) The initial function is composed from the large-scale signal identical to that used in b) but with a random noise. The same weighting function and truncation distance as in b) were used.

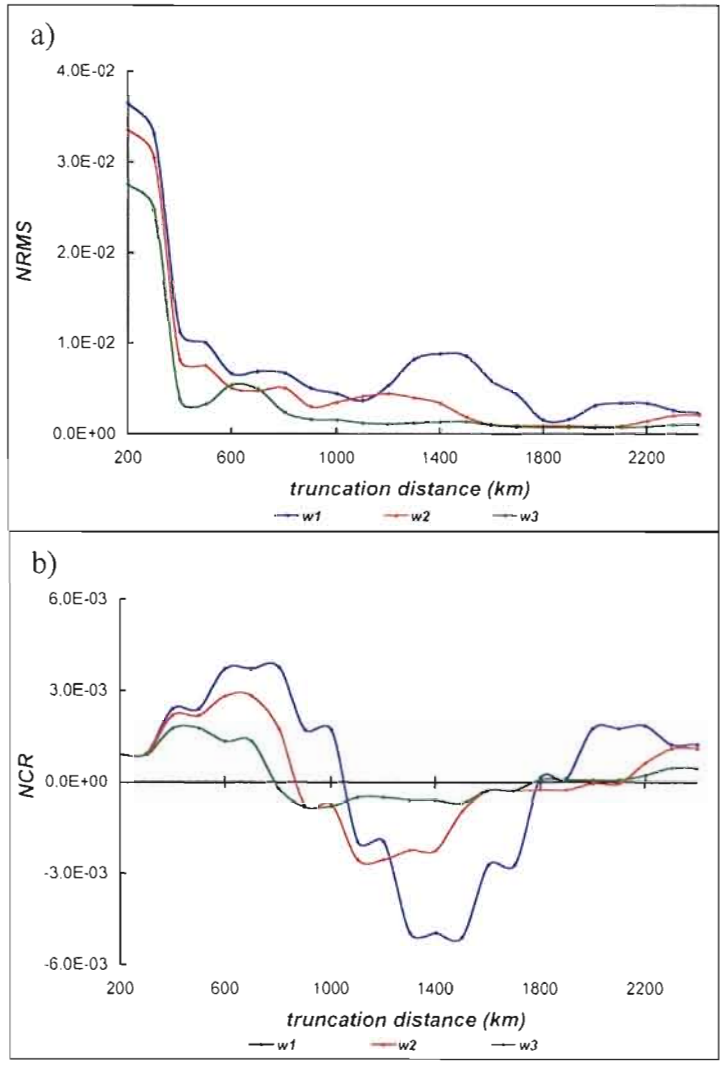


Figure 2.3 The *NRMS* (a) and the *NCR* (b) scores as a function of the truncation distance, for three convolution filters with weighting functions $w1:\begin{cases} L_a = 2{,}400\,\text{km} \\ L_b = 1{,}000\,\text{km} \end{cases}$, $w2:\begin{cases} L_a = 2{,}400\text{km} \\ L_b = 800\text{km} \end{cases}$ and $w3:\begin{cases} L_a = 2{,}400\text{km} \\ L_b = 600\text{km} \end{cases}$, applied on the same test function as in Fig. 2.2a with a noise with $L_n = 500\,\text{km}$.

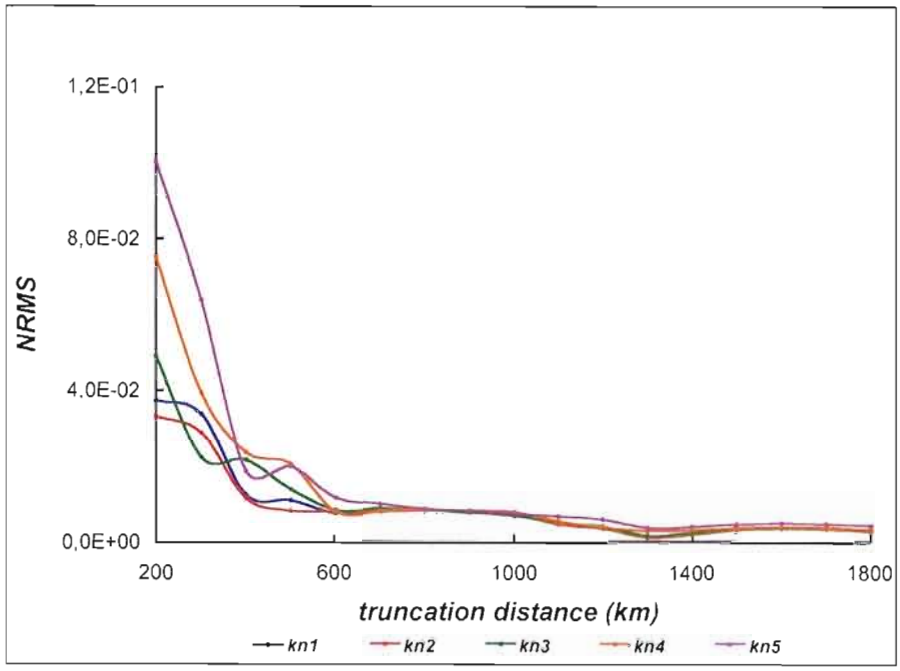


Figure 2.4 The NRMS score as a function of the truncation distance when a filter with a weighting function $w:\begin{cases} L_a = 4{,}000\,\text{km} \\ L_b = 1{,}000\,\text{km} \end{cases}$ is applied for five test-functions containing a small-scale signal with weightlengths of $L_{n_1} = 500\text{km}$, $L_{n_2} = 600\text{km}$, $L_{n_3} = 700\text{km}$, $L_{n_4} = 800\text{km}$ and $L_{n_5} = 900\text{km}$.

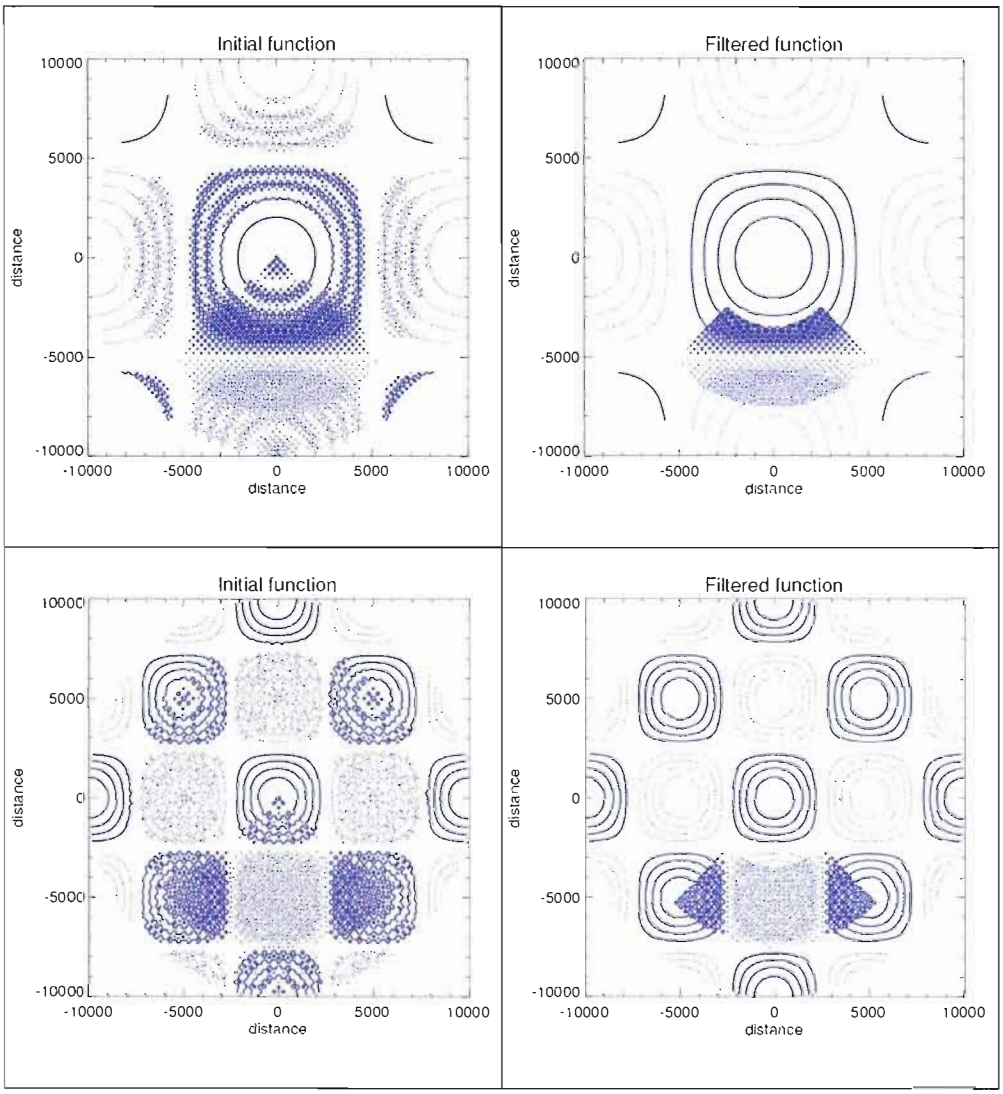


Figure 2.5 The test functions composed of a large-scale cosine as signal and a small-scale cosine as noise are represented on the polar stretched-grid with $S_r \cong S_\lambda \cong 6$ (left panels); the filtered functions are represented in the right panels. In the first case (right upper panel) the convolution filter uses the weighting function $w\left(L_a = 2,400\,\text{km}; L_b = 1,000\,\text{km}\right)$ and a truncation distance of 2,300km to remove a noise with $L_n$ = 400km . In the second case (right bottom panel) the convolution filter uses the weighting function $w\left(L_a = 2,400\,\text{km}; L_b = 600\,\text{km}\right)$ and a truncation distance of 1,000km to remove a noise with $L_n$ = 500km .

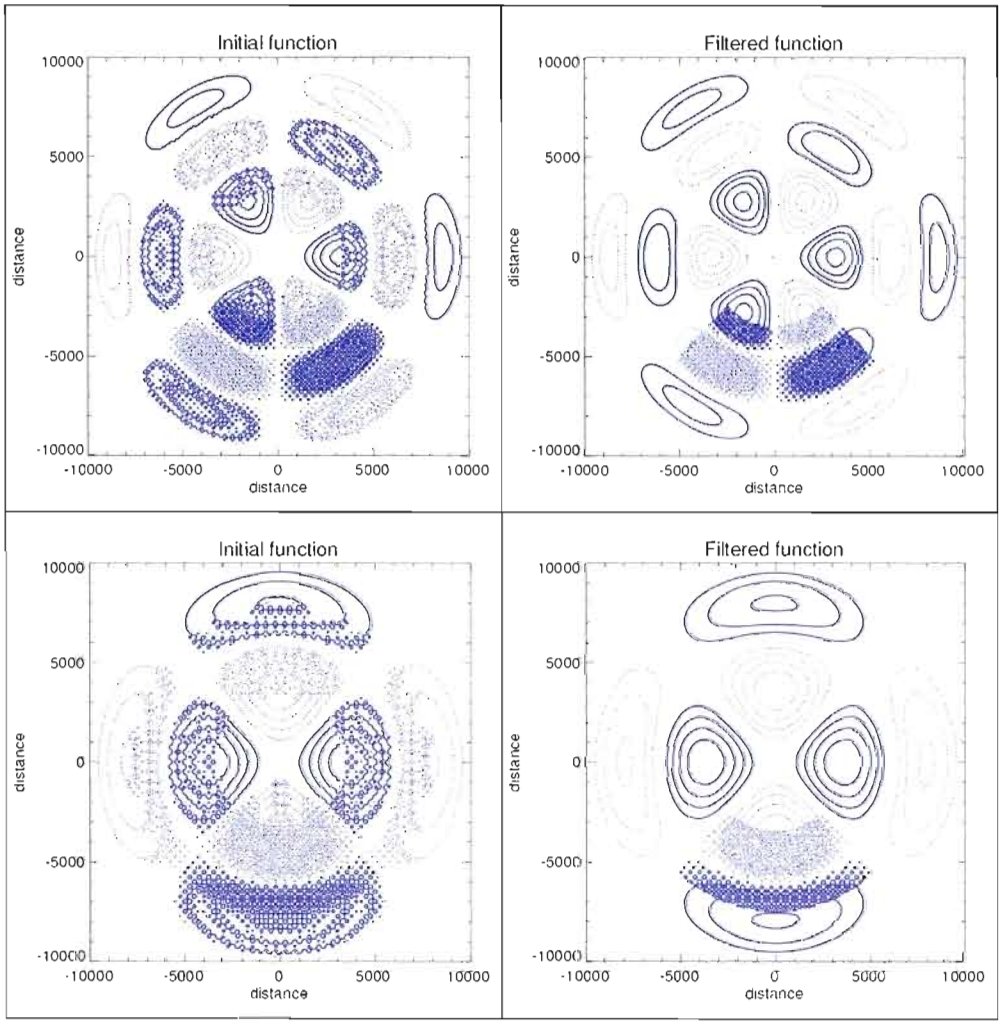


Figure 2.6 The initial test functions composed of a large-scale cylindrical harmonic as signal and small-scale cosines as noises are represented on the polar stretched-grid with $S_r \cong S_\lambda \cong 6$ (left panels); the filtered functions are represented in the right panels. In the first case (right upper panel) the convolution filter uses the weighting function $w\left(L_a = 2{,}400\,\text{km}; L_b = 1{,}000\,\text{km}\right)$ and a truncation distance of 2,300km to remove a noise with $L_n = 400\text{km}$. In the second case (right bottom panel) the convolution filter uses the weighting function $w\left(L_a = 2{,}400\,\text{km}; L_b = 600\,\text{km}\right)$ and a truncation distance of 1,000km to remove a noise with $L_n = 500\text{km}$.

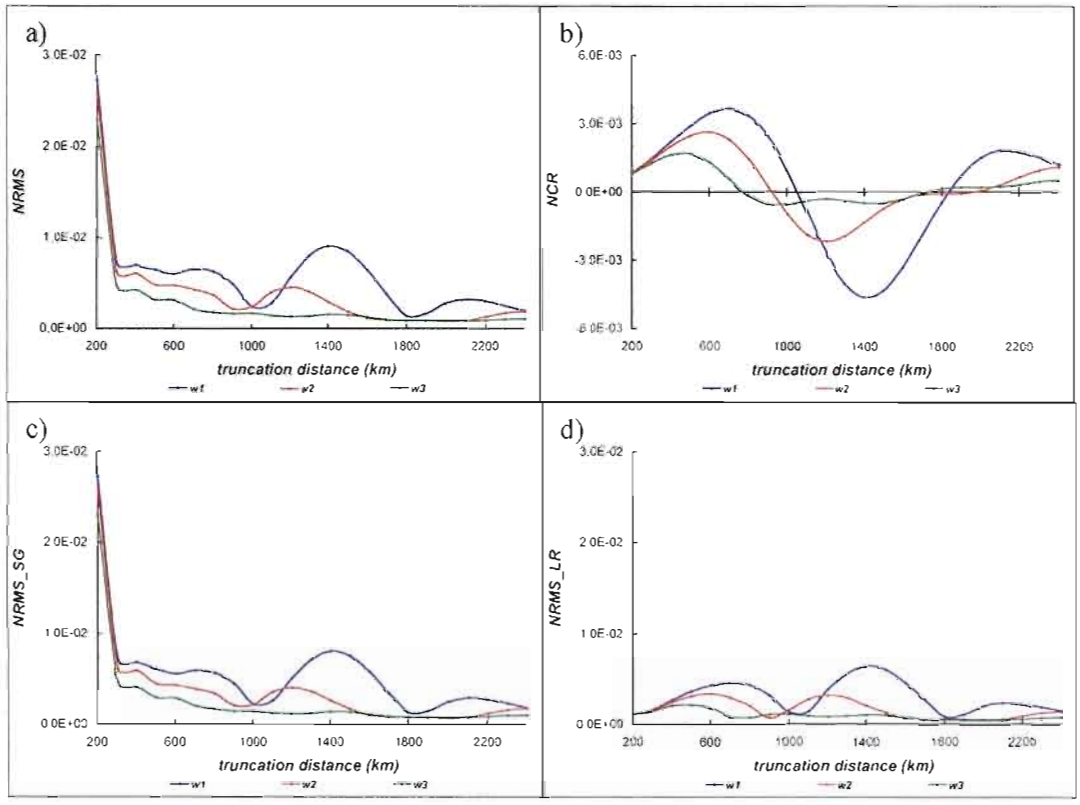


Figure 2.7 The *NRMS* (a) and the *NCR* (b) scores as a function of the truncation distance, for three convolution filters with weighting functions $w1:\begin{cases} L_a = 2{,}400\text{km} \\ L_b = 1{,}000\text{km} \end{cases}$, $w2:\begin{cases} L_a = 2{,}400\text{km} \\ L_b = 800\text{km} \end{cases}$ and $w3:\begin{cases} L_a = 2{,}400\,\text{km} \\ L_b = 600\,\text{km} \end{cases}$ applied on the same test function containing a noise with $L_n = 400\text{km}$ ; c) *The NRMS_SG* score is calculated only in the stretching areas; d) The *NRMS_LR* score is calculated in the uniform low-resolution area.

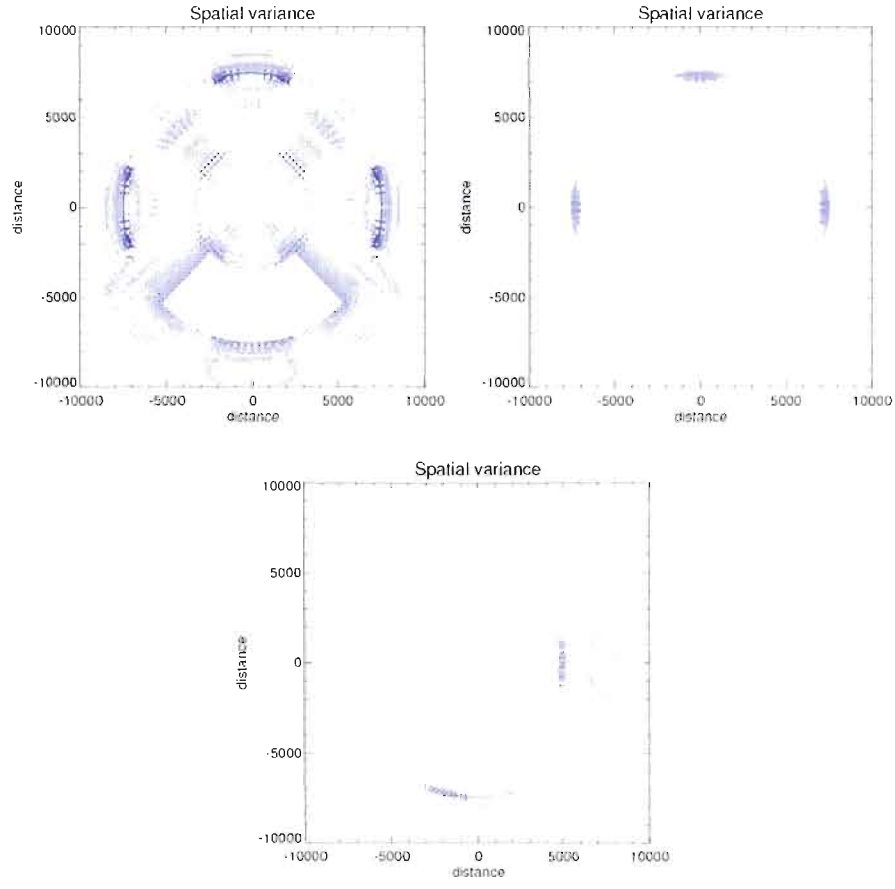


Figure 2.8 The spatial distribution of the quadratic error for the same test as that shown in Fig. 2.5 (left upper panel). The convolution filter used the weighting function $w1:\begin{cases} L_a = 2400\,\mathrm{km} \\ L_b = 1000\,\mathrm{km} \end{cases}$. The quadratic error is shown for three different truncation distances of 400km, 1,000km and 1,400km, respectively.

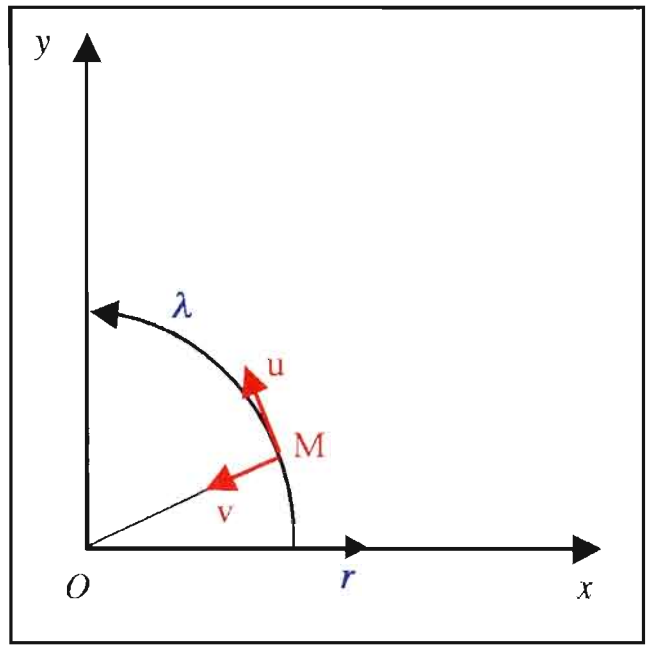


Figure 2.9 The representation of horizontal velocity components in polar coordinates.

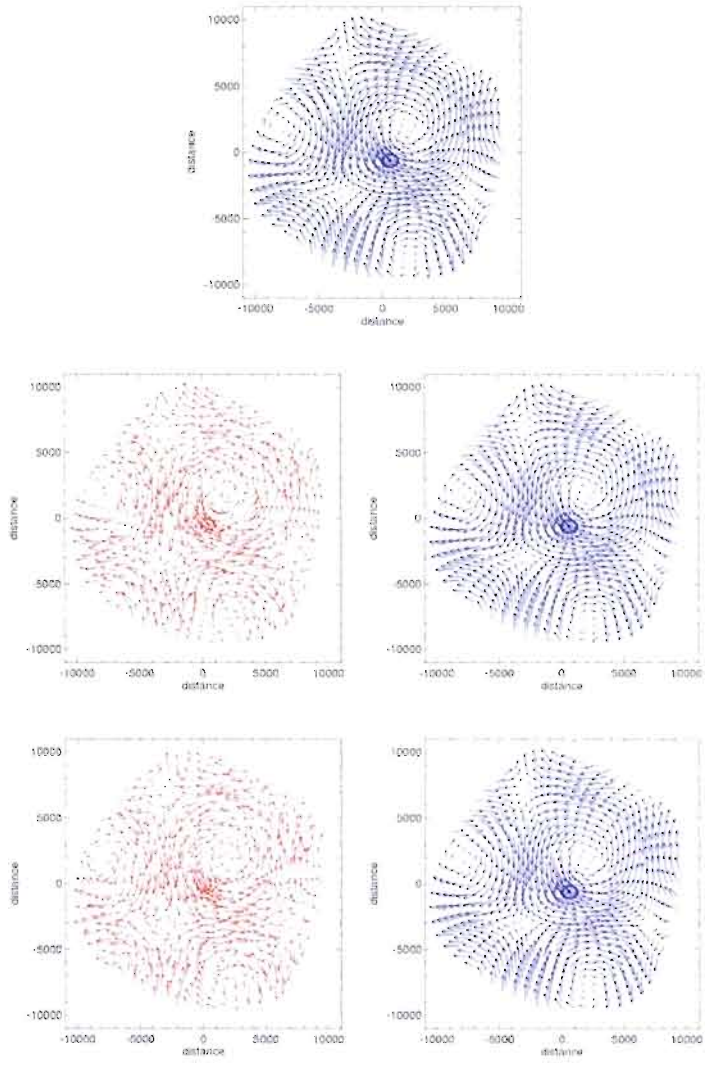


Figure 2.10 The large-scale rotational wind field (upper panel) is perturbed by a small-scale divergent wind field (middle left panel) or by a small-scale rotational wind field (bottom left panel). The filtered fields are represented in the right panels. The large-scale field is built using a scalar cosine function as streamfunction similar with those used when we tested the convolution filter for scalar variables with wavelength $L_l = 20{,}000$ km. For both tests the small-scale-field (the noise) was built using cosine scalar functions as velocity potential or streamfunction with $L_n = 500\text{km}$. For all tests, the convolution filter uses the weighting function $w\left(L_a = 3{,}000\,\text{km}; L_b = 800\,\text{km}\right)$ and a truncation distance of 1,100 km.

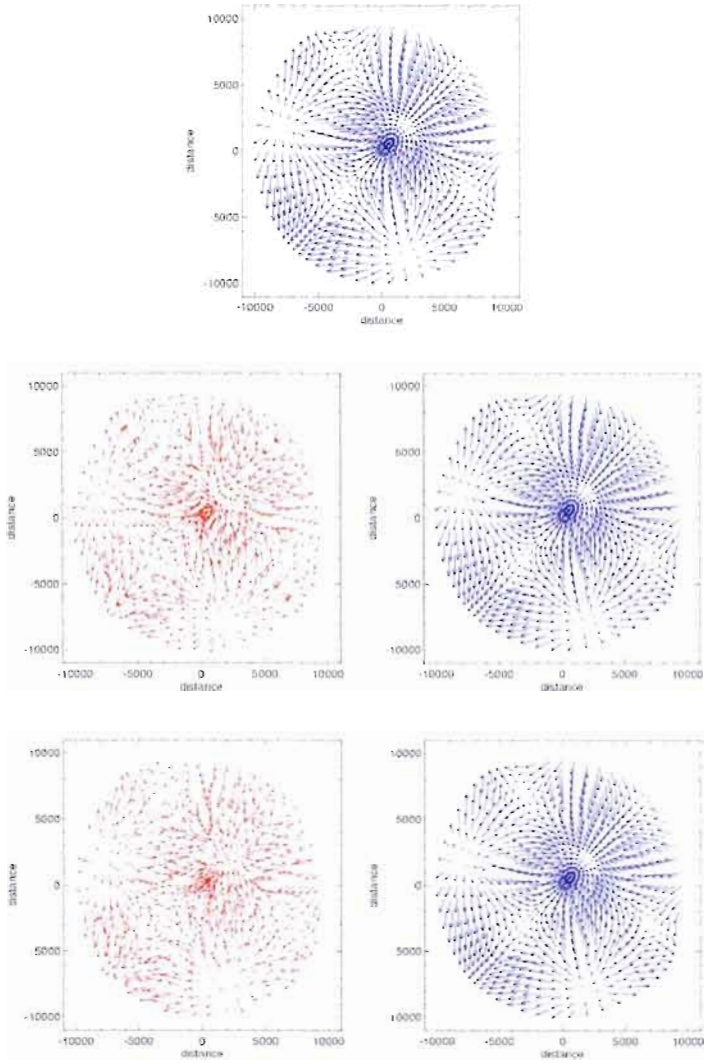


Figure 2.11 The large-scale divergent wind field (upper panel) is perturbed by a small-scale divergent wind field (middle left panel) or by a small-scale rotational wind field (bottom left panel). The filtered fields are represented in the right panels. The large-scale field is built using a scalar cosine function as velocity potential similar with those used when we tested the convolution filter for scalar variables and it has the wavelength $L_l = 20{,}000\text{km}$. For both tests the small-scale field (the noise) was built using cosine scalar functions as velocity potential or streamfunction with $L_n = 500\text{km}$. For all tests, the convolution filter uses the weighting function $w\left(L_a = 3{,}000\,\text{km}; L_b = 600\,\text{km}\right)$ and a truncation distance of 900km.

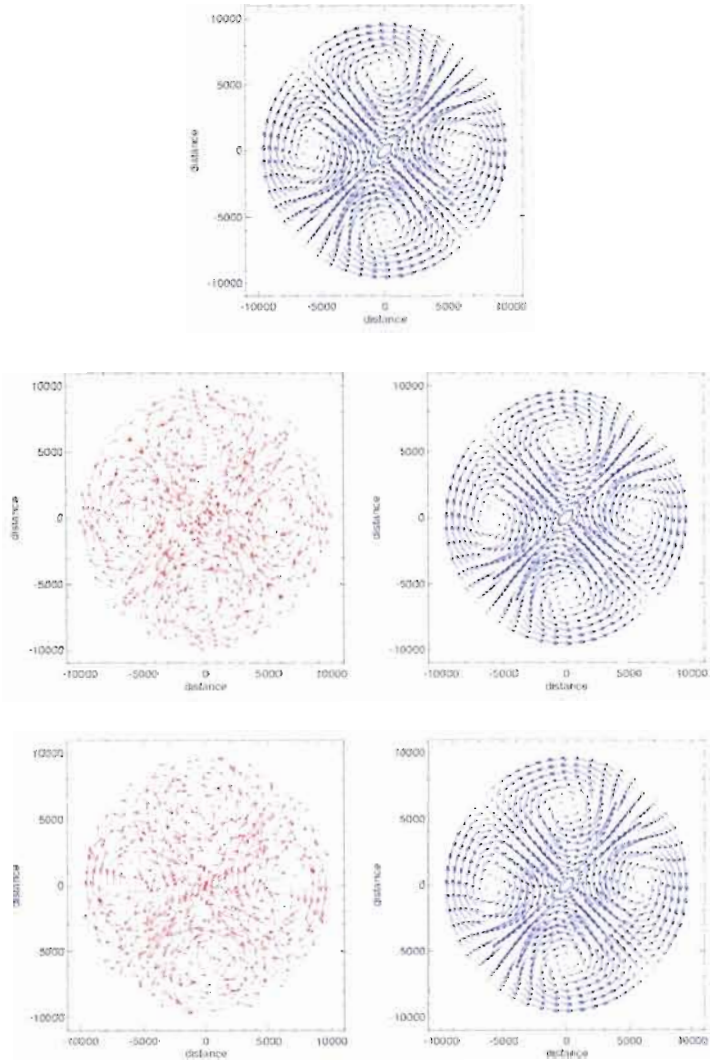


Figure 2.12 The large-scale rotational wind field (upper panel) is perturbed by a small-scale divergent wind field (middle left panel) or by a small-scale rotational wind field (bottom left panel). The filtered fields are represented in the right panels. The large-scale field is built using a scalar cylindrical harmonic function as streamfunction similar with those used for scalar variables with wavenumbers $k_l = 1$ and $l_l = 2$. For both tests the small-scale field (the noise) was built using double cosine scalar functions as velocity potential or streamfunction with $L_n = 500\text{km}$. For the tests presented the convolution filter used the weighting function $w\left(L_a = 3{,}000\,\text{km}; L_b = 800\,\text{km}\right)$ and a truncation distance of 1,100km.

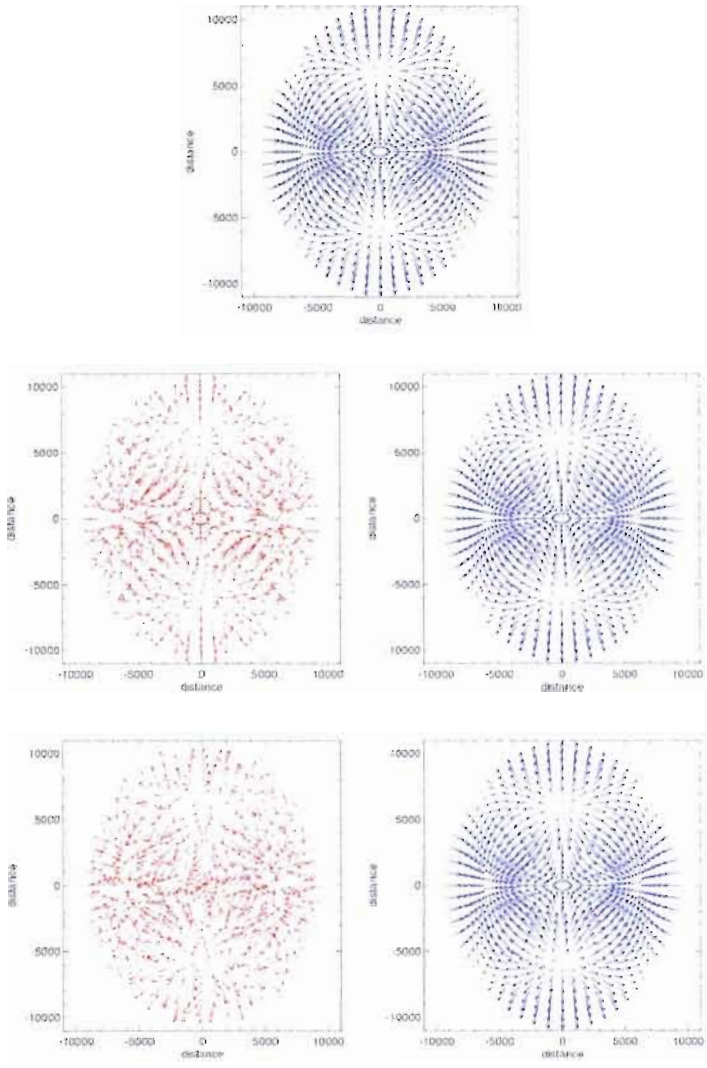


Figure 2.13 The large-scale divergent wind field (upper panel) is perturbed by a small-scale divergent wind field (middle left panel) or by a small-scale rotational wind field (bottom left panel). The filtered fields are represented in the right panels. The large-scale field is built using a scalar cylindrical harmonic function as velocity potential similar with those used for scalar variables with wavenumbers $k_l = 1$ and $l_l = 2$. For both tests the small-scale field (the noise) was built using cosine scalar functions as velocity potential or streamfunction with $L_n = 500\text{km}$. For the test presented the convolution filter used the weighting function $w\left(L_a = 3,000\,\text{km}; L_b = 600\,\text{km}\right)$ and a truncation distance of 900km.

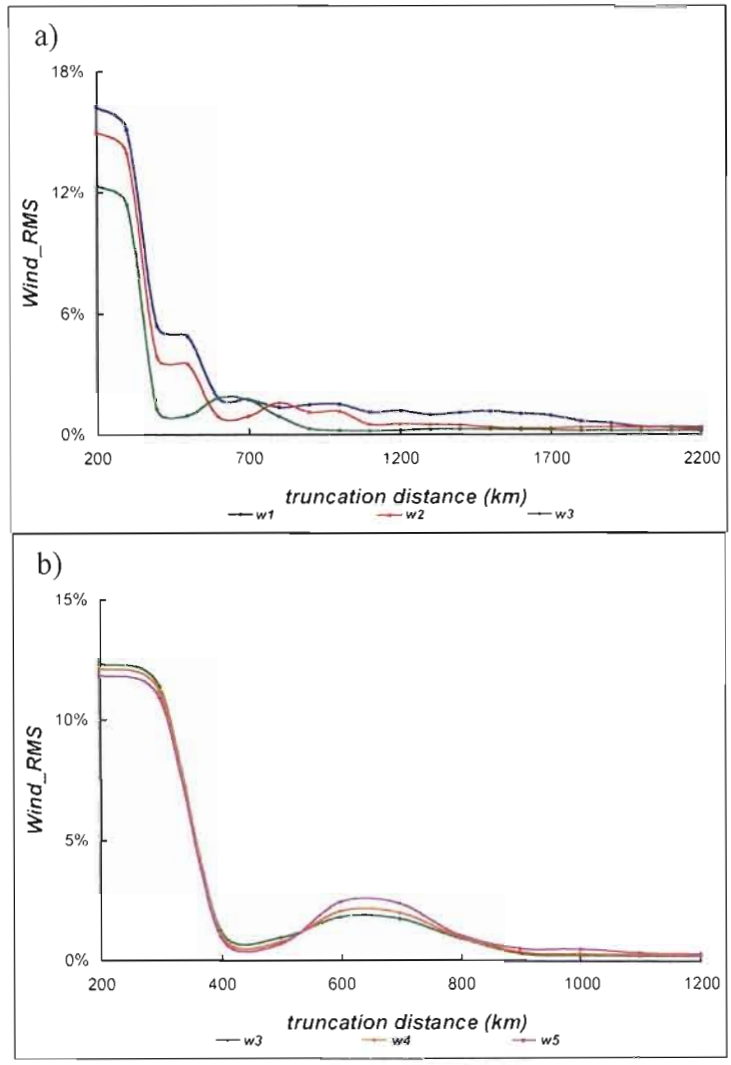


Figure 2.14 a) The *Wind_RMS* score as a function of the truncation distance, for three convolution filters with weighting functions $w1:\begin{cases} L_a = 3{,}000\,\text{km} \\ L_b = 1{,}000\,\text{km} \end{cases}$, $w2:\begin{cases} L_a = 3{,}000\,\text{km} \\ L_b = 800\,\text{km} \end{cases}$ and $w3:\begin{cases} L_a = 3{,}000\,\text{km} \\ L_b = 600\,\text{km} \end{cases}$ applied on the same test function containing a noise with $L_n = 500\,\text{km}$; b) The *Wind_RMS* score as a function of the truncation distance, for three convolution filters with weighting functions $w3:\begin{cases} L_a = 3{,}000\,\text{km} \\ L_b = 600\,\text{km} \end{cases}$, $w4:\begin{cases} L_a = 2{,}600\,\text{km} \\ L_b = 600\,\text{km} \end{cases}$ and $w5:\begin{cases} L_a = 2{,}200\,\text{km} \\ L_b = 600\,\text{km} \end{cases}$ applied on the same test function containing a noise with $L_n = 500\,\text{km}$.

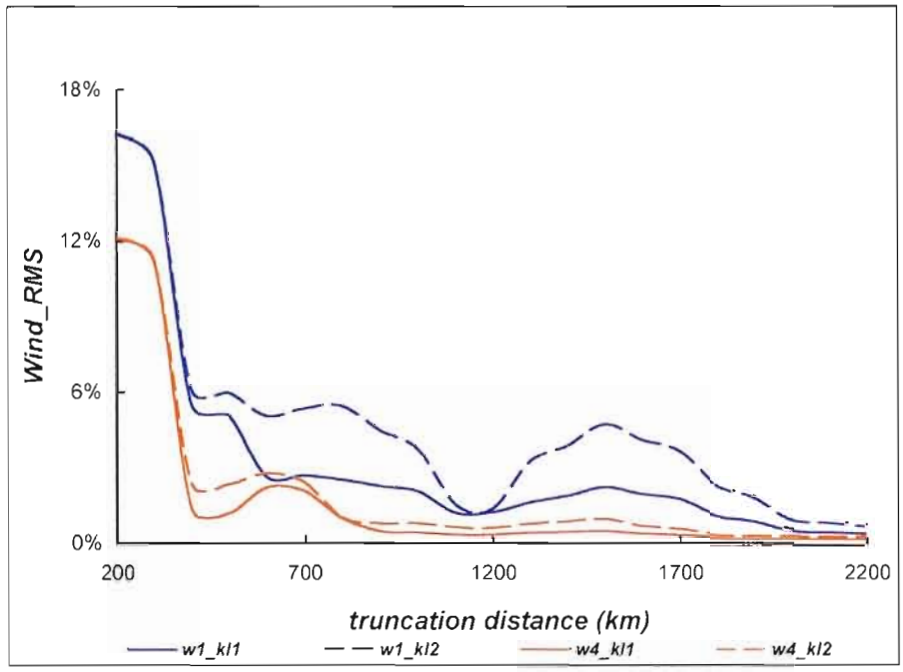


Figure 2.15 The *Wind_RMS* score as a function of the truncation distance, for two convolution filters with weighting functions $w1:\begin{cases} L_a = 3{,}000\text{km} \\ L_b = 1{,}000\text{km} \end{cases}$ and $w4:\begin{cases} L_a = 2{,}600\text{km} \\ L_b = 600\text{km} \end{cases}$. The test functions have different large-scale signals with wavelengths $L_{l_1} = 16{,}000\text{km}$ and $L_{l_2} = 12{,}000\text{km}$.

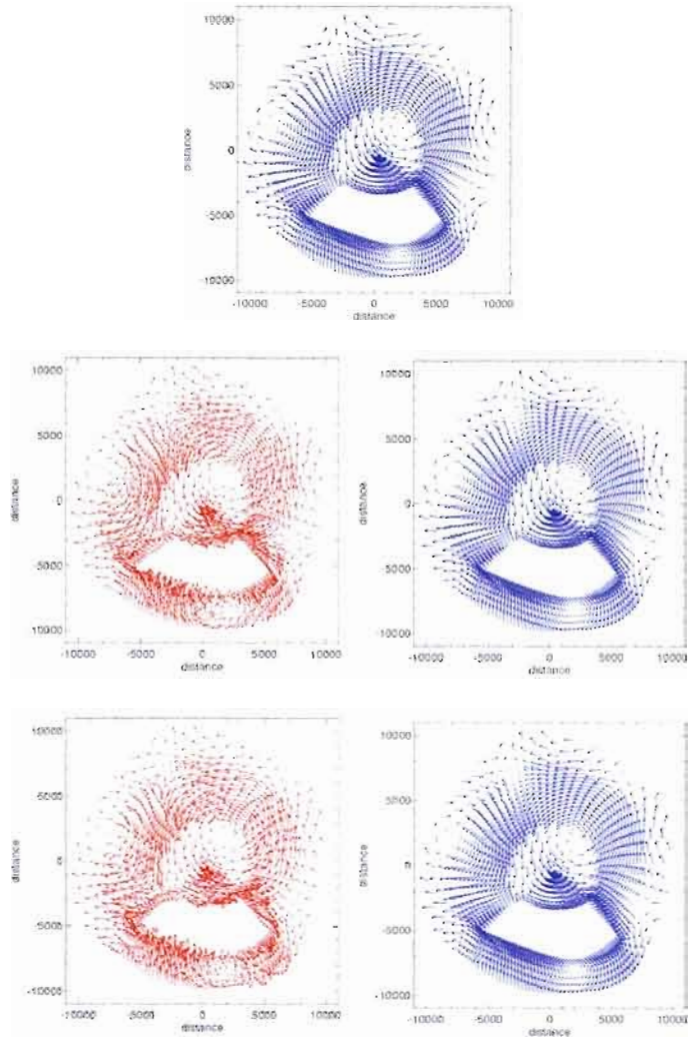

Figure 2.16 The large-scale rotational wind field (upper panel) is perturbed by a small-scale divergent wind field (middle left panel) or by a small-scale rotational wind field (bottom left panel). The filtered fields are represented in the right panels. The large-scale field is built using a scalar cosine function as streamfunction similar with those used when we tested the convolution filter for scalar variables. For both test-fields the small-scale signal (the noise) was built using cosine scalar functions as velocity potential or streamfunction with $L_n = 400\,\text{km}$. For the tests presented the convolution filter used the weighting function $w\left(L_a = 3,000\,\text{km}; L_b = 1,000\,\text{km}\right)$ and a truncation distance of 2,000km. The convolution filter is applied outside the uniform-high resolution area and the test-functions are represented only in the regions where the filter is applied.

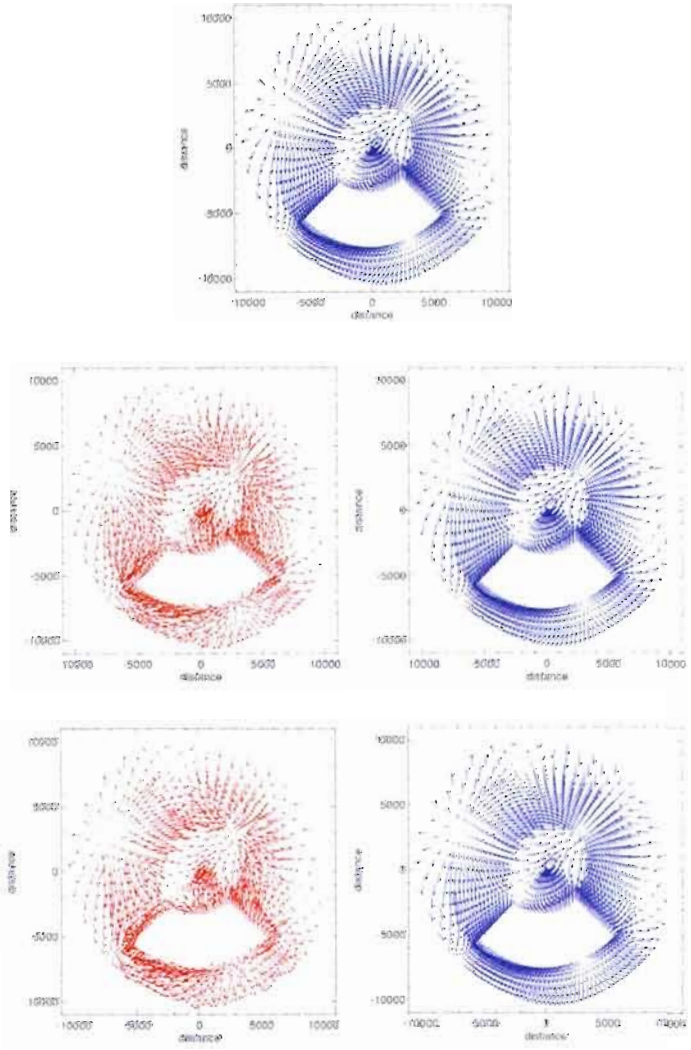

Figure 2.17 The large-scale divergent wind field (upper panel) is perturbed by a small-scale divergent wind field (middle left panel) or by a small-scale rotational wind field (bottom left panel). The filtered fields are represented in the right panels. The large-scale field is built using a scalar cosine function as velocity potential similar with those used when we tested the convolution filter for scalar variables. For both test-fields the small-scale signal (the noise) was built using cosine scalar functions as velocity potential or streamfunction with $L_n = 400\,\text{km}$. For the tests presented the convolution filter used the weighting function $w\left(L_a = 3{,}000\,\text{km}; L_b = 600\,\text{km}\right)$ and a truncation distance of 900km . The convolution filter is applied outside the uniform-high resolution area and the test-functions are represented only in the regions where the filter is applied.

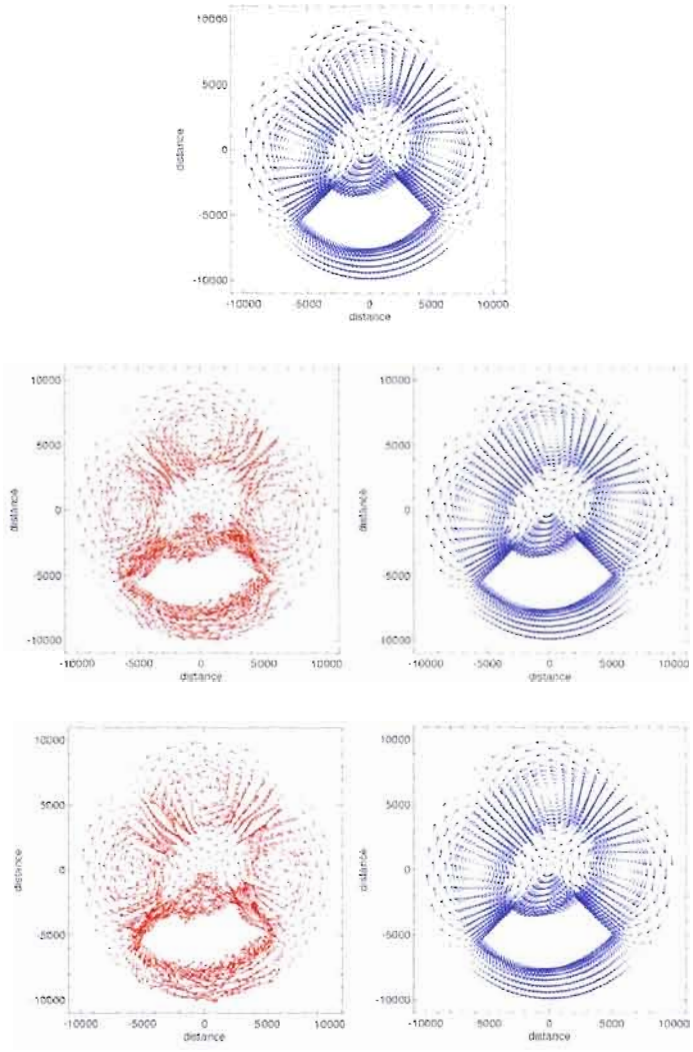


Figure 2.18 The large-scale rotational wind field (upper panel) is perturbed by a small-scale divergent wind field (middle left panel) or by a small-scale rotational wind field (bottom left panel). The filtered fields are represented in the right panels. The large-scale field is built using a scalar cylindrical harmonic function as streamfunction similar with those used when we tested the convolution filter for scalar variables. For both test-fields the small-scale signal (the noise) was built using cosine scalar functions as velocity potential or streamfunction with $L_n = 400\,\text{km}$. For the tests presented the convolution filter used the weighting function $w\left(L_a = 1,800\,\text{km}; L_b = 600\,\text{km}\right)$ and a truncation distance of 1,200km. The convolution filter is applied outside the uniform-high resolution area and the test-functions are represented only in the regions where the filter is applied.

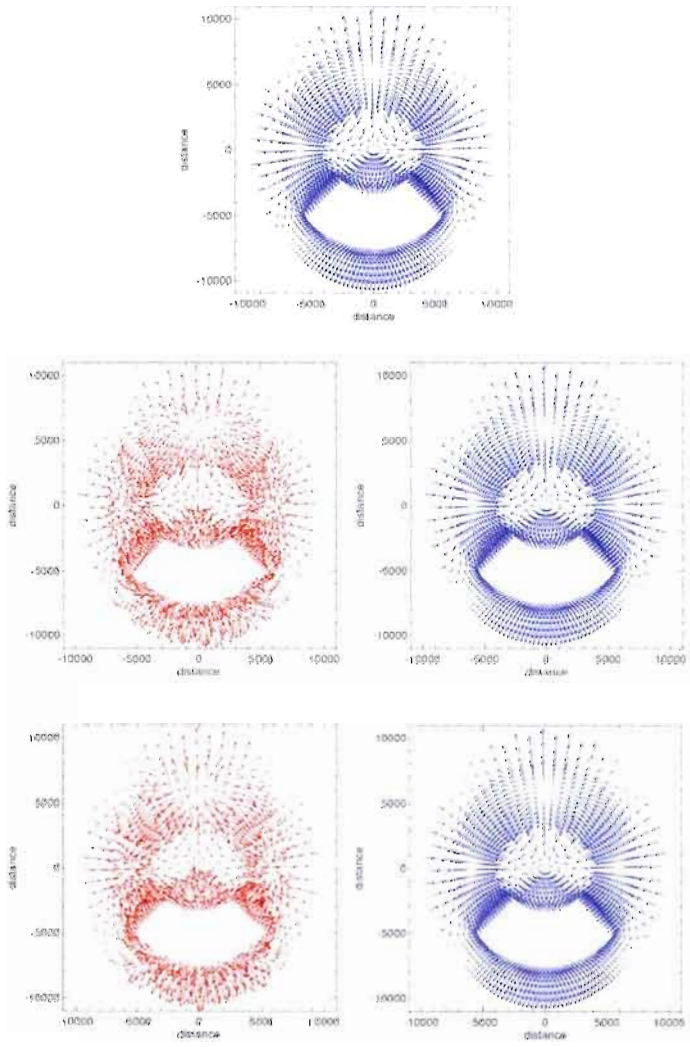

Figure 2.19 The large-scale divergent wind-field (upper panel) is perturbed by a small-scale divergent wind field (middle left panel) or by a small-scale rotational wind field (bottom left panel). The filtered fields are represented in the right panels. The large-scale field is built using a scalar cylindrical harmonic function as velocity potential similar with those used when we tested the convolution filter for scalar variables. For both test-fields the small-scale signal (the noise) was built using cosine scalar functions as velocity potential or streamfunction with $L_n = 400\,\text{km}$. For the tests presented the convolution filter used the weighting function $w\left(L_a = 1{,}000\,\text{km}; L_b = 600\,\text{km}\right)$ and a truncation distance of 1,800km . The convolution filter is applied outside the uniform-high resolution area and the test-functions are represented only in the regions where the filter is applied.

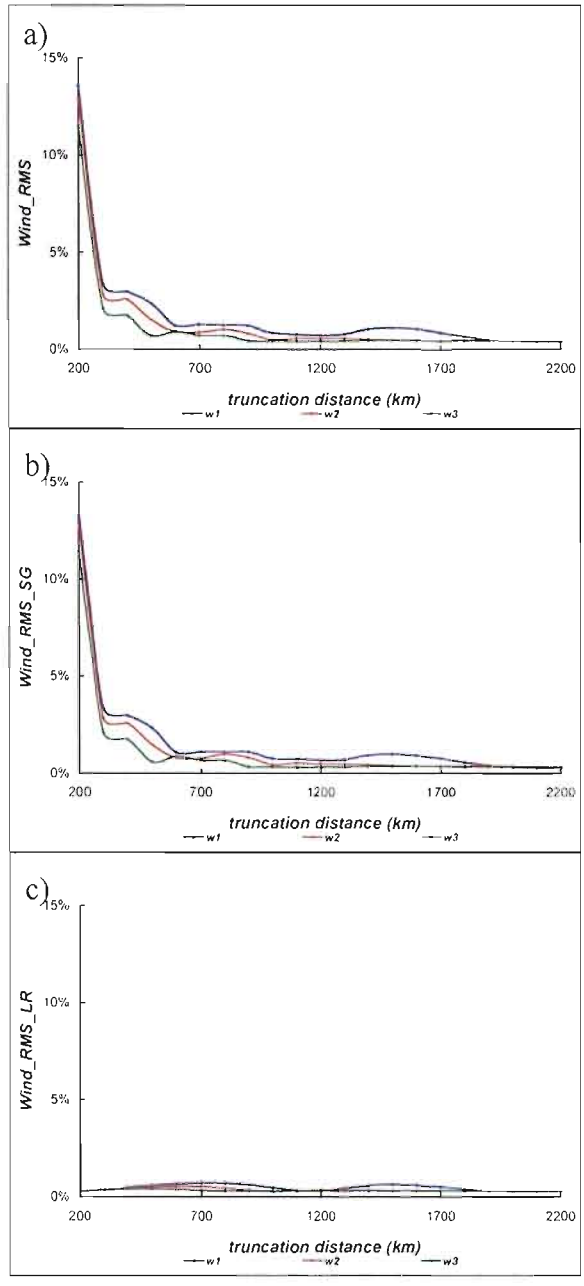


Figure 2.20 a) The *Wind_RMS* score as a function of the truncation distance, for three convolution filters with weighting functions $w1:\begin{cases} L_a = 3{,}000\,\text{km} \\ L_b = 1{,}000\,\text{km} \end{cases}$, $w2:\begin{cases} L_a = 3{,}000\,\text{km} \\ L_b = 800\,\text{km} \end{cases}$ and $w3:\begin{cases} L_a = 3{,}000\,\text{km} \\ L_b = 600\,\text{km} \end{cases}$ applied on the same test function containing a noise with $L_n = 400\,\text{km}$; b) The *Wind_RMS_SG* score is calculated only in the stretching areas; c) The *Wind_RMS_LR* score is calculated in the uniform low-resolution area.

# CONCLUSIONS

L'approche de résolution variable représente une alternative viable aux modèles sur aire limitée. Choisie par plusieurs centres de recherche, cette approche permet d'effectuer des simulations avec une haute résolution dans une région d'intérêt, utilisant un seul modèle et gardant les coûts de calculs inférieurs à ceux qui sont demandés par un modèle mondial de haute résolution. Toutefois, une grille qui change la résolution ne peut pas représenter correctement toute la gamme des échelles en même temps dans le domaine de haute résolution ainsi que dans le domaine de basse résolution. Pour réduire l'impact de la variation de la grille de calcul, des conditions sont imposées sur les facteurs local et total d'étirement (Fox Rabinovitz *et al.* 2006). Même pour une grille variable localement isotrope, comme celle qui utilise la transformée conforme de Schmidt (1978), des limitations concernant la variation de la résolution sont imposées (Caian et Geleyn 1995). C'est pour ces raisons que nous avons eu l'idée de créer un opérateur qui permettra de garder l'information acquise par l'utilisation d'une haute résolution à l'intérieur de la zone d'intérêt et en même temps d'éliminer toutes les échelles qui ne sont pas bien représentées en dehors de cette zone.

La première partie de cette thèse reprend l'idée présentée dans Surcel (2005) pour la construction d'un filtre numérique en utilisant l'opérateur du produit de convolution. Ce produit de convolution entre une fonction qu'on va appeler « initiale » ou « non filtrée » et une fonction de pondération représente le résultat du filtrage. La fonction de pondération est déterminée à partir de la réponse de filtrage désirée après l'application du filtre. La nouveauté dans cette approche est que la fonction de pondération dépend de la distance physique sur la grille de calcul et non pas du nombre de points de grille sur lesquels est appliquée. Le produit de

convolution exprimé en principe par une somme infinie sera tronqué pour des raisons de coût de calcul. La troncature se fait quand la distance entre le point d'application (le point où le produit de convolution est calculé) et tout autre point qui entre dans cette somme est plus grande qu'une distance prédéfinie.

Une condition nécessaire pour qu'une méthode de filtrage applicable sur une grille variable soit performante est qu'elle ait une efficacité élevée sur une grille uniforme. Le calcul de l'erreur quadratique moyenne normalisée *(Normalized Root-mean Square Error - NRMS)* et du taux de conservation normalisé *(Normalized Conservation Ratio - NCR)* montre que la réponse de filtrage reproduit la réponse spectrale imposée soit en choisissant une distance de troncature élevée, soit en appliquant plusieurs fois le filtre avec une distance de troncature plus petite. Pour une fonction-test périodique représentée dans un domaine périodique avec résolution uniforme, les quantités filtrées sont parfaitement conservées.

L'application du filtre construit à l'aide d'un produit de convolution sur une grille unidimensionnelle à résolution variable est testée en considérant une grille périodique étirée. La configuration choisie est typique pour la résolution variant autour d'un cercle de latitude dans la région qui se trouve à l'extérieur de la région de haute résolution uniforme sur une grille de type latitude-longitude étirée (similaire à la ligne A-A' sur la Figure 1.1).

L'objectif des tests réalisés sur la grille variable unidimensionnelle était de vérifier la capacité du filtre à enlever l'anisotropie causée par la variation de la résolution, donc de rendre les variables isotropes, bien que la grille varie. Les fonctions tests utilisées sur la grille unidimensionnelle variable sont similaires à celles utilisées sur la grille unidimensionnelle uniforme, à l'exception du fait que le bruit est introduit graduellement dans les zones d'étirement ainsi que dans la zone de haute résolution uniforme. L'efficacité de cette approche a permis l'utilisation du filtre dans un domaine bidimensionnel cartésien pour supprimer l'anisotropie dans

« les bras de la croix », c'est-à-dire les régions où la résolution varie différemment en direction de l'abscisse et de l'ordonné. Sur la grille bidimensionnelle cartésienne, le produit de convolution a été calculé par des applications successives du produit de convolution unidimensionnel. Cette méthode permet de réduire les coûts de calcul en produisant des analyses comparables avec un schéma qui utilise un produit de convolution bidimensionnelle (Thatcher et McGregor 2009).

Pour tous les tests effectués sur la grille étirée unidimensionnelle ou bidimensionnelle, le filtre de convolution a fonctionné correctement. Avec des paramètres judicieusement sélectionnés, le bruit est éliminé dans les régions choisies par l'utilisateur, comme les régions d'étirement et/ou sur le domaine entier, la masse totale est relativement bien conservée, et il n'y a pas d'atténuation du signal initial. En pratique, le choix entre une fonction de pondération qui corresponde à une réponse spectrale assez nette mais qui nécessite une distance de troncature grande, et une fonction de pondération qui corresponde à une réponse spectrale plus étalée mais dont la distance de troncature nécessaire est plus petite, sera un compromis entre les coûts de calcul et la précision du filtre.

En conclusion, dans cette première partie de la thèse, un nouvel opérateur de filtrage est présenté. Cette approche est une alternative viable aux opérateurs de filtrage plus conventionnels, comme le filtre de Shapiro, qui sont basés sur une formulation en points de grille. Le filtre construit à l'aide d'un produit de convolution utilise une fonction de pondération dépendante de la distance physique sur la grille de calcul. L'adaptation pour le domaine bidimensionnel en utilisant la même fonction de pondération est obtenue par des applications successives du filtre unidimensionnel. Simple et efficace, cette méthode peut être appliquée sur une grille uniforme ainsi que sur une grille variable.

La deuxième partie de la thèse traite les objectifs suivants : le filtre devrait enlever l'anisotropie en dehors de la zone de haute résolution uniforme, le filtre

devrait résoudre des problèmes caractéristiques aux modèles qui utilisent une grille sphérique et aussi le filtre devrait être applicable pour toutes les variables d'un modèle numérique.

Le filtre numérique développé dans la première partie de la thèse est maintenant adapté pour la grille polaire. Son application consiste dans l'application successive du produit de convolution unidimensionnel en direction azimutale et en direction radiale. La fonction de pondération utilisée dans le produit de convolution est définie en fonction de la distance physique sur la grille polaire. En étant indépendant du choix de la grille de calcul, le filtre produit une réponse presque isotrope, ce qui convient à son utilisation dans les zones d'étirement pour contrôler les petites échelles ou dans la région polaire pour résoudre le « problème du pôle ».

Les premiers tests effectués sur la grille polaire ont utilisé des fonctions scalaires représentées par des signaux sinusoïdaux bidimensionnels ou des harmoniques cylindriques. Le filtre a été appliqué sur une grille polaire uniforme où un signal initial de grande échelle a été perturbé par un bruit de courte échelle. En choisissant une fonction de pondération correspondant à une réponse spectrale définie telle qu'elle élimine les échelles représentant le bruit et en utilisant une distance de troncature appropriée, le filtre a réussi à éliminer le bruit et le signal initial n'a pas été affecté. L'erreur quadratique moyenne normalisée ainsi que le taux de conservation normalisé ont été étudié pour différents choix de fonctions de pondération utilisant diverses distances de troncature. Les tests ont montré que ces erreurs diminuent pour des distances de troncature grandes et aussi ils ont montré que le filtre conserve les quantités filtrées.

Ensuite, l'application du filtre a été testée sur une grille étirée. Les mêmes coefficients statistiques ont été évalués sur la grille entière ou seulement dans les régions d'étirement ou dans la région de basse résolution uniforme. Sur la grille polaire variable le filtre a été appliqué en dehors de la zone de haute résolution

uniforme et aussi le bruit a été introduit graduellement dans les zones d'étirement et dans la zone de haute résolution uniforme. Dans ce contexte l'erreur quadratique normalisée calculée sur la grille entière (*NRMS*) montre un impact net de l'application du filtre dans les zones d'étirement, la courbe *NRMS_SG* ayant un profil qui ressemble à la courbe *NRMS*. La différence entre les deux courbes représente l'effet de l'application du filtre sur le signal de grande échelle. Il faut remarquer qu'il n'y a pas de déformation ou d'atténuation du signal initial en dehors de la zone de haute résolution uniforme si une distance de troncature suffisante est utilisée.

Un objectif important de cette thèse a été l'application du filtre pour toutes les variables d'un modèle numérique. Les méthodes de filtrage sont généralement appliquées pour des variables comme la température, l'humidité ou la pression. Si une méthode de filtrage est nécessaire pour la quantité de mouvement, alors le filtrage est appliqué pour les variables scalaires correspondantes comme la fonction de courant, le potentiel de vélocité, la divergence ou le tourbillon. L'idée originale de cette thèse est d'appliquer le filtre directement aux vecteurs représentant le vent. Les deux composantes du vent horizontal sont filtrées simultanément en appliquant le produit de convolution successivement en direction azimutale et en direction radiale. Pour ce faire, tous les vecteurs pris en compte dans le calcul du produit de convolution sont représentés dans le même système de référence centré dans le point d'application du filtre.

Les tests effectués sur une grille polaire uniforme et sur une grille polaire étirée ont montré que le filtre est capable d'enlever le bruit présent dans les zones d'étirement et de réduire l'effet de l'excès de résolution dans la région polaire. L'analyse de l'erreur quadratique pour le vent (*Wind_RMS*), qui représente l'erreur de conservation de l'énergie cinétique des variables filtrés, donne des indications sur le choix de la fonction de pondération en considérant les coûts impliqués qui sont exprimés par l'utilisation d'une certaine distance de troncature.

En conclusion, dans la deuxième partie de la thèse, la conversion du filtre pour la grille polaire a été abordée comme une étape nécessaire pour une éventuelle application du filtre sur la grille sphérique. La méthode proposée est applicable pour toutes les variables d'un modèle numérique et aussi elle s'attaque en même temps à la résolution de plusieurs cibles comme l'anisotropie de la grille de calcul ou le problème du pôle.

Par analogie avec la grille polaire, l'application du filtre sur une grille sphérique latitude-longitude consiste dans l'application succesive du produit de convolution en direction zonale et en direction méridienne. La fonction de pondération nécessaire dans le produit de convolution sera dépendante de la distance physique en direction zonale ou en direction méridienne sur la grille de calcul. Les principes de base qui devraient être suivis dans l'application du filtre sur une grille variable latitude-longitude sont présentés dans l'appendice D.

Cette étude présente dans un mode simple la construction d'un filtre numérique en utilisant le produit de convolution. Cet opérateur mathématique est souvent utilisé dans le traitement numérique des signaux (Radix 1970, Gasquet et Witomski 1990) pour développer des techniques d'analyse et d'interprétation des données. Dans ce travail, par une approche similaire, la propriété fondamentale du produit de convolution est exploitée pour définir une fonction de pondération analogue à la fonction de transfert dans le traitement des signaux. En appliquant cette procédure pour une fonction définie dans le domaine spatial unidimensionnel, la fonction de pondération obtenue est fonction de la distance physique sur la grille spatiale. Cette dépendance est l'ingrédient principal de cet opérateur de filtrage qui fait son application possible sans tenir compte de la maille du domaine.

Généralement les modèles atmosphériques à résolution variable utilisent plus qu'une méthode de filtrage pour résoudre les problèmes reliés à la variation de la grille et pour enlever les instabilités numériques (par ex. Fox Rabinovitz *et al.* 2001,

Côté *et al.* 1998). Avec l'approche que nous proposons, il serait possible de réaliser en même temps les objectifs suivants :

- enlever l'anisotropie en dehors de la zone de haute résolution uniforme : après l'application du filtre les variables contiennent juste les échelles qui peuvent êtres supportées par la grille de calcul ;

- résoudre le problème du pôle : après l'application du filtre les variables ne contiennent plus les échelles qui nécessitaient l'utilisation d'un pas temporel réduit ;

- appliquer le filtre pour toutes les variable du modèle : avec des conditions bien spécifiées, le filtre est applicable tant pour les scalaires que pour les vecteurs ;

- enlever les instabilités numériques caractéristiques aux modèles : avec des coefficients judicieusement choisis, le filtre peut éliminer en même temps une vaste gamme d'échelles.

Bien que la méthode présentée soit simple et facile à implémenter, elle a été testée juste pour des fonctions classiques comme les composantes de Fourier ou les harmoniques cylindriques. L'utilisation de cette méthode dans un modèle simplifié sur une grille étirée de type latitude-longitude pourrait donner des indications supplémentaires concernant le choix des paramètres qui définissent la fonction de pondération et aussi des informations précises concernant les coûts de calcul impliqués en dépendant du choix de la fonction de pondération. Ces étapes sont nécessaires dans le but d'utiliser un tel opérateur dans un modèle climatique à résolution variable.

# APPENDICE A

# A FORMAL APPROACH FOR SMOOTHING ON VARIABLE-RESOLUTION GRID

# PART I: DESIGN AND APPLICATION FOR CARTESIAN COORDINATES

Dorina Surcel and René Laprise

ESCER, Université du Québec à Montréal, Montréal, Québec, Canada

Publié dans Research activities in Atmospheric and Oceanic Modelling, WMO/TD, A. Zadra Ed., 1578 (41): 3.13-3.14.

Global climate models with variable resolution are used to improve the representation of regional scales over an area of interest, avoiding the nesting issues of the limited-area models and reducing the computational costs compared to global uniform high-resolution models. To address some potential problems associated with the stretching and anisotropy of the computational grid, a general convolution filter operator was developed. The main feature of this filter is to locally remove scales shorter than a user-prescribed spatially varying length scale.

Over non-uniform grids, the only scales that can be represented over the entire domain are those with length scales larger than or equal to twice the maximum grid spacing $\Delta x_{\max}$. In a stretched-grid model, it would be possible to remove anisotropic features associated with fine-scale structure of the mesh in only one dimension, such as in the arms-of-the-cross region surrounding the high-resolution area of interest. This may be an effective means of controlling aliasing of fine-scale features while

they exit the high-resolution region and enter in the low-resolution part of the domain. In this case, the numerical filtering operator could suitably remove the unwanted small scales outside the uniform high-resolution area.

The convolution operator was chosen to design the filtering formula. For a signal $\psi$, the filtered value $\overline{\psi}$ is: $\overline{\psi}(x) = (\psi * w)(x) = \int_{-\infty}^{\infty} \psi(x) \cdot w(x-s) ds$. Using the convolution theorem and taking the Fourier transform of the initial $\psi$ and the filtered $\overline{\psi}$ fields to evaluate the ratio of their spectral amplitudes, one finds that the required weighting function $w$ is the inverse Fourier transform of the desired response function (e.g. Surcel 2005). The numerical filtering operator that will remove all the waves that are not correctly represented outside the high-resolution region has a spectral response that corresponds to keeping unchanged the large scales with wavenumber smaller than $a = 2\pi/2\Delta x_{\max}$ (corresponding to wavelengths larger than $2\Delta x_{\max}$ that are resolved everywhere on the grid), and removing entirely small scales with wavenumber larger than a chosen value of $b \le 2\pi/2\Delta x_{\min}$, with a gradual transition in between to reduce Gibbs' phenomenon. The convolution theorem then gives $w(d) = \frac{\pi}{2} \cdot \frac{\sin ad + \sin bd}{d} \cdot \frac{1}{\pi^2 - d^2(b-a)^2}$, where $d = x - s$. Although the formal definition of the convolution exists for continuous space, its practical application needs a definition using a discrete set of points. Also, the presence of non-vanishing values over the entire domain is problematic because of excessive computational costs. Given that the values become small after some distance from the origin, truncating the weighting function after some distance can result in an important reduction in computational costs. While the truncation distance is an important parameter for the precision of the filter, the distance between the wavenumbers $a$ and $b$ affects also the choice of the truncation distance and subsequently the precision of the filter. A weighting function corresponding to an abrupt change in the spectral response contains large oscillations, and needs a large truncation distance, while a

more gradually varying response function gives rise to a narrow weighting function, and thus to a much smaller acceptable truncation distance, in order to approximate adequately the theoretical response.

The application of the convolution filter for a variable resolution domain is tested considering a periodic 1D stretched grid $[0,2\pi]$ with a stretching factor $S = \Delta x_{\max}/\Delta x_{\min} \cong 4$. This grid contains 60 to 64% from the total number of grid points in the high-resolution area, even if the area represents only 1/3 from the entire domain. The filter is tested using the 1D test-function as $\psi(x) = \psi_l(x) + \psi_n(x)$, where $\psi_l$ is a large-scale wave representing the physical signal that is properly represented on the entire domain, and $\psi_n$ is a small-scale wave representing the noise which is chosen to be zero in the low-resolution part of the domain, gradually increased in the stretching areas, and is maximum in the high-resolution area of the domain. The skill of the filter is quantitatively evaluated by comparing the filtered solution $\overline{\psi}$ with the expected analytical solution $\psi_l$, using two scores: the normalized root-mean square error (*NRMS*) that is computed between the filtered solution and the expected analytical solution, and the normalized conservation ratio (*NCR)* calculated as the mean error between the filtered and unfiltered solution (Surcel and Laprise, 2011).

A first example presents a test function containing a noise with wavenumber $k_n = 2\pi/4\Delta x_{\min}$. The convolution filter used a weighting function $w_1$ defined by $a = 2\pi/2\Delta x_{\max}$ and $b = 1.5a$; in this case a truncation distance $d_{\max} = 5\Delta x_{\max}$ was adequate to completely remove the noise while maintaining the large-scale signal. The effects of using different weighting functions was studied employing the same test function and two different weighting functions: $w_1$ ($a = 2\pi/2\Delta x_{\max}$; $b = 1.5a$) and $w_2$ ($a = 2\pi/2\Delta x_{\max}$; $b = 2a$). The *NRMS* score (Fig. A1b) shows that the noise is completely removed if an adequate truncation distance is used and this distance is shorter for the filter with a more gradual response ($w_2$). In this case we note also a

better conservation expressed by a *NCR* score, which approaches zero for a truncation distance larger than $10\Delta x_{\min}$ as it can be seen in Fig. A1c.

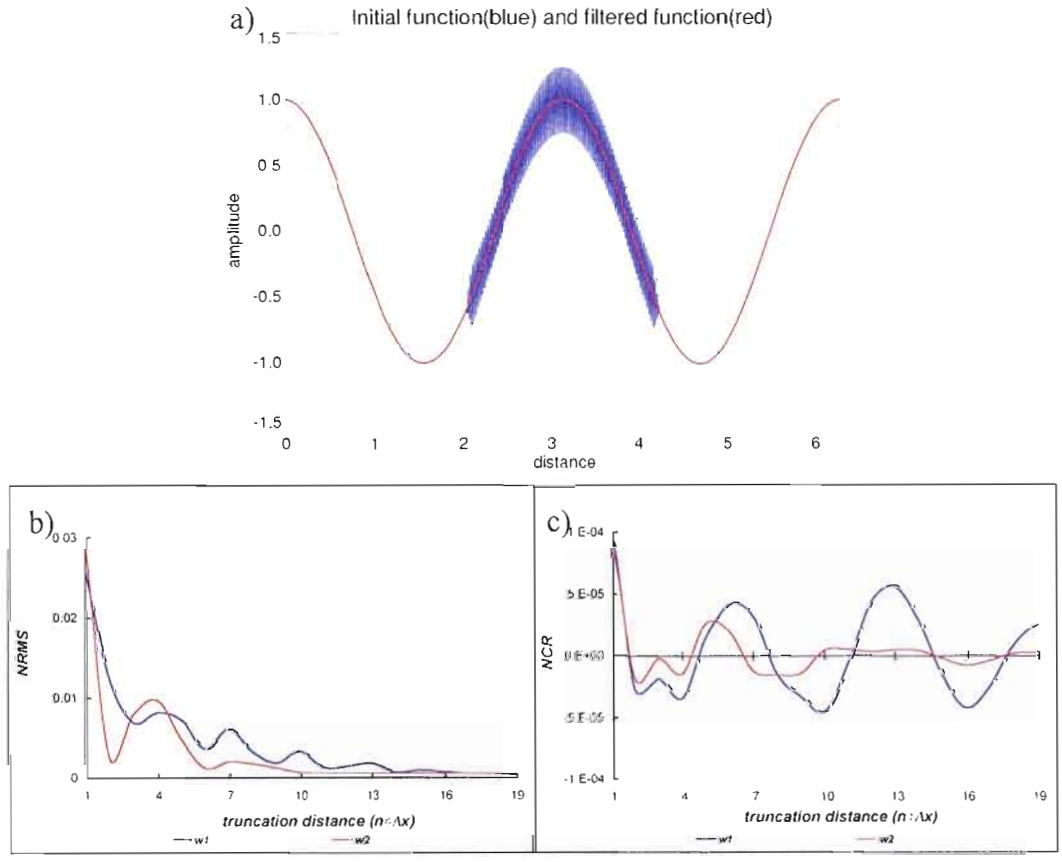


Figure A.1 (a) The initial test function (blue) containing a noise with wavenumber $k_n = 2\pi/4\Delta x_{\min}$ and the filtered field (red) are represented on a grid with $S \cong 4$. The convolution uses the weighting function $w_1$ and a truncation distance $d_{\max} = 5\Delta x_{\max}$. The *NRMS* (b) and the *NCR* (c) scores as a function of the truncation distance, for two different weighting functions.

The formal approach developed in 1D is generalized for two-dimensional domains. The 2D convolution uses a weighting function that is the product of two 1D functions, similar with those used in one-dimensional case. In practice, the 2D filtered function is obtained conveniently by successive applications of 1D filter in each direction. It is important to reiterate that in our proposed convolution filter

approach, the weights are calculated using physical distances rather than grid-point indices.

Similarly to our tests in 1D, test functions using 2D sinusoidal waveforms were chosen to represent the large-scale signal that will be retained by the filter and the noise that will be removed. The example presented in Fig. A.2 shows the initial signal (a) and the filtered function when the convolution uses the weighting function $w_1$ and truncation distances of $d_{max} = 10\Delta x_{min}$ (b) and $d_{max} = 21\Delta x_{min}$ (c).

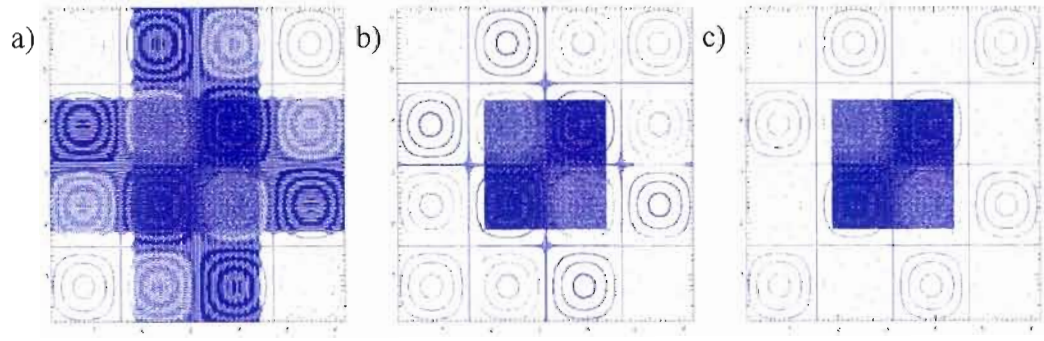


Figure A.2 The initial test field on the 2D stretched-grid with $S \cong 4$ (a). The filtered fields after application of a convolution filter with 1D weighting function $w_1$ and truncation distances of $10\Delta x_{min}$ (b) and $21\Delta x_{min}$ (c).

The proposed approach appears to be a valuable alternative to a conventional grid-point based smoothing operator for stretched-grid models. The filter can be used to render quasi-isotropic fields on variable-resolution grids. A key element of this approach is that the weighting function is based on the physical distance rather than grid point indices. The convolution filter developed in 1D and generalised for 2D Cartesian geometry will next be adapted for polar geometry.

**References**

Surcel, D., 2005: Filtres universels pour les modèles numériques à résolution variable. Mémoire de maîtrise en Sciences de l'atmosphère,Département des Sciences de la Terre et de l'Atmosphère, Université du Québec à Montréal, 104pp.

Surcel, D., and R. Laprise, 2011: A General Filter for Stretched-Grid Models: Application in Cartesian Geometry. *Mon. Wea. Rev.* **139**, 1637-1653.

# APPENDICE B

# A FORMAL APPROACH FOR SMOOTHING ON VARIABLE-RESOLUTION GRID

# PART II: FILTERING THE SCALARS ON THE POLAR GRID

Dorina Surcel and René Laprise

ESCER, Université du Québec à Montréal, Montréal, Québec, Canada

Publié dans Research activities in Atmospheric and Oceanic Modelling, WMO/TD, A. Zadra Ed., 1578 (41): 3.15-3.16.

The filter formulation developed in 1D and generalized in 2D Cartesian domain (Surcel and Laprise 2011) is here adapted to 2D cylindrical polar geometry, as a step towards spherical polar geometry. The filter is tested for different scalar test-functions, first to control the "pole problem" specific of the latitude-longitude models, and second to remove the anisotropic noise outside the high-resolution area of a polar stretched grid.

On the polar grid the formulation of the filter is obtained by separate applications of the filter in radial and azimuthal directions. The filtered function can be written in integral form as

$$\overline{\psi}(r,\lambda) = \overline{\left(\overline{(\psi)}^{\lambda}\right)}^{r}(r,\lambda) = \int_{r'=0}^{\infty}\int_{\lambda'=0}^{2\pi} \psi(r',\lambda')\, w\left(r'(\lambda-\lambda')\right) w(r-r')\, r'\, dr'\, d\lambda' .$$

On a discrete polar grid $(r_i,\lambda_j)$, the field to be filtered is represented by $\psi_{i,j}=\psi(r_i,\lambda_j)$, with $i=1,\ldots,n; j=1,\ldots,m$ and $r_i\in[0,R_e], \lambda_j\in[0,2\pi[$ where $R_e$ is the distance from the centre of the grid to the boundary (henceforth referred to as the equator). Then the convolution formula is discretized as follows:

$$\overline{\psi}^{r,\lambda}(r_i,\lambda_j)=\frac{\sum_k \overline{\psi}^{\lambda}(r_k,\lambda_j)\cdot w(d^r_{i-k})\cdot s(r_k)}{\sum_k w(d^r_{i-k})\cdot s(r_k)}$$
$$=\frac{\sum_k\sum_l \psi(r_k,\lambda_l)\cdot w(d^{\lambda}_{j-l})\cdot w(d^r_{i-k})\cdot s(r_k)\cdot s(\lambda_l)}{\sum_k\sum_l w(d^{\lambda}_{j-l})\cdot w(d^r_{i-k})\cdot s(r_k)\cdot s(\lambda_l)},$$

where $d^r_{i-k}$ and $d^{\lambda}_{j-l}$ are the radial and azimuthal distances, and $s(r_k)\cdot s(\lambda_l)=s(r_k,\lambda_l)$ is the unit area surface. It must be noted that the weighting function varies with the physical distances, and is not based on grid-point count, which is in fact the critical ingredient in the design of the proposed convolution filter.

To test the skill of the filter at alleviating the "pole problem", we employ a discrete uniform polar grid. The test functions are composed of a large-scale field referred to as the signal or physical component and a small-scale field referred to as the noise. The large-scale signal will be represented by a double cosine in physical space or by a cylindrical harmonic (eigenfunction of the Laplacian on the polar grid). The small-scale noise will be represented by a double cosine in physical space.

A first example regarding the application of the filter to remove the "pole problem" is presented in Fig. B.1a. The test function is composed from a large-scale signal in form of a double cosine with wavelength 20,000 km and a similar noise with wavelength of 500 km. The convolution filter is defined such as to keep unchanged all scales larger than 2,400 km and to remove all scales smaller than 800 km. With

these parameters the quadrature requires a minimum truncation distance of 1,600 km for an adequate accuracy of the convolution. The second example presented in Fig. B.1b uses a large-scale signal in form of cylindrical harmonic with radial and azimuthal wavenumbers equal to 2 and a noise with wavelength of 600 km. For this example the filter is designed such as to keep unchanged all scales larger than 2,400 km, but to remove all scales smaller than 1,000 km. Because the weighting function corresponds to a more abrupt response function, the convolution needs a larger truncation distance of 2,300 km to properly remove the noise and to preserve the large-scale signal. To quantitatively assess the influence of the cut-off distance, three different weighting functions were tested. The normalized root mean square error (*NRMS*) is computed between the filtered solution and the expected analytical solution. The parameters characterizing these weighting functions are $w1\left(L_a = 2{,}400\,\text{km}; L_b = 1{,}000\,\text{km}\right)$, $w2\left(L_a = 2{,}400\,\text{km}; L_b = 800\,\text{km}\right)$ and $w3\left(L_a = 2{,}400\,\text{km}; L_b = 600\,\text{km}\right)$, where $L_a$ represents the minimal wavelength to be preserved and $L_b$ the maximal wavelength to be removed by the filter. The *NRMS* curve represented in Fig.1c for truncation distance between 200 km and 2,400 km shows that the error decreases as the truncation distance increases, although not monotonically. The oscillations are larger for $w1$ than for $w3$ due to Gibbs' phenomenon associated with the narrower response function, which necessitates wider stencil for accurate representation.

We now present the skill of the filter at removing the anisotropy on the stretched polar grid. This grid contains a "uniform" high-resolution domain in the sector $(r_1, r_2) = (3{,}500; 7{,}500)$ km and $(\lambda_1, \lambda_2) = (5/8 \cdot 2\pi, 7/8 \cdot 2\pi)$. A gradual stretching zone is used adjacent to the high-resolution area: $r \in (2{,}500; 3{,}500) \cup (7{,}500; 8{,}500)$ and

$\lambda \in (4.5/8 \cdot 2\pi, 5/8 \cdot 2\pi) \cup (7/8 \cdot 2\pi, 7.5/8 \cdot 2\pi)$, with local stretching rate of $s_r = 8\%$

in the radial direction and $s_\lambda = 3.8\%$ in the azimuthal direction. Low resolution is used elsewhere in the domain resulting in a total stretching factor of $S_r \cong S_\lambda \cong 6$.

An example of the application of the filter on the polar stretched-grid is presented in Figs B.2a and B.2b. The first panel represents the initial test function composed from a cylindrical harmonic with radial and azimuthal wavenumbers equal to 3 and a noise in form of a double cosine with wavelength 400km. The noise is gradually added in the stretching zones and in the high-resolution area and the filter is applied outside the uniform high-resolution region. The convolution filter uses the weighting function $w1$ and a truncation distance of 2,300km. We note that the noise is completely removed and not deformations or attenuations of the large-scale signal were observed. We verify the performance of the filter to conserve the filter quantities computing the normalized conservation ratio (*NCR*) between the initial and the filtered function. Figure B.2c presents the *NCR* for a test function similar with those used for the uniform grid, but with the noise added gradually in the stretching areas and the high-resolution domain. Using the same weighting functions as in the first case we note a better conservation for weighting functions that need a smaller truncation distance, but all *NCR* curves eventually approach zero when using large truncation distances.

The experiments realized on the polar grid demonstrated the ability of the convolution filter to adequately remove small-scale noise both in the polar region and also in the anisotropic "arms-of-the-cross" regions of the variable polar stretched grid. The convolution filter can be concomitantly applied to address the pole problem and also to remove anisotropic noise in the stretching region of the grid, by choosing appropriate parameters for the convolution weighting function.

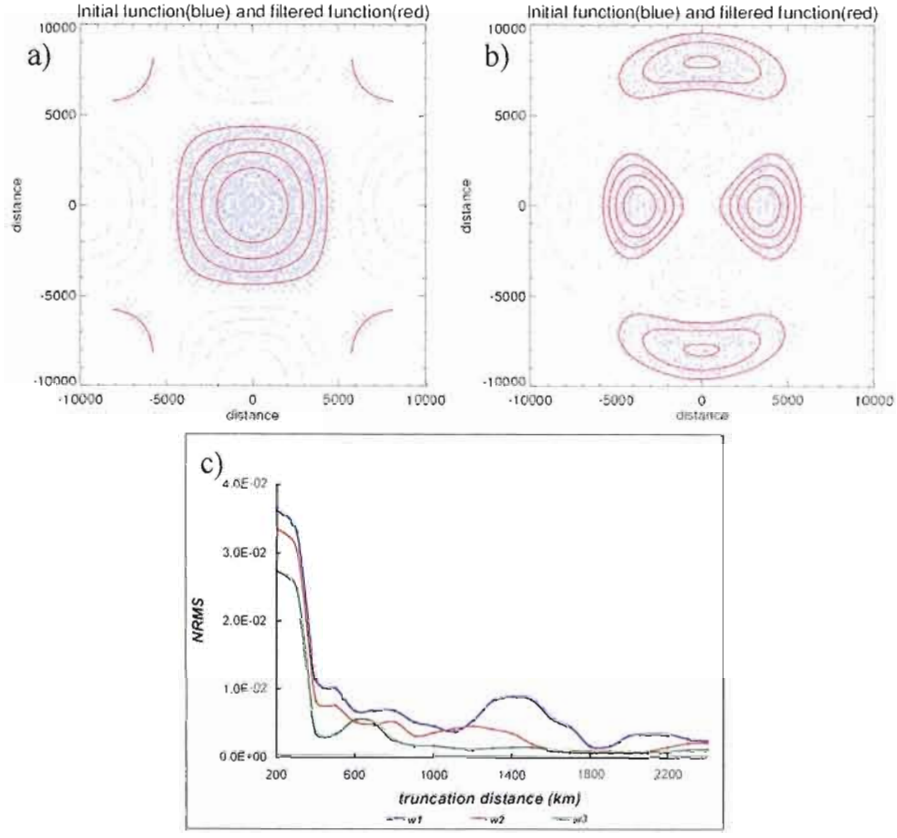


Figure B.1 An initial function shown in blue and the filtered function is shown in red. The filter uses the weighting function $w2$ (a) and $w1$ (b) and truncation distances of 1,600 km (a) and 2,300 km (b). c) The NRMS curves as function of the truncation distance for the three weighting functions presented above.

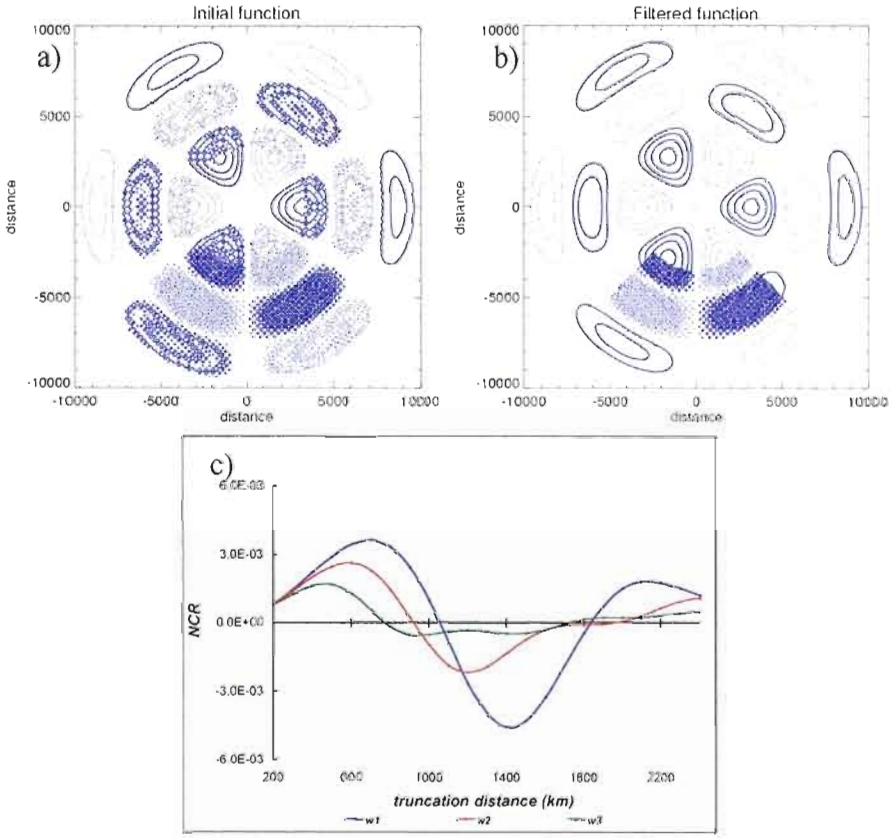


Figure B.2 The initial (a) and the filtered (b) signal when the convolution filter uses the weighting function $w1$ and a truncation distance of 2,300km. c) The NCR curves as function of the truncation distance for the three weighting functions presented above.

**Reference**

Surcel, D., and R. Laprise, 2011: A General Filter for Stretched-Grid Models: Application in Cartesian Geometry. *Mon. Wea. Rev.* **139**, 1637-1653.

# APPENDICE C

# A FORMAL APPROACH FOR SMOOTHING ON VARIABLE-RESOLUTION GRID

# PART III: FILTERING THE VECTORS ON THE POLAR GRID

Dorina Surcel and René Laprise

ESCER, Université du Québec à Montréal, Montréal, Québec, Canada

Publié dans Research activities in Atmospheric and Oceanic Modelling, WMO/TD, A. Zadra Ed., 1578 (41): 3.17-3.18.

It is common practice to filter the fields (or sometimes their tendencies) in order to remove high wavenumbers that otherwise would affect the accuracy of a climate model. Generally, these damping methods are applied to variables such as temperature, pressure and humidity, and if filtering is needed for momentum, it is often applied to the corresponding scalar quantities, such as streamfunction and velocity potential, or vorticity and divergence. In this study we proceed to the filtering of the wind vectors themselves. The convolution filter developed by Surcel and Laprise (2011a) and adapted for scalar variables on the polar grid (Surcel and Laprise 2011b) is now generalized for vector fields.

When the convolution is applied to vectors such as the horizontal wind, care has to be taken to use a representation of the vector components relative to the same reference system, chosen here to correspond to the application point. As the polar grid

used in this paper is an intermediate step to the application of the filter on a spherical latitude-longitude stretched grid, the representation of the vector components is made by analogy with the spherical grid.

On a polar grid defined by $(r,\lambda)$, with $r$ the radius and $\lambda$ the azimuth angle, the horizontal wind is defined related to the local coordinate system, as $\mathbf{V}_h = (u, v) = \left( r\frac{d\lambda}{dt}, -\frac{dr}{dt} \right)$, where $(u, v)$ correspond to the "zonal" and "meridional" wind components (using the terminology on the sphere), with the sign convention that $u$ is positive eastward and $v$ is positive northward.

The filter is applied simultaneously for both wind components and the convolution is applied successively in radial and azimuthal directions. Following the meteorological tradition, the wind components are defined relative to a locally orthogonal reference system whose base vectors change with location (only with longitude in fact for the polar grid). Therefore the application of the filter operator requires representing the wind components contributing to the convolution at a point in the same coordinate system as that point. For each point $P_0(r_i,\lambda_j)$ where the convolution filter is applied for $(u,v)$, we transform all wind vectors in the neighbouring points $P(r_k,\lambda_l)$ contributing to the convolution, i.e. those for which their distance is within the chosen truncation distance for the convolution. The wind components at point $P(r_k,\lambda_l)$ are expressed in the coordinate system relative to the application point $P_0$ as follows:

$$\begin{pmatrix} u \\ v \end{pmatrix}_{P_0}(k,l) = \begin{bmatrix} \cos(\lambda_l - \lambda_j) & -\sin(\lambda_l - \lambda_j) \\ \sin(\lambda_l - \lambda_j) & \cos(\lambda_l - \lambda_j) \end{bmatrix} \begin{pmatrix} u \\ v \end{pmatrix}_P (k,l).$$

We note that the conversion only involves the longitude angle, not the radial distance, thus no transformation is required for points aligned on the same meridian.

To verify the efficiency of the convolution filter we define test wind fields by constructing rotational and divergent motions using the Helmholtz theorem for two-dimensional vector field $\mathbf{V}_h$ as

$$\mathbf{V}_h = \mathbf{V}_R + \mathbf{V}_D = \mathbf{k} \otimes \nabla\psi + \nabla\chi$$

where $\psi$ is the streamfunction and $\chi$ the velocity potential. We then employ scalar test functions, for use as streamfunction or velocity potential, and we develop analytically the corresponding zonal and meridional wind components in polar coordinates. We use a signal corresponding to either a pure rotational or divergent large-scale motion, and then add to it a small-scale noise that is also either rotational or divergent.

The filter's ability for application to vectors was tested first on a uniform polar grid and we checked the performance of the filter around the pole. To verify the performance of the convolution filter we represent a large-scale wind field, considered as analytical solution, a perturbed wind field created by adding a noise to the analytic wind field, and the filtered wind field that must be identical with the analytical solution if the filter works properly.

In Fig. C.1 (right panel), a streamfunction represented by a double cosine with wavelengths of 20,000 km defines a purely rotational large-scale wind field. To this large-scale field a small-scale divergent wind noise with wavelength of 500 km is added (middle panel). The convolution filter uses a weighting function that keeps unchanged all signals with wavelengths larger than 3,000km and removes all signals with wavelengths smaller than 800km. The convolution is calculated for truncation distance of 1,100 km. The filtered field (right panel) shows that the large-scale signal is preserved and the noise removed. For this test the large-scale field was located specifically such as to have not zero winds at the pole. Numerically the pole is considered as $(r_1, \lambda_j)$ with $j = 1,\ldots,m$ and the convolution filter is applied there as for

all other grid-points. The tests revealed that the convolution filter works properly in the vicinity of the pole, and the large-scale fields are recovered without distortions near the pole.

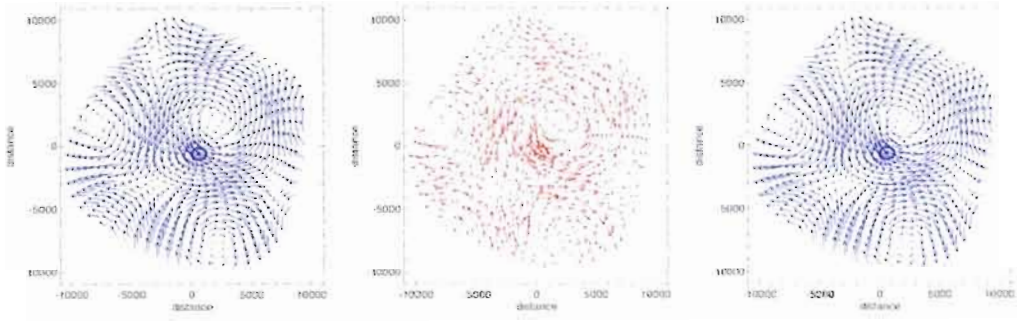

Figure C.1 A large-scale rotational wind field (left panel) is perturbed by a small-scale divergent wind field (middle panel). The filtered field is represented in the right panel.

A similar experiment was repeated on a polar stretched grid. A test field wind composed from a large scale purely divergent wind developed using a velocity potential in form of cylindrical harmonic with radial wavenumber 1 and azimuthal wavenumber 2 (Fig. C.2 left panel) was perturbed by a rotational noise developed using a streamfunction in form of double cosine with wavelength 400km (Fig. C.2 middle panel). The filter uses a weighting function that keeps unchanged all signals with wavelengths larger than 3,000km and removes all noises with wavelengths smaller than 600km. These parameters correspond to a smoother spectral response than in the first example and thereafter necessitate a truncation distance of only 900 km to remove the noise. Because the filter is applied outside the uniform high-resolution region and to better display the effect of the filter in the stretching zones, we present only the test-function outside the high-resolution zone. In Fig. C.2 (right panel) we show the filtered function; visually we note that the convolution filter is able to remove the noise and after the application of the filter the large scale signal is

recovered. No deformations were noted around the high-resolution domain and the filter works properly in the stretching zones as well as around the pole.

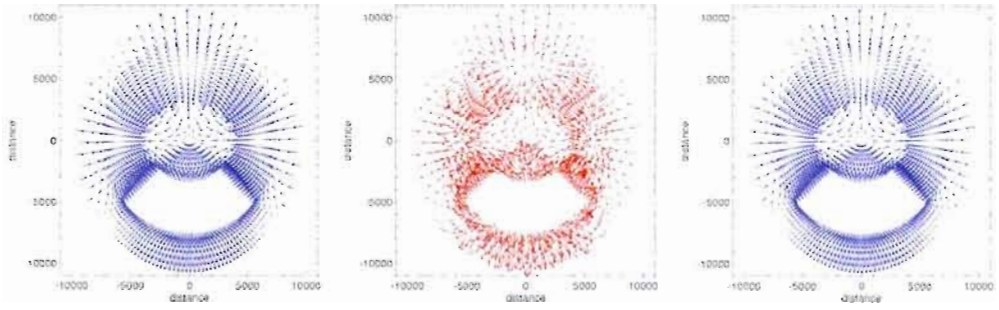

Figure C.2 A large-scale divergent wind field (left panel) is perturbed by a small-scale rotational wind field (middle panel). The convolution filter is applied outside the uniform high-resolution region and the filtered field is represented in the right panel.

The present study shows that with appropriate definition constraints, and representing the winds components for all points contributing to the convolution relative to the same reference system as the application point, we were able to remove small-scale noise superimposed on large-scale signals.

## Reference

Surcel, D., and R. Laprise, 2011a: A General Filter for Stretched-Grid Models: Application in Cartesian Geometry. *Mon. Wea. Rev.* **139**, 1637-1653.

Surcel, D., and R. Laprise, 2011b: A Theoretical Approach for a Smoothing operator on a variable grid. Part II: Filtering the scalars on the polar grid, Research activities in Atmospheric and Oceanic Modelling, edited by A. Zadra, WMO/TD, Report No. 40.

# APPENDICE D

# ADAPTATION DU FILTRE CONSTRUIT À L'AIDE D'UN PRODUIT DE CONVOLUTION POUR UNE GRILLE SPHÉRIQUE LATITUDE-LONGITUDE

L'approche développée pour une grille cartésienne et adaptée pour la grille polaire sera maintenant généralisée pour l'application du filtre sur une grille sphérique latitude-longitude. En coordonnées sphériques, un point est représenté par son rayon $r$, la latitude $\varphi$ et la longitude $\lambda$. Les coordonnées cartésiennes $x$, $y$ et $z$ sont reliées aux coordonnées sphériques par :

$$\begin{cases} x = r \cdot \cos\varphi \cdot \cos\lambda \\ y = r \cdot \cos\varphi \cdot \sin\lambda \\ z = r \cdot \sin\varphi \end{cases} \tag{D.1}$$

où $\begin{cases} r = \left(x^2 + y^2 + z^2\right)^{1/2} = \text{const.} \\ \lambda = \tan^{-1}\left(\dfrac{y}{x}\right) \\ \varphi = \sin^{-1}\left(\dfrac{z}{a}\right) \end{cases}$ , $-\pi/2 \le \varphi < \pi/2$ et $0 \le \lambda \le 2\pi$.

Le filtre construit à l'aide du produit de convolution sera appliqué sur chaque surface $r = a = \text{const.}$, et alors chaque point sur la sphère sera représenté seulement par la latitude $\varphi$ et la longitude $\lambda$.

La formulation du filtre est obtenue par l'application du produit de convolution successivement en direction zonale et en direction méridienne. La fonction de

pondération utilisée dans le produit de convolution dépend de la distance physique en direction zonale et en direction méridienne sur la grille. La fonction filtrée sera exprimée par :

$$\begin{aligned}\overline{\psi}(\varphi,\lambda) &= \overline{\left(\overline{(\psi)}^{\lambda}\right)}^{\varphi}(\varphi,\lambda) \\ &= \int_{\varphi'=-\frac{\pi}{2}}^{\frac{\pi}{2}} \int_{\lambda'=0}^{2\pi} \psi(\varphi',\lambda') \cdot w\left(d(\varphi,\varphi')\right) \cdot w\left(d(\lambda,\lambda')\right) \cdot a^2 \cdot \cos\varphi \cdot d\varphi \cdot d\lambda\end{aligned} \quad , \qquad \text{(D.2)}$$

où $d(\varphi,\varphi') = a \cdot (\varphi' - \varphi)$ représente la distance en direction méridienne, c'est-à-dire poure $\lambda = \text{const.}$, et $d(\lambda,\lambda') = a \cdot \cos\varphi \cdot (\lambda' - \lambda)$ représente la distance en direction zonale, c'est-à-dire pour $\varphi = \text{const.}$

Pour un champs scalaire $\psi_{i,j} = \psi(\varphi_i,\lambda_j)$ représenté sur une grille discrète latitude-longitude $(\varphi_i,\lambda_j)$ ($i = 1,\ldots,n; j = 1,\ldots,m$, $\varphi_i \in [-\pi/2,\pi/2]$, $\lambda_j \in [0,2\pi)$), la fonction filtrée sera exprimée à l'aide du produit de convolution par:

$$\begin{aligned}\overline{\psi}^{\varphi,\lambda}(\varphi_i,\lambda_j) &= \frac{\sum_k \overline{\psi}^{\lambda}(\varphi_k,\lambda_j) \cdot w\left(d^{\varphi}_{i-k}\right) \cdot s(\varphi_k)}{\sum_k w\left(d^{\varphi}_{i-k}\right) \cdot s(\varphi_k)} \\ &= \frac{\sum_k \sum_l \psi(\varphi_k,\lambda_l) \cdot w\left(d^{\lambda}_{j-l}\right) \cdot w\left(d^{\varphi}_{i-k}\right) \cdot s(\varphi_k) \cdot s(\lambda_l)}{\sum_k \sum_l w\left(d^{\lambda}_{j-l}\right) \cdot w\left(d^{\varphi}_{i-k}\right) \cdot s(\varphi_k) \cdot s(\lambda_l)}\end{aligned} \qquad \text{(D.3)}$$

où $d^{\lambda}_{j-l}$ et $d^{\varphi}_{i-k}$ sont les distances en direction zonale et méridienne entre deux points de grille $(\varphi_i,\lambda_j)$ et $(\varphi_k,\lambda_l)$, et $s(\varphi_k) \cdot s(\lambda_l) = s(\varphi_k,\lambda_l)$ représente la surface de pondération considérée pour chaque point de grille $(\varphi_k,\lambda_l)$.

Comme nous avons procédé sur la grille cartésienne ainsi que sur la grille polaire, les sommes dans l'équation (D.3) serons calculées pour une distance de troncature maximale $d_{\max}$. La fonction filtrée en direction zonale s'exprime par :

$$\overline{\psi}^{\lambda}\left(\varphi_k,\lambda_j\right)=\frac{\sum\limits_{l}\psi\left(\varphi_k,\lambda_l\right)\cdot w\left(d^{\lambda}_{j-l}\right)\cdot s\left(\lambda_l\right)}{\sum\limits_{\substack{l\\ d^{\lambda}_{j-l}\le d_{\max}}} w\left(d^{\lambda}_{j-l}\right)\cdot s\left(\lambda_l\right)} \qquad (D.4)$$

avec $d^{\lambda}_{j-l}=a\cdot\cos\varphi_k\cdot\left(\lambda_j-\lambda_l\right)$ la distance entre les points de grille $\left(\varphi_k,\lambda_j\right)$ et $\left(\varphi_k,\lambda_l\right)$ situés sur le même cercle $\varphi_k=\text{const.}$, et $s\left(\lambda_l\right)=a\cdot\cos\varphi_k\cdot\left[\left(\lambda_{l+1}-\lambda_{l-1}\right)/2\right]$ le facteur d'échelle qui correspond au point de grille $\left(\varphi_k,\lambda_l\right)$.

Le produit de convolution appliqué ensuite en direction méridienne est:

$$\overline{\psi}\left(\varphi_i,\lambda_j\right)=\overline{\left(\overline{\psi}^{\lambda}\right)}^{\varphi}\left(\varphi_i,\lambda_j\right)=\frac{\sum\limits_{k}\overline{\psi}^{\lambda}\left(\varphi_k,\lambda_j\right)\cdot w\left(d^{\varphi}_{i-k}\right)\cdot s\left(\varphi_k\right)}{\sum\limits_{\substack{k\\ d^{\varphi}_{i-k}\le d_{\max}}} w\left(d^{\varphi}_{i-k}\right)\cdot s\left(\varphi_k\right)} \qquad (D.5)$$

avec $d^{\varphi}_{i-k}=a\cdot\left(\varphi_i-\varphi_k\right)$ la distance entre les points de grille $\left(\varphi_i,\lambda_j\right)$ et $\left(\varphi_k,\lambda_j\right)$ situés sur le même cercle $\lambda_j=\text{const.}$, et $s\left(\varphi_k\right)=a\cdot\left(\varphi_{k+1}-\varphi_{k-1}\right)/2$ le facteur d'échelle qui correspond au point de grille $\left(\varphi_k,\lambda_j\right)$.

Quand le produit de convolution est appliqué pour des vecteurs sur une grille sphérique, il faut considérer la représentation des vecteurs relative au même système des coordonnées. Cette opération est nécessaire pour prendre en compte l'effet de courbature de la sphère. Dans la pratique météorologique, les vecteurs, comme le vent horizontal, sont définis en termes de coordonnées facilement identifiables en tout point

sur la sphère. Nous allons considérer un système cartésien local avec l'axe $x$ vers l'est et l'axe $y$ vers le nord. Pour un point $P(\varphi,\lambda)$ce système est défini par :

$$\begin{aligned} dx &= a\cdot\cos\varphi\cdot d\lambda \\ dy &= a\cdot d\varphi \end{aligned} \tag{D.6}$$

Le vent horizontal en coordonnées sphériques est :

$$\mathbf{V} = (u,v) = \left(a\cos\varphi\frac{d\lambda}{dt}, a\frac{d\varphi}{dt}\right) \tag{D.7}$$

où $(u,v)$ correspondent aux composantes zonale et méridienne du vent avec les conventions mentionnées que $u$ est positif vers l'est et $v$ est positif vers le nord.

Pour un point de grille $(\varphi_i,\lambda_j)$ les composantes du vent horizontal sont:

$$\begin{cases} u_{i,j} = u(\varphi_i,\lambda_j) \\ v_{i,j} = v(\varphi_i,\lambda_j) \end{cases} \tag{D.8}$$

avec $i=1,\ldots,n;\quad j=1,\ldots,m;\varphi_i\in[-\pi/2,\pi/2];\quad \lambda_j\in[0,2\pi)$ .

L'application du filtre construit à l'aide d'un produit de convolution pour des vecteurs nécessite que tous les vecteurs qui participent dans le produit de convolution soient représentés relatifs au même système de coordonnées. Nous allons décrire brièvement une méthode pour obtenir cette représentation.

Cette méthode décrite dans Tanguay *et al* .(1990) consiste à représenter les vecteurs dans un plan polaire stéréographique avec la projection vraie à la latitude où le filtre est appliqué. Comme pour les scalaires, le produit de convolution sera appliqué premièrement en direction zonale et par la suite en direction méridienne.

Quand le filtre est appliqué en direction zonale, alors pour chaque point $P_0(\varphi_0, \lambda_0)$ où le filtre est appliqué, il faut exprimer les composantes $(u, v)$ des points voisins $P(\varphi_0, \lambda)$ pour lesquels $dx = \left| a \cdot \cos\varphi_0 \cdot (\lambda - \lambda_0) \right| \leq d_{\max}$ où $d_{\max}$ est la distance maximale de troncature. En suivant Tanguay *et al.* (1990), nous allons retrouver :

- le facteur d'échelle $m$ correspondant à cette projection

$$m = \frac{1 + \sin\varphi_0}{1 + \sin\varphi_0} = 1, \tag{D.9}$$

- les distances dans le nouveau système de coordonnées

$$\begin{pmatrix} dX \\ dY \end{pmatrix} = \begin{bmatrix} -\sin(\lambda - \lambda_0) & -\cos(\lambda - \lambda_0) \\ \cos(\lambda - \lambda_0) & -\sin(\lambda - \lambda_0) \end{bmatrix} \begin{pmatrix} dx \\ 0 \end{pmatrix} \tag{D.10}$$

- les composantes du vent

$$\begin{pmatrix} U \\ V \end{pmatrix} = \begin{bmatrix} -\sin(\lambda - \lambda_0) & -\cos(\lambda - \lambda_0) \\ \cos(\lambda - \lambda_0) & -\sin(\lambda - \lambda_0) \end{bmatrix} \begin{pmatrix} u \\ v \end{pmatrix} \tag{D.11}$$

En appliquant le filtre en direction zonale nous allons obtenir $(\overline{U}^{\lambda}, \overline{V}^{\lambda})$ et, par la relation inverse à (D.11), nous allons retrouver $(\overline{u}^{\lambda}, \overline{v}^{\lambda})$.

Par la suite le filtre sera appliqué en direction méridienne. Dans ce cas pour chaque point $P_0(\varphi_0, \lambda_0)$ où le filtre est appliqué, il faut exprimer les composantes $(u, v)$ des points voisins $P(\varphi, \lambda_0)$ pour lesquels $dy = \left| a \cdot (\varphi - \varphi_0) \right| \leq d_{\max}$ où $d_{\max}$ est la distance maximale de troncature. Encore une fois en suivant Tanguay *et al.* (1990), nous allons retrouver :

- le facteur d'échelle $m$ correspondant à cette projection

$$m = \frac{1+\sin\varphi_0}{1+\sin\varphi}, \tag{D.12}$$

- les distances dans le nouveau système de coordonnées

$$\begin{pmatrix} dX \\ dY \end{pmatrix} = m \cdot \begin{bmatrix} -\sin\lambda_0 & -\cos\lambda_0 \\ \cos\lambda_0 & -\sin\lambda_0 \end{bmatrix} \begin{pmatrix} 0 \\ dy \end{pmatrix} \tag{D.13}$$

- les composantes du vent

$$\begin{pmatrix} U \\ V \end{pmatrix} = \frac{1}{m} \cdot \begin{bmatrix} -\sin\lambda_0 & -\cos\lambda_0 \\ \cos\lambda_0 & -\sin\lambda_0 \end{bmatrix} \begin{pmatrix} \overline{u}^{\lambda} \\ \overline{v}^{\lambda} \end{pmatrix} \tag{D.14}.$$

En appliquant le filtre en direction méridienne nous allons obtenir $\left(\overline{U}^{\lambda,\varphi}, \overline{V}^{\lambda,\varphi}\right)$ et, par la relation inverse à (D.14), nous allons retrouver $\left(\overline{u}^{\lambda,\varphi}, \overline{v}^{\lambda,\varphi}\right) = \left(\overline{u}, \overline{v}\right)$.

# BIBLIOGRAPHIE


Bracewell, R. N., 2000: *The Fourier transform and its applications.* McGraw-Hill International Editions, third edition, 640 pp.

Caian, M., and J.-F. Geleyn, 1997: Some limits to the variable mesh solution and comparison with the nested-LAM solution. *Quart. J.Roy. Meteor. Soc.,* **123,** 743–766.

Côté, J., M. Roch, A. Staniforth, and L. Fillion, 1993: A variable-resolution semi-Lagrangian finite-element global model of the shallow-water equations. *Mon. Wea. Rev.,* **121,** 231–243.

Côté, J., S. Gravel, A. Méthot, A. Patoine, M. Roch, and A. Staniforth, 1997: Preliminary results from a dry global variable-resolution primitive equations model. *Numerical methods in Atmospheric and Oceanic Modelling: The André J. Robert Memorial Volume*, edited by C. Lin, R. Laprise and H. Richie, 245-259, CMOS, Ottawa, Canada.

Côté, J., S. Gravel, A. Méthot, A. Patoine, M. Roch, and A. Staniforth, 1998: The operational CMC-MRB Global Environmental Multiscale (GEM) Model. Part I: Design considerations and formulation. *Mon. Wea. Rev.*, **126**, 1373-1395.

Courtier, P., and J.-F. Geleyn, 1988: A global numerical weather prediction model with variable resolution: Application to the shallow-water equations. *Quart. J. Roy. Meteor. Soc.,* **114,** 1321– 1346.

Déqué, M., and J.P. Piédelièvre, 1995: High resolution climate simulation over Europe. *Climate Dyn.*, **11**, 321-339.

Fox-Rabinovitz, M.S., L. Stenchikov, M. Suarez, and L. Takacs, 1997: A finite-difference GCM dynamical core with a variable-resolution stretched grid. *Mon. Wea. Rev.*, **125**, 2943-2968.

Fox-Rabinovitz, M.S., L. Takacs, R.C. Govindaraju, and M. Suarez, 2001: A variable- resolution stretched-grid general Circulation Model : Regional climate simulation, *Mon. Wea. Rev.*, **129**, 453-469.

Fox-Rabinovitz, M.S., J. Côté, B. Dugas, M. Déqué, and J.L. McGregor, 2006: Variable resolution general circulation models: Stretched-grid model

intercomparison project (SGMIP). *J. Geophys. Res.*, **111**, D16104, doi:10.1029/2005JD006520.

Fox-Rabinovitz, M.S., J. Côté, B. Dugas, M. Déqué, J.L. McGregor, and A. Belochitski, 2008: Stretched-grid Model Intercomparison Project: decadal regional climate simulations with enhanced variable and uniform-resolution GCMs. *Meteor. Atmos. Phys.*, **100**, 159-177.

Gasquet, C., and P. Witomski, 1990: *Analyse de Fourier et applications. Filtrage, calcul numérique, ondelettes*. Mason, Paris, 354 pp.

Gibelin A.L., and M. Déqué, 2003: Anthropogenic climate change over the Mediterranean region simulated by a global variable resolution model. *Clim. Dyn.* **20,** 327-339.

Hardiker, V., 1997: A global numerical weather prediction model with variable resolution. *Mon. Wea. Rev.* **125**, 59-73.

Hortal, M., and A.J. Simmons, 1991: Use of reduced Gaussian grids in spectral models. *Mon. Wea. Rev.*, **119**, 1057-1074.

Laprise R., 2008: Regional climate modelling. *J. Comput. Phys.*, **227**, 3641-3666.

McGregor, J.L., K.C. Nguyen, and J.J. Katzfey, 2002: Regional climate simulations using a stretched-grid global model. Research Activities in Atmospheric and Oceanic Modelling, Report 32 WMO/TD- No. 1105, 3.15-16.

Paegle, J., 1989: A variable resolution global model based upon Fourier and finite element representation. *Mon.Wea. Rev.*, **117**, 583-606.

Paegle, J., Q. Yang, and M. Wang, 1997: Predictability in limited area and global models. *Meteorol. Atmos. Phys.*, **63**, 53-69.

Purser, R.J., 1988: Degradation of numerical differencing caused by Fourier filtering at high latitudes. *Mon. Wea. Rev.*, **116**, 1057-1066.

Radix, J.C., 1970: *Introduction au filtrage numérique, Lissage de données, Estimation de parameters, Identification de processus, Exercices et solutions*. Éditions Eyrolles, Paris, 240 pp.

Schmidt, F., 1977: Variable fine mesh in the spectral global models. *Beitr. Phys. Atmos.*, **50,** 211–217.

Shapiro, R., 1970: Smoothing, filtering and boundary effects. *Rev. Geophys. Space Phys.*, **8**, 359-387.

Staniforth, A., 1997: Regional modeling: a theoretical discussion. *Meteorol. Atmos. Phys.*, **63**, 15-29.

Surcel, D., 2005: Filtres universels pour les modèles numériques à résolution variable. Mémoire de maîtrise en Sciences de l'atmosphère, Université du Québec à Montréal. 104 pp.

Takacs, L., W. Sawyer, M.J. Suarez, and M.S. Fox-Rabinovitz, 1999: Filtering techniques on a stretched grid General Circulation Model. *NASA Tech. Memo. 104606*, Vol. 16, 45 pp. [Available from Data Assimilation Office, NASA GSFC, Greenbelt, MD 20771].

Tanguay, M., A. Robert, and R. Laprise, 1990: A semi-implicit semi-Lagrangian fully compressible regional forecast model. *Mon.Wea. Rev.*, **118,** 1970–1980.

Thatcher, M., and J.L. McGregor, 2009: Using a scale-selective filter for dynamical downscaling with the Conformal Cubic Atmospheric Model. *Mon. Wea. Rev.*, **137**, 1742-1752.

Yessad, K., and P. Bénard, 1996: Introduction of a local mapping factor in the spectral part of the Meteo-France global variable mesh numerical weather forecast model. *Quart. J. Roy. Meteorol. Soc.*, **122**, 1701-1719.

Zadra, A., D. Caya, J. Côté, B. Dugas, C. Jones, R. Laprise, K. Winger, and L.-P. Caron, 2008: The next Canadian Regional Climate Model. *Physics in Canada*, **64**, 75-83.